FUELS JOINT RESEARCH GROUP

CHECK

Band 31

Martin Unglert, Tobias Köstner, Markus Jakob, Anja Singer, Michael Rossner, Olaf Schröder, Thomas Garbe, Jürgen Krahl

Development of an on-board sensor system for early identification of deposit formations in fuels containing biodiesel

Herausgeber: Jürgen Krahl, Axel Munack, Peter Eilts, Jürgen Bünger

Cuvillier Verlag Göttingen

Development of an on-board sensor system for early identification of deposit formations in fuels containing biodiesel

Union zur Förderung von
Oel- und Proteinpflanzen e. V.

Federal Ministry
of Education
and Research

COBURG UNIVERSITY
of applied sciences and arts

Research Project Final Report

Development of an on-board sensor system for early identification of deposit formations in fuels containing biodiesel

Edited by: Martin Unglert
Tobias Köstner

Funding code: UFOP project 540/151
BMBF13FH028PX5

Grantee: Coburg University of Applied Sciences
Friedrich-Streib-Str. 2
96450 Coburg

Project management: Markus Jakob (HS-Coburg)
Anja Singer (HS-Coburg)
Michael Rossner (HS-Coburg)
Olaf Schröder (HS-Coburg)
Thomas Garbe (HS-Coburg)
Jürgen Krahl (TH OWL)

Term of the research project: 01/11/2016 – 31/01/2021

Bibliografische Information der Deutschen Nationalbibliothek
Die Deutsche Nationalbibliothek verzeichnet diese Publikation in der
Deutschen Nationalbibliografie; detaillierte bibliographische Daten sind im Internet
über http://dnb.d-nb.de abrufbar.
1. Aufl. - Göttingen: Cuvillier, 2021

Nonnenstieg 8, 37075 Göttingen
Telefon: 0551-54724-0
Telefax: 0551-54724-21
www.cuvillier.de

1. Auflage, 2021
Gedruckt auf umweltfreundlichem, säurefreiem Papier aus nachhaltiger Forstwirtschaft.

ISBN 978-3-7369-7492-0
eISBN 978-3-7369-6492-1

Table of contents

1 Introduction 7
2 Theory – State of Research 8
2.1 Autoxidation 8
2.2 Thermal oxidative ageing 9
2.3 Radical stability 9
2.4 Reaction mechanisms used for explanation from the literature 10
3 Utilised fuels 12
3.1 Biodiesel 12
3.2 Hydrogenated vegetable oil (HVO) 13
3.3 Polyoxymethylene dimethyl ether (OME) 13
4 Measurement and evaluation methods used and sensor details 14
4.1 Accelerated artificial ageing 14
4.1.1 Rancimat method 14
4.1.2 Petrooxy method 15
4.2 Fourier transform infrared spectrometry (FTIR) 15
4.3 Near infrared spectroscopy with laboratory measuring device 15
4.4 Partial least squares Regression (PLS) 15
4.4 Liquid chromatography coupled mass spectrometry 16
4.5 Spectroscopic methods of the developed sensor technology 17
4.5.1 Dielectric sensor 19
4.5.2 Optical sensor 20
5 Evaluation of the mass spectrometric investigations 22
5.2 Chromatographic separation 22
5.3 Structure elucidation of the ageing products with MS/MS fragmentation pattern 23
6 Ageing tests by RME 26
6.1 Overview of the ageing test 26
6.2 Identified ageing products and statements about the underlying mechanisms 27
6.2.1 Simple oxidation products 27
6.2.2 Multiple oxidation products 33
6.2.3 Short-chain degradation products 36
6.2.4 Dimerization 37
6.2.5 Acids 42
6.3 Time course of RME ageing 44
6.3.1 Starting products 46
6.3.2 Simple oxidation products 46

6.3.3 Twofold oxidation products 46
6.3.4 Triple oxidation 47
6.3.5 Fourfold oxidation 49
6.3.6 Short-chain degradation products 49
6.3.7 Dimer formation 50
6.4 Influence of the fuel composition on the ageing behaviour 50
6.4.1 Simple oxidation 52
6.4.2 Double oxidation 54
6.4.3 Triple oxidation 54
6.4.4 Fourfold oxidation 55
6.4.5 Short-chain degradation products and acids 56
6.4.6 Influence of the volume fraction of RME 57
7 additive tests 59
8 Developed fuel sensors 64
8.1 Empirical variance and measurement accuracy of the developed sensors 65
8.1.1 Dielectric measurements (permittivity and conductivity) 65
8.1.2 Optical measurements (near infrared, fluorescence and VIS spectroscopy) 67
8.2 Fluorescence measurement data 70
8.3 Determination of the fuel composition and the degree of ageing 71
8.3.1 Partial Least Square evaluation 71
8.3.2 Fuels used 72
8.3.3 PLS evaluation using reference analysis 73
8.3.4 Sensor-based prediction 79
9 Summary 84
10 Outlook 85
11 Bibliography 86

1 Introduction

The environmental pollution that arises in connection with increasing mobility must be reduced.[1] In order to achieve set climate targets, a holistic approach must be pursued that includes not only electromobility but also renewable fuels.[2] As so-called drop-in fuels, regenerative fuels can be used with the existing infrastructure, and cars that are already on the market can thus be operated in a more environmentally friendly way.[3] However, increasing the regenerative share of fuel is only part of the reduction in emissions.[4] Since the design of the internal combustion engine is always a compromise between stable operation, low emissions and high efficiency, the importance of the three parameters must be determined during development (Figure 1). For example, high operational reliability and high efficiency play a decisive role in aircraft engines. This is where the fuel plays a crucial role, as the influence of the fuel on the combustion can minimise emissions. [5] Sensors for recognising the fuel composition in automobiles are useful in order to reduce emissions in the best possible way.[6]

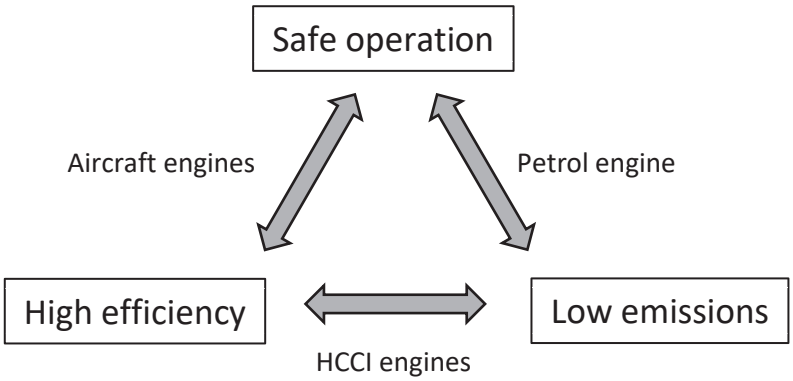

Figure 1: Compromise in engine combustion design.

By recognising the fuel composition and the degree of ageing or oxidation, the engine control device can be set specifically to the fuel present. A sensory fuel detection can also be used to detect regenerative fuels. Because the emissions of the combustion engine are mainly caused by the operation of the automobile (only a small part of the emissions are generated by production), a contribution can be made through regenerative fuel.[7] In combination with tax relief for regenerative fuels, an effective control mechanism can be implemented in the car that documents the use of regenerative fuels. In order to replace fossil fuels in the future, different raw material sources can be used to produce synthetic fuels.[8] This results in fuels that can differ greatly in their chemical composition.[9][33][10] For optimal combustion, the fuel components or the fuel composition must be recognised in the future so that the engine management can be optimally adjusted. Subsidised electromobility is also increasingly influencing electrification in the form of plug-in hybrids. In plug-in hybrids, the advantages of both technologies (electric drive and combustion engine) are combined: This means that local emission-free driving and a long range can be guaranteed.[11] The short driving cycles in everyday life make it possible to charge the accumulator in a stationary manner from the mains. The short driving cycles mean that the fuel in plug-in hybrid vehicles is exposed to far more critical conditions than before. The fuel remains in the tank for longer, which can lead to changes in the physical and chemical properties of the fuel. Accordingly, the detection of the degree of ageing is an important property for a fuel sensor system.

The first part of the research project presented here discusses a detailed investigation of the ageing of rapeseed oil methyl ester (RME). For the increased use of biodiesel in the future, also in connection with new regenerative fuels, understanding ageing is an important aspect in order to be able to ensure stable fuel formulations. As a result, the ageing of biodiesel in its pure form must be understood and

since fuel ageing is not the same for all fuels, the ageing in biodiesel blends must also be examined. For RME ageing, the investigations presented below aim to answer the following questions:

- What products are produced by fuel ageing?
- What is the mechanism behind the creation of the products?
- What is the development of the individual products over time like?
- Influence of the fuel matrix on ageing behaviour?

The answer to these questions is based on the investigation of fuel ageing with high-resolution mass spectrometry, which describes the different stages of oxidation that increases over the ageing process. By identifying the structures of ageing products, new insights into the ageing behaviour are presented in the area of the oligomerisation of RME. The second part presents the developed sensor system for recognising the fuel composition and the degree of ageing. In the following, the theoretical basics, the fuels used, the measuring methods and the procedure for evaluating high-resolution mass spectra for the structure identification of the ageing products are presented initially. After that, the results obtained in the course of this research project will then be discussed.

2 Theory – State of Research

The fuel ageing of RME or fatty acid methyl esters in general has already been discussed many times in literature. [12,13,14,15] The following section summarises the most important principles of autoxidation. Three mechanisms from literature are used for the discussion of the results, which are presented below in their original interpretation.

2.1 Autoxidation

Autoxidation is the process of a chemical compound being slowly oxidised by oxygen from the air. This process takes place autocatalytically and, among other things, leads to the formation of hydroperoxides. Some examples of autoxidation reactions are the formation of acetic acid from alcohols, the fading of colours, fats turning rancid and in everyday life the browning of cut apples.[16]

The process of autoxidation can be divided into three phases. The first phase is called the start reaction, in which homolytic bond splitting is initiated. If radicals have formed in the initial reaction, chain propagation describes the further reaction with renewed formation of a radical. Chain termination occurs when two radicals form stable products with one another.[17] In autoxidation, hydroperoxides (ROOH) are of particular importance. Hydroperoxides are formed during chain propagation (equations 4 and 5) and are also starting compounds for the start reaction (equation 2). The great influence of the hydroperoxides results from the branching of the reaction process, since two radicals are formed from one hydroperoxide (equation 2). This process is known as chain branching.[18]

Start reaction:

$$R\text{–}H \xrightarrow{activation} R^{\bullet} + H^{\bullet} \quad (1)$$

$$ROOH \longrightarrow RO^{\bullet} + {}^{\bullet}OH \quad (2)$$

$$2ROOH \longrightarrow RO^{\bullet} + RO_2^{\bullet} + H_2O \quad (3)$$

Chain propagation:

$$R^{\bullet} + O_2 \longrightarrow RO_2^{\bullet} \quad (4)$$

$$RO_2^{\bullet} + RH \longrightarrow ROOH + R^{\bullet} \quad (5)$$

$$RO^{\bullet} + R\text{–}H \longrightarrow ROH + R^{\bullet} \quad (6)$$

Chain termination:

$2R^{\bullet} \rightarrow R–R$ (7)

$2RO_2^{\bullet} \rightarrow$ stable products (8)

2.2 Thermal oxidative ageing

The autoxidation depends on the temperature.[19] The ageing of substances is thus an interplay of radical stability and temperature. According to the Arrhenius equations, the logarithm of the reaction rate constant (k) is subject to a linear dependence on the reciprocal absolute temperature.

$$\ln k = \ln A - \frac{E_a}{RT} \quad (9)$$

In the equation, R represents the universal gas constant, E_a the activation energy, T the temperature in Kelvin and A an empirical constant that includes various probability parameters and oscillation constants of molecules.[20] Fuel ageing occurs faster as the temperature increases, which is why the investigations on fuel ageing must always be considered in relation to the selected ageing temperature.[19]

2.3 Radical stability

The formation of the ageing products depends largely on the stabilisation of the radicals involved. The more stable a radical is, the more easily it is formed and the easier the oxidation of the compounds that can form these radicals.[21] The stability is determined by mesomerism (delocalisation), substituent effects (hyperconjugation), steric effects and the reactivity of the radical centre affects and results in a lower bond dissociation energy. In addition, the solvent has an influence on the stabilisation of the educts formed as well as products (dimers) or can itself react with the radical. Figure 2 shows the increasing stability of selected organic radicals. The stability increases from primary to secondary to tertiary alkyl radicals. The cause is the hyperconjugation of the binding electrons of the C–H bond into the half-occupied p-orbital on the sp2 hybridised carbon (Figure 2) due to the methyl group. Aryl and benzyl radicals have a significantly higher stability due to mesomerism (Figure 3).[22]

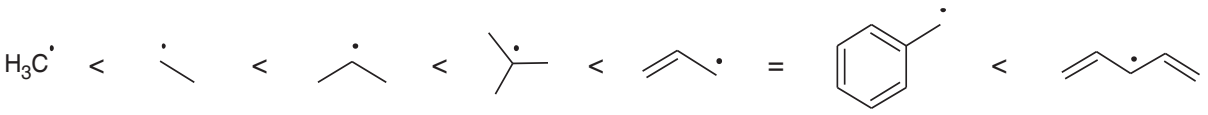

Figure 2: *Radical stability.* [23][24][25]

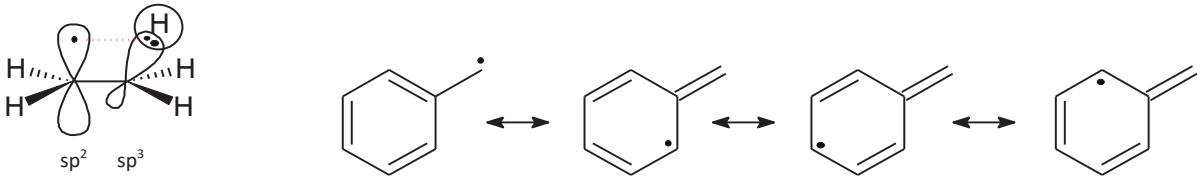

Figure 3: *Hyperconjugation and resonance stabilisation.* [26][27]

2.4 Reaction mechanisms used for explanation from the literature

The aspects described in Sections 2.1 to 2.3 represent the generally accepted general mechanism of the autoxidation of fatty acid methyl esters.[29] The autoxidation is based on the spontaneous formation of radicals (initiation) and a subsequent reaction with molecular oxygen in which up to two radicals are formed from one radical (chain branching). However, these generally formulated reactions can be further differentiated and discussed. The general influences of autoxidation and radical stabilities must be extended to the structure of the fuel molecules for a detailed consideration of fuel ageing, since the structure influences the mesomeric stabilisation of radicals and these in turn influence the oxidation and the formation of ageing products. The core aspect of autoxidation is represented by the peroxides formed by the reaction of radicals and molecular oxygen.[29] Starting from these peroxides, a number of different functional groups can be observed that are formed in secondary reactions. In addition, the greater the number of double bonds, the greater the diversity of the compounds that are formed. However, this does not affect the variety of functional groups that form. The investigation of FAME ageing is such a complex project that there are currently no studies that consider ageing in its entirety. Research on the mechanisms is often based on a selective consideration of individual steps, such as the formation of different peroxides and the reaction mechanisms derived from them. [29] Thus, through targeted synthesis of individual products, the evaluation leads to an interpretation limited to this reaction. However, if the ageing is examined as a whole, a further interpretation of the subsequent reactions must be carried out using the selective interpretation. Products such as hydroperoxides do not represent completely stable products with the low dissociation energy of the oxygen-oxygen bond.[28] Although they can be detected, the thermodynamically more stable products are of greater importance for the investigation of overall ageing or for ageing after defined time intervals. For the interpretation of these thermodynamically more stable products, however, the studies of intermediates and their reaction mechanisms are an indispensable contribution to understanding the products observed. Three reactions that are important for a deeper understanding of ageing and that are used below for the discussion of results are described in more detail below.

The first reaction mechanism relevant to the results section of this report relates to the mechanism of the radical reaction with molecular oxygen and the various subsequent reactions that follow the initial reaction with molecular oxygen (Figure 4). Figure 4 shows the hydrogen abstraction in the α-position of the double bond of C18:1 ME, as described in literature.[29] The allyl radical formed in the first step reacts with molecular oxygen to form a peroxide radical in the second step. The reaction with RH with the release of a radical leads to hydroperoxides. Hydroperoxides, in turn, can break down into hydroxyl radicals and alkoxy radicals. Several reactions are possible starting from alkoxy radicals. By reacting RH with renewed release of a radical, alcohols can be formed, which can be further oxidised to ketones under the oxidative conditions. Alternatively, an epoxide can be formed by reaction of the alkoxy radical with an electron in the adjacent double bond (blue arrow). The alkoxy radical can, however, also react with cleavage of C-C bonds to form short-chain degradation products (red and green arrows). The initially formed radical in FAME is caused by several positions at which hydrogen abstraction can occur. As a result of the mesomeric stabilization the hydroperoxides can be located in different places in the molecule. The subsequent reactions that also occur there are then correspondingly in different positions. This results in a large number of ageing products that can be formed from a few starting materials (C18:1 ME, C18: 2 ME, ...). For further discussion see section 6.2.[29]

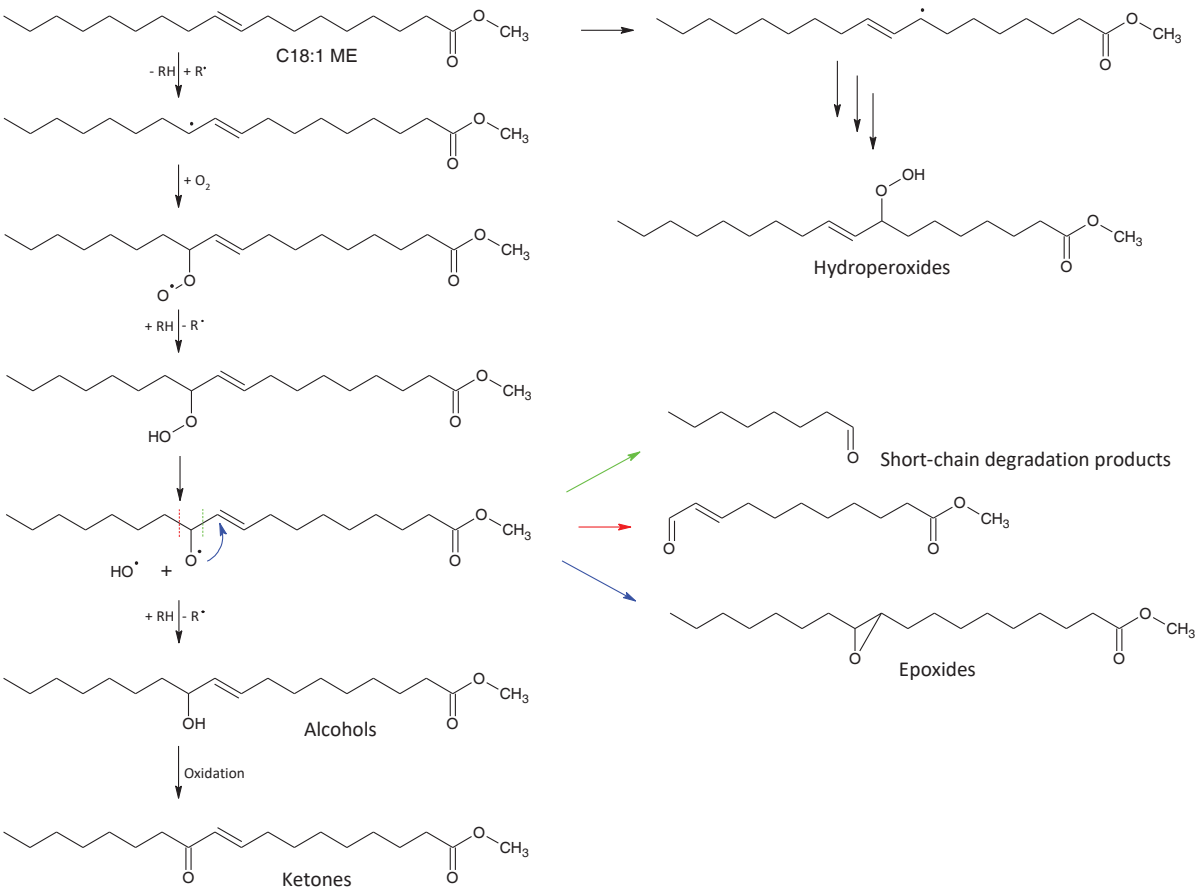

Figure 4: Mechanism of hydroperoxide formation and the possible subsequent reactions.[29]

The second basic-relevant reaction for the discussion in the results section is directly related to the product distribution of the epoxides in monounsaturated fatty acid methyl ethers and other reactions in which the products formed cannot be explained by the mechanism shown in Figure 4. The second mechanism for epoxide formation found in connection with retinoic acid as a cooxidant is described.[30] The oxidation products of retinoic acid found by Samokyszyn et al exclude the sole reaction mechanism from Figure 4. As here the epoxide is found at the position of the double bond and is necessary for a further explanation of identified products. For this reason, direct epoxidation through a peroxide radical with the double bond is suggested. The significance of this reaction in the ageing of fatty acid methyl esters is discussed in detail in Section 6.2 using the identified product ratio.

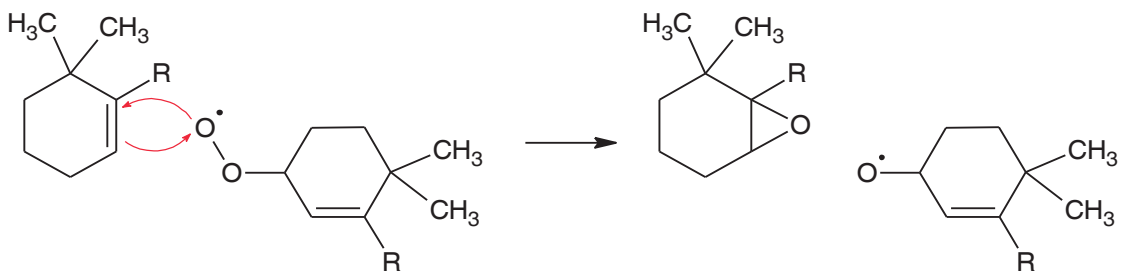

Figure 5: Epoxide formation through reaction of the double bond with a peroxide radical.[30]

The third reaction is a secondary reaction that can occur with epoxides. The formation of ketones from epoxides as a result of a rearrangement reaction depending on various substituents is part of Winstein and Henderson's studies (Figure 6).

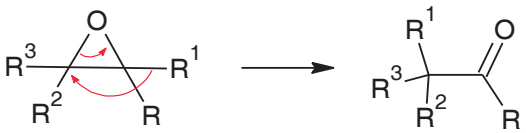

Figure 6: Ring opening reaction of monosubstituted epoxides.[31]

By opening the C-O bond and rearranging R1, epoxides are converted into ketones. With a symmetrical arrangement of the radicals (R1 = R3 and R = R2) the two possible ketones are formed in equal parts, whereby either one or the other C-O bond can break. Both ketones are then available with a theoretical ratio of 1:1.

3 Utilised fuels

3.1 Biodiesel

Biodiesel is a fuel name that is used either as a pure fuel or as a blend component in fossil diesel fuel. Biodiesel is made from different oils and fats (triglycerides).[32] Triglycerides consist of three fatty acids that are triple esterified with glycerine. In the biodiesel manufacturing process, the triglycerides are transesterified with methanol. Biodiesel therefore consists of fatty acid methyl esters (FAME), which differ in their fatty acid composition depending on the oil used.[33]

Table 1: *Fatty acid composition for different oils and fats.*[33]

Oil	Fatty acid composition [%]								
	C10:0	C12:0	C14:0	C16:0	C18:0	C18:1	C18:2	C18:3	C22:1
Rapeseed oil			0–1.5	1-6	0.5-3.5	8-60	9.5-23	1-13	5-64

The fatty acid composition of various oils used for biodiesel production is given in Table 1. The fatty acids are named according to their number of carbons (number before the colon) and the number of double bonds in the fatty acid (number after the colon). Based on the fatty acid composition, biodiesel consists of a mixture of unsaturated fatty acid methyl esters (compounds with a double bond) and saturated fatty acid methyl esters (compounds without a double bond). The composition of biodiesel affects the low temperature properties of the fuel. FAME with double bonds have a lower melting point than saturated FAME.[34] For this reason, the biodiesel component in diesel fuel used in winter mainly comes from rapeseed oil, which contains a high proportion of unsaturated FAME. In summer, the biodiesel content can have a higher proportion of saturated FAME, which means that biodiesel based on palm oil can be used.[35] In the context of this report, only biodiesel made from rapeseed oil is used. The biodiesel made from rapeseed oil is called rapeseed oil methyl ester (RME). The most frequently occurring FAMEs in RME are shown in Figure 7 with their structural formulas. For identification and differentiation from the fatty acids, the FAMEs have an addition of methyl ester (ME) in their designation. With the distinction between summer and winter diesel based on the fatty acid composition of the FAME, an important aspect is taken into account when using biodiesel, which plays an important role in the ageing investigation of RME.[35] For this purpose, the molecular structures are examined more closely in Figure 7. The presence of a double bond in the molecule changes the geometry of the molecules. If two molecules come together, the contact areas of the molecules are reduced in comparison to saturated FAMEs if double bonds are present. There are fewer intermolecular interactions. The result is lower melting points, as less energy has to be expended to

separate the molecules from one another in the solid state.[22] The aspect of the size of the intermolecular interactions affects not only the melting point, but also the miscibility of the fuels (see Section 6.4) and the chromatographic separation (see Section 5.2).

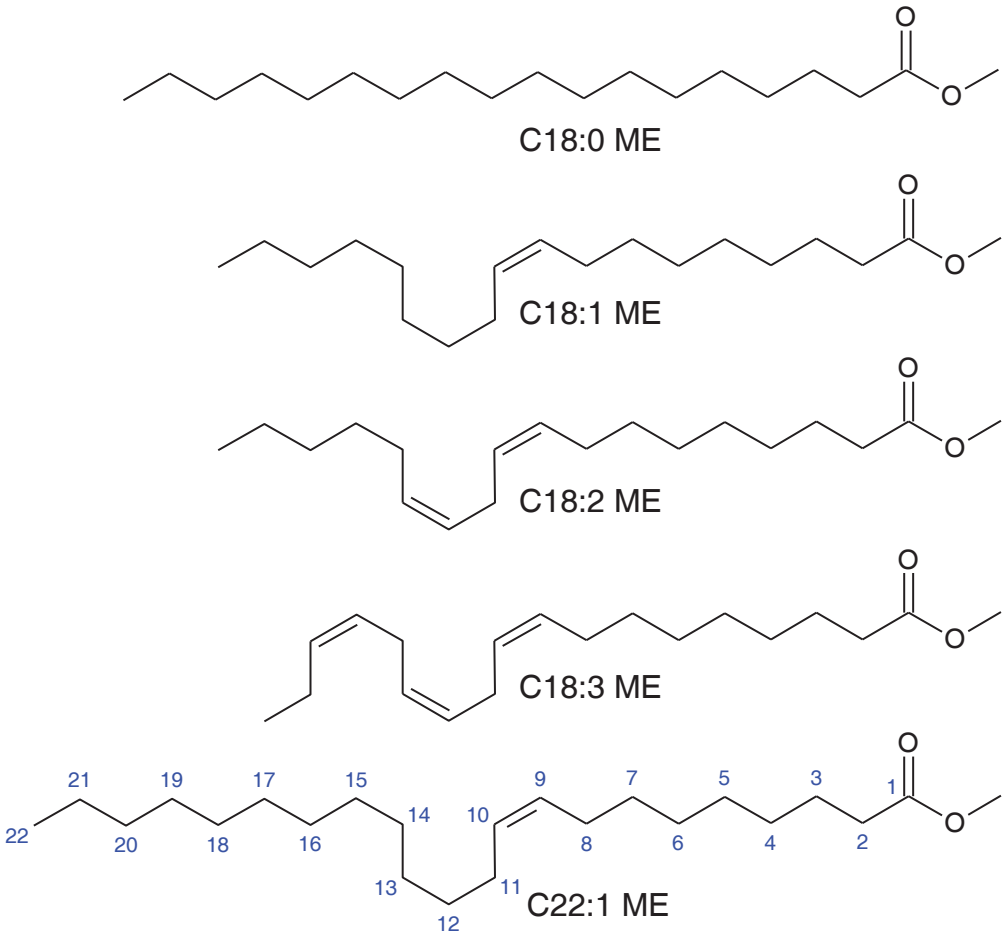

Figure 7: Structural formulas of C18:0 ME, C18:1 ME, C18:2 ME, C18:3 ME and C22:1 ME. For C22:1 ME the numbering of the carbons is shown, with which the position in the molecule is defined.

3.2 Hydrogenated vegetable oil (HVO)

Hydrogenated vegetable oil (HVO) is obtained from triglycerides in the same way as biodiesel. In contrast to biodiesel, HVO does not use transesterification, but rather the triglyceride is catalytically hydrogenated. The hydrogenation converts the triglycerides into alkanes, water and CO_2. Any unsaturated fatty acids present are converted into saturated hydrocarbons by hydrogenation. In addition, the hydrogenation causes an isomerisation of the hydrocarbons, whereby at the end the HVO is composed of n- and iso-alkanes.[9]

3.3 Polyoxymethylene dimethyl ether (OME)

Polyoxymethylene dimethyl ether (OME) is a polyether with different chain lengths. The general structural formula is shown in Figure 8, with the chain length of the batch used being between n = 3 and n = 6. The large proportion of oxygen atoms in the OME leads to a higher polarity compared to HVO and RME. This creates a field of tension between HVO and OME, which affects the miscibility.[36]

Due to the miscibility gap in HVO and OME, the influence of miscibility on fuel ageing can be examined in Section 6.4.

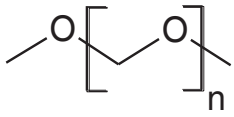

Figure 8: Structural formula of polyoxymethylene dimethyl ether.

4 Measurement and evaluation methods used and sensor details

4.1 Accelerated artificial ageing

To investigate the oxidation stability of fuels in the laboratory, a method must be used that allows the fuel to age within a short period of time. There are two methods according to DIN EN 590 which subject the fuel to accelerated thermo-oxidative ageing with a temperature increase and excess oxygen.

4.1.1 Rancimat method

The so-called Rancimat test determines the time from when the fuel begins to oxidise. The time it takes for oxidation to occur is known as the induction time. To determine the induction time, the fuel is heated to 110 °C in a defined reaction vessel (Figure 9). Through a glass tube, air is passed through the fuel with a volume flow of 10L / hour. If, for example, volatile acids are formed due to oxidation, these lead to an increase in conductivity in a separate conductivity measuring cell. The induction time can thus be determined by evaluating the conductivity over time. The induction time results from naturally occurring antioxidants, for example in rapeseed oil methyl ester, or from artificially added antioxidants that trap free radicals and thus suppress oxidation. The length of the induction time depends on the type and composition of the antioxidant and the interaction with the susceptibility of the fuel to oxidation. When the fuel is stored, the induction time of the fuel decreases continuously over time, depending on external influencing factors such as temperature, since the antioxidants are consumed over time.[37]

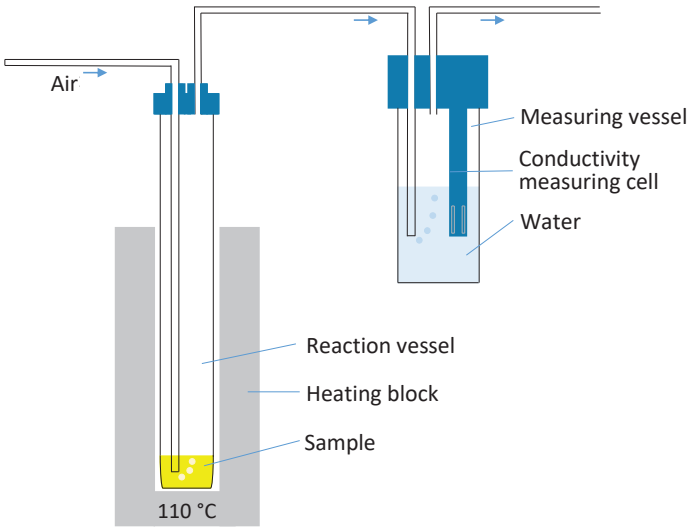

Figure 9: Schematic sketch of the ageing device Rancimat 873 Biodiesel for thermoxidative ageing of fuels.

4.1.2 Petrooxy method

The second test method is the so-called petrooxy test. In the petrooxy test, the fuel is tempered in a closed system together with pure molecular oxygen. The test cell is set to a pressure of 700 kPa by the molecular oxygen. When the oxidation occurs, the molecular oxygen is incorporated into the fuel molecules, which reduces the pressure in the test cell. According to the standard, the induction time is reached when the pressure drop is 10%. According to the standard, the test parameters are set at a temperature of 140 °C. The high pressure applied and the higher temperature compared to the Rancimat test result in a shorter measuring time. Another advantage is that the closed system enables even volatile fuels to be examined for oxidation stability. The respective induction time from Rancimat and Petrooxy refers exclusively to the measuring method. A direct general comparison of the induction times of both measurement methods is not possible due to the different test procedures.[38]

4.2 Fourier transform infrared spectrometry (FTIR)

The analysis of functional groups through the wavelength-dependent absorption in the mid-infrared range is measured with a Nicolet 6700 FTIR spectrometer from Thermo Scientific. The measurement is carried out using the ATR measuring principle (*attenuated total reflection*) in the wave number range from 4000 cm^{-1} to 650 cm^{-1}. The measurements are carried out at room temperature and evaluated with the Omnic software from Thermo Scientific.

4.3 Near infrared spectroscopy with laboratory measuring device

The near-infrared spectra are carried out with a NIRS XDS Rapid Liquid Analyser from Methrom. An Xds Monochromator Type XM – 1000 is used as the light source. The samples are taken with 8 mm cuvettes in a measuring range from 400 nm to 2400 nm at 35 °C. The evaluation was carried out with the VISION 4.0.3.0 software. Near-infrared spectroscopy is based on overtone or combination oscillations of the fundamental molecular oscillation, which leads to broad absorption bands and superimpositions. For this reason, the near-infrared data are further interpreted for detailed evaluations using multivariate methods.

4.4 Partial least squares Regression (PLS)

Partial least squares regression (PLS) is a multivariate method can be used in chemistry, for example, to determine properties from spectra. The PLS is based on the principal component analysis of independent variables X and the dependent variables Y. The matrices X and Y are each divided into two matrices T (score matrix) and P'' (loading matrix) or U and Q plus a respective error matrix E and F.

$$X = T \cdot P' + E$$

$$Y = U \cdot Q' + F$$

The basic idea is that the main components of the matrices X and Y are calculated independently and that a regression model is created between the score matrices T and U. The target data Y are therefore included in the principal component analysis for the X data in the PLS. The aim of the PLS is to minimise the norm of the error matrix F while maintaining a correlation between X and Y. This is done using the relationship U = B·T. Thus, the PLS can determine the target variable Y for unknown samples based on the measured values X.[39]

4.4 Liquid chromatography coupled mass spectrometry

Mass spectrometry is an analytical method for determining the mass of molecules and is used as a detector in liquid chromatographic separation. The sample to be examined is separated with the aid of a chromatographic separation column. The separation column consists of silica gel modified with alkane chains, the so-called stationary phase. A solvent (liquid phase) separates the components according to the interaction between sample, stationary phase and liquid phase. If the separation is good or if there are only a few compounds in the sample, the individual components are eluted from the separation column at different times (retention time). The eluted components are then detected with the mass spectrometer. All elements can be determined based on their masses, whereby compounds can be identified by their different composition of the elements. An Agilent Time of Flight mass spectrometer with upstream liquid chromatography is used for the investigations. A schematic sketch of the time-of-flight mass spectrometer is shown in simplified form in Figure 10. The analyte is first separated by liquid chromatography and ionised by the ionisation source. The ions generated are accelerated and focused by the Octopole 1 (Figure 10). The uncharged species are gradually removed by the vacuum pumps. With the help of lens 1 and 2 (Figure 10), the ion beam is further focused and adapted to the downstream quadrupole. The quadrupole acts as a filter for the masses passing through, whereby either the entire ions are allowed through or individual masses can be selected. Optionally, MS/MS spectra can be recorded in the collision cell. To do this, the ions are stimulated to fragment by colliding with nitrogen gas. The fragmentation depends on the energy exposed to the ions, the gas used and the molecule itself. The ion beam is then accelerated into the flight chamber by the ion pulser. The mass is determined by measuring the flight time. The time of arrival of the ions is determined by the detector and the start time is specified by the ion pulse. After passing through an electrical voltage (U), the ions of charge q have the energy Ep = U · q in the form of kinetic energy. Due to the relationship with the equation $E = ½ mv^2$, the flight time is proportional to the mass-to-charge ratio of the ions. Since the accuracy of the mass determination correlates with the length of the flight path, the high-resolution mass with which the elemental composition can be determined can be established in the time-of-flight mass spectrometer.[40]

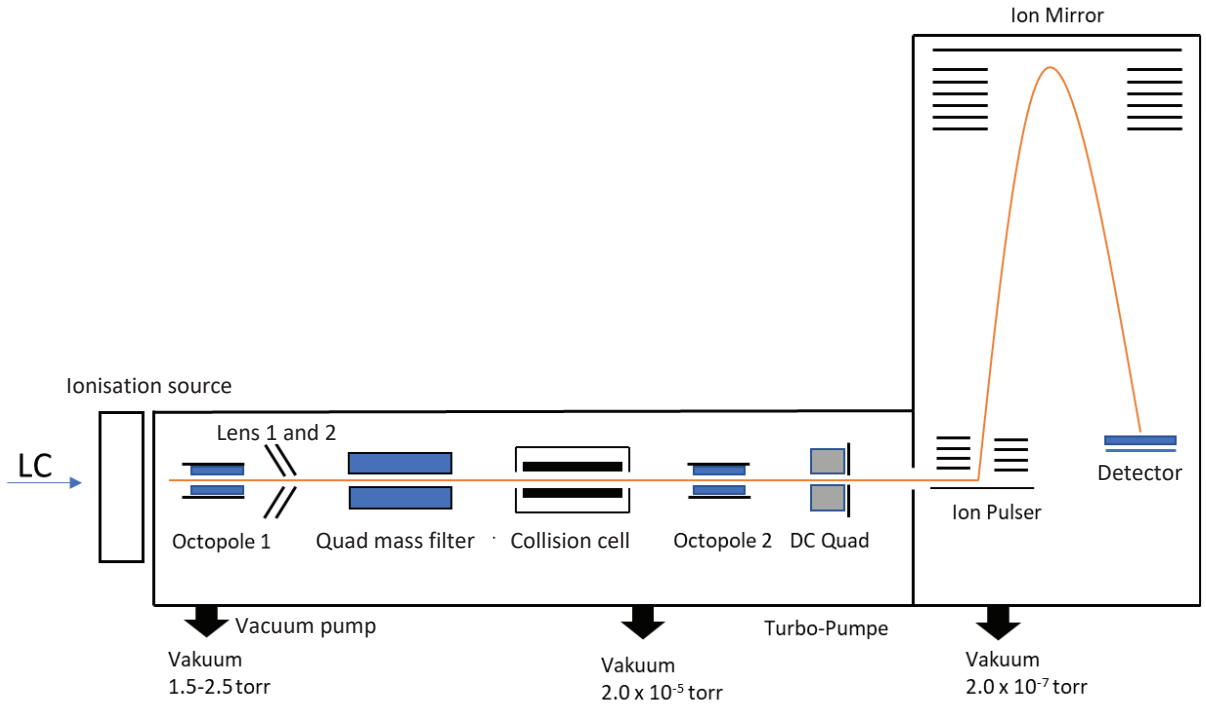

Figure 10: Sketch of the simplified schematic structure of a Q-TOF mass spectrometer.[40]

In principle, only ions can be detected in the mass spectrometer. That is why the process of ionisation is of particular importance. Since ionisation is highly dependent on the analyte, there are several ionisation sources, each of which is more or less suitable for different compounds.

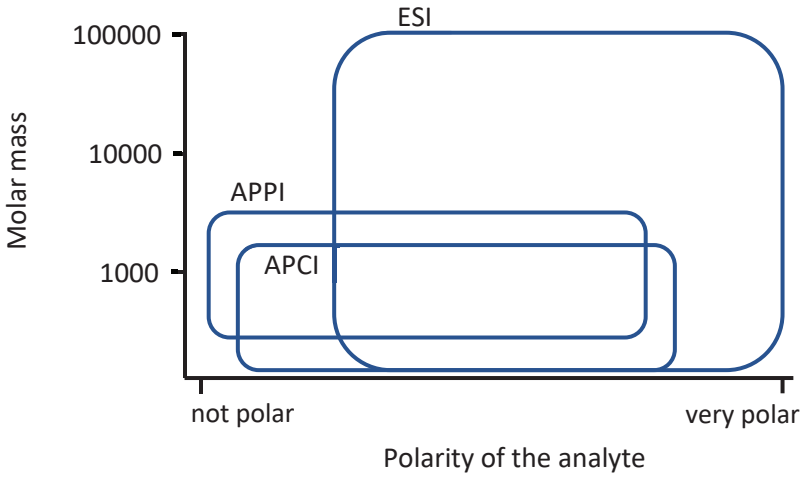

Figure 11: Application range of the different ionisation sources depending on the molar mass and polarity.[41]

The areas of application of the three ionisation sources APCI (Atmospheric-pressure chemical ionisation), APPI (atmospheric pressure photo ionisation) and ESI (Electrospray ionisation) are shown in Figure 11 depending on the molar mass and the polarity of the analyte. The APCI ionisation source covers the largest possible range of compounds for the fatty acid methyl esters (FAME) and their oxidation products to be examined. The non-oxidised FAMEs have a low polarity, which can just be ionised with the APCI. With the APCI, reactants and oxidation products can be recorded together in one measurement, which is why this ionisation source is used for all investigations in this report. APCI is a soft ionisation method that leads to a low residual energy in the molecule and thus only causes a low level of fragmentation. The advantage of soft ionisation is that the molecular ions of the analytes can be examined without fragmentation occurring. With this, the sum formulas of the analytes can be determined with high-resolution mass spectrometry. [41]

4.5 Spectroscopic methods of the developed sensor technology

The following section discusses the physical fundamentals of the spectroscopic method on which the developed fuel sensor is based. In general, to determine the fuel parameters, the interaction of the fuel samples with different electromagnetic fields or waves is analysed and conclusions about the composition of the fuel sample are drawn with the help of the measured values. The analysis methods used can be divided into two main categories:

1. Dielectric spectroscopy (low frequencies / long wavelengths) and
2. the optical spectroscopy method (high frequencies / small wavelengths).

In dielectric spectroscopy, the complex dielectric constant (relative permittivity)

$$\underline{\epsilon_r}(f) = \epsilon_r'(f) - j\epsilon_r''(f) \tag{10}$$

of a medium is recorded depending on the measuring frequency (f). The complex permittivity ($\underline{\epsilon_r}$) describes how a substance interacts with the electric field. The real part ϵ_r' describes the polarisation processes in the medium, which are often also simply described by the real polarisation number ε_r. The imaginary part ϵ_r'' describes the polarisation losses that occur. Figure 12 schematically shows the

course of the complex permittivity ($\underline{\epsilon_r}(f)$) in a broad frequency spectrum. Depending on the medium in which the electric field spreads, different physical processes occur at different frequencies, which is why different measurement methods are necessary to examine a sample in the entire spectrum shown. Depending on how strong and which physical processes occur at which frequency or wavelength, the medium interacts differently with the electric field or the electromagnetic waves.

For a better illustration, the frequency spectrum in Figure 12 is divided into 5 differently coloured areas. In areas 1 and 2, dielectric spectroscopy is commonly used – the frequency-dependent permittivity is measured according to Eq. 10. In areas 3 and 4, optical methods such as near infrared spectroscopy or fluorescence spectroscopy are used for analysis. Instead of the complex permittivity ($\underline{\epsilon_r}$) , the reflection factor (n) or the absorption (E) depending on the wavelength (λ) or wave number (k) are commonly used as physical quantities in optics. The assignment of the developed sensors to the various physical processes is indicated on the right-hand side of *Figure 12*. The sensors themselves are explicitly described in Sections 4.5.1 and 4.5.2.

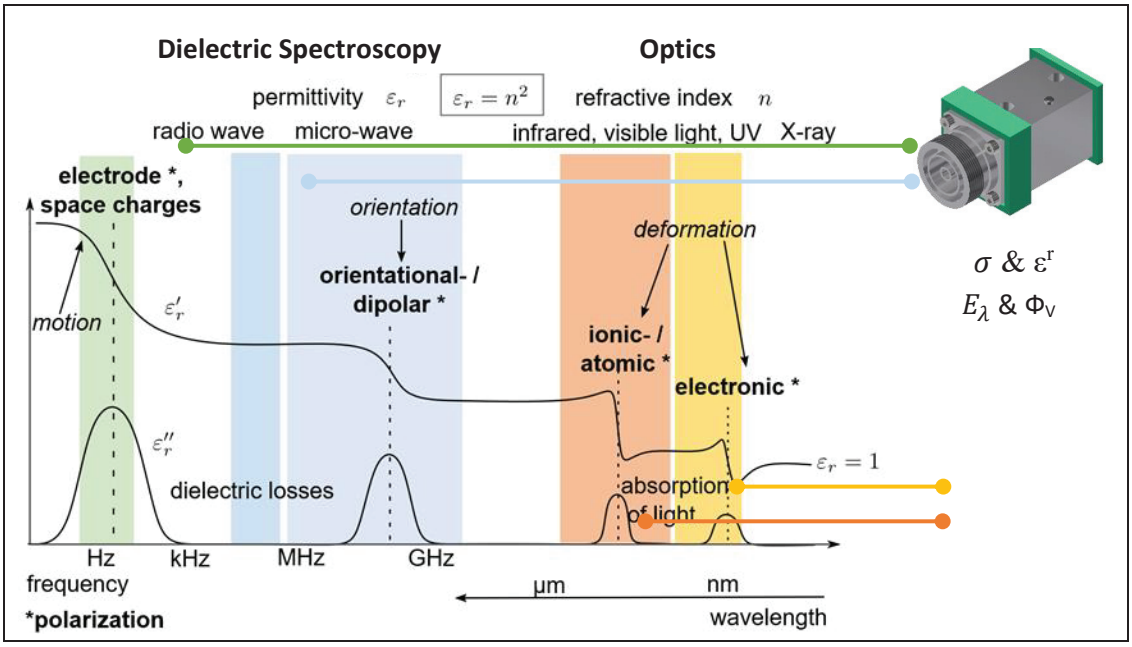

Figure 12: Left: Overview of dielectric and optical spectroscopy. Right: Sensor technology for recording the physical phenomena that occur. [42]

The following first describes the general course of the two curves (ϵ_r' and ϵ_r'') from Figure 12. A detailed explanation of the physical processes that occur and the underlying measuring principle of the sensor then follows in Sections 4.5.1 and 4.5.2.

When the medium interacts with electromagnetic radiation or the electric field, different processes play a role depending on the excitation frequency or wavelength. At low frequencies, the different polarisation mechanisms occur together and overlap, which leads to a high interaction with the electric field and thus high permittivity ϵ_r'. Each of these processes takes a certain amount of time to align the structures that contribute to polarisation in the electric field. If the excitation frequency or wavelength corresponds to this material- and process-specific time constant, a resonance point occurs at which the losses (ϵ_r'') that occur become maximum (Figure 12 dashed lines). If the excitation frequency is increased further, one process after the other stops and the permittivity ϵ_r' drops, the structures to be polarised can no longer follow the rapid field change. In area 5, the medium shows no interaction with electromagnetic radiation – it behaves like a vacuum and its relative permittivity ϵ_r is 1. The relative permittivity ϵ_r or the physical effects that occur are not only dependent on the frequency but also on the temperature and the field strength of the electric field. [42], [43], [44], [45]

Since the possible superimpositions of different resonance processes are known from the previous text passage, the four polarisation processes shown and their features are described in detail below. The processes shown in Figure 12 are:

1. Electrode polarisation and space charges
2. Orientation / dipole polarisation
3. Ionic / atomic polarisation
4. Electron polarisation

The electrode polarisation (1) is primarily caused by the migration of ions in the medium, which corresponds to a conductivity (σ) that can be recorded using the dielectric sensor (see Section 4.5.1). The orientation / dipole polarisation (2) describes the alignment of dipoles in the alternating electric field and can be detected with the dielectric sensor via the permittivity (ϵ_r). In area 3, various molecular vibrations can be excited using a broadband light source. If the substance resonates in this area, some of the radiation is absorbed. This effect can be measured with the help of a photo detector suitable for the wavelength of the resonance. The measurement of the absorption in the range of near-infrared radiation is called near-infrared spectroscopy and can be recorded with the help of the optical sensor (see Section 4.5.2). The electron polarisation in area 4 is caused by the distortion of the electron cloud that surrounds the atoms. When excited in this area of the spectrum, various substances can also absorb radiation/energy. When the energy is absorbed, individual electrons of an atom can be raised to higher energetic states. If these electrons fall back to low-energy states, a photon can be emitted. This process is called fluorescence and generates diffuse radiation, which can be measured using the fluorescence detector of the optical sensor (see Section 4.5.2). [42], [43]

4.5.1 Dielectric sensor

The structure of the dielectric sensor is presented in the following section. Figure 13 (left) shows the functional diagram of the dielectric sensor. The sensor is based on the measuring principle of the capacitive measuring cell. During operation, an alternating voltage (U (f)) is applied to the electrodes, which leads to an alternating electric field E between the electrodes. This electric field creates two effects in the fuel sample: On the one hand, free charge carriers (electrons or ions) through charge carrier transport lead to an active current that results from the ohmic conductivity σ of the medium. On the other hand, the polarisable material components generate a so-called dielectric displacement current (D), which is linked to the permittivity ε_r , since the polarisation charges of the aligned dipoles have to be replenished. In general, both processes can be described by a complex current density $\underline{J}$, or a complex current flow $\underline{I}$, which results from the integration of the current density over the area under consideration.

The right side of Figure 13 shows the mechanical structure of the dielectric sensor. The two essential components of the sensor are the inner conductor within the sensor, which serves as the inner electrode, and the outer housing, which is also the outer electrode. The sample volume between the inner conductor and the sensor housing acts as a dielectric. The system is accessible via two connections, the inlet and the outlet. Commercially available sealing rings are used between the individual parts to prevent leaks. So that the measurements are not falsified by parasitic effects outside the measurement volume, the sensor is provided with a guard ring on the connector side, which derives both capacitive and ohmic stray components, caused by field components in the edge areas, so that these are not measured.

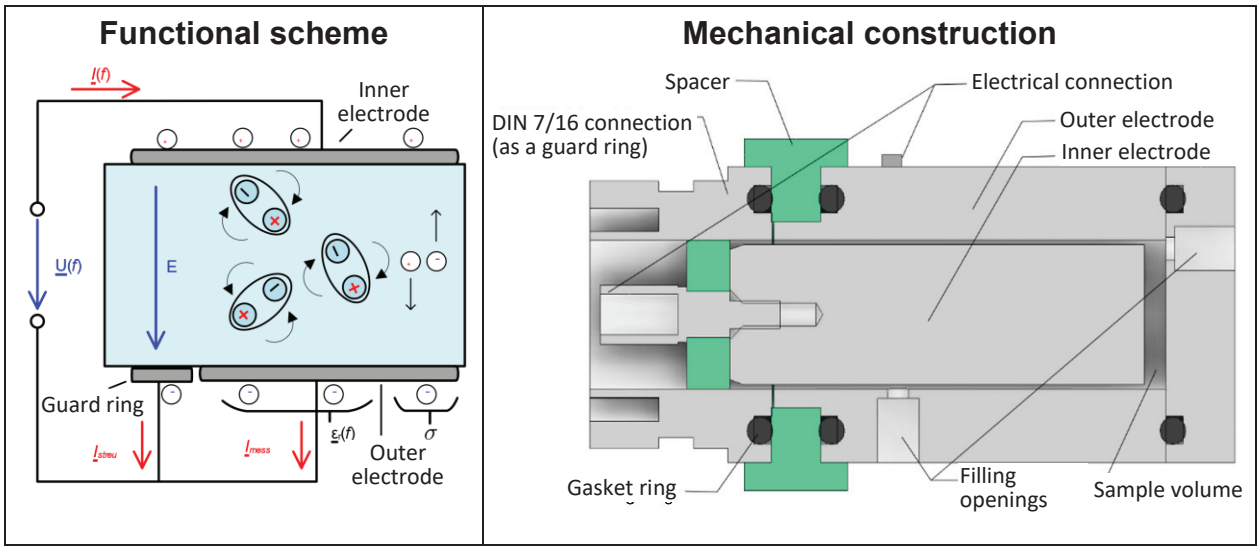

Figure 13: Functional diagram and sectional view of the dielectric sensor.

The passive dielectric sensor shown in Figure 13 (right) is suitable for frequencies from 1 Hz to about 1 MHz and can be used with conventional impedance measuring devices (reference devices). Test measurements with an impedance analyser show that the permittivity at 100 kHz and the conductivity (at very low frequencies) are particularly meaningful for fuel samples, which is why an application-optimised measurement setup is being developed so that the sensor can also be used inexpensively and in miniaturised form. In combination with the sensor, this measurement setup can record the permittivity ϵ_r' at 100 kHz and optionally the conductivity σ at 10 Hz (dielectric sensors). The permittivity measurement is designed for organic fluids in the range of $\epsilon_r' = 1 \dots 6$ and offers a resolution of $< \pm 0.005$. The conductivity can be measured in the range from approximately $10^{-9}\ S/m$ to $10^{-13}\ S/m$. In addition, the sensor system offers options such as monitoring the measured variables over time, and also temperature monitoring. With the help of an external temperature control, temperature-dependent series of measurements in the range of -15… + 40 °C can be carried out.

4.5.2 Optical sensor

Figure 14 shows the functional diagram of the optical measurement technology of the fuel sensor. The sensor housing consists of two screwable main components (yellow and orange) with different measuring connections, which enclose a quartz flow-through cuvette (see Figure 10) with a light path within the medium of 5 mm (alternatively, a conventional cuvette with a light path of 10 mm can be used). This cuvette serves as a sample container and optical window for fluorescence and near-infrared spectroscopy. Both the excitation light sources and the detectors are connected to the passive sensor via optical fibres.

In the upper part of the sensor, the fuel sample is optically stimulated using a laser diode which, according to the manufacturer, only emits light in a narrow spectral range (of $\lambda \cong 405\ \mathrm{nm}$). If the fuel fluoresces, the emitted diffuse radiation is guided from the sample to a fluorescence detector (FLU detector) via a second light guide connection, which is arranged at a 90 ° angle to the first laser diode. Inside the detector, the emitted radiation is spectrally split in a polychromator in order to then measure the radiation intensity of the individual spectral components in parallel. The built-in fluorescence sensor is based on the Hamamatsu C12880MA mini spectrometer chip which can detect wavelengths from λ =340 nm to 850 nm and offers a spectral resolution of 15 nm. The measured variable of the FLU detector is recorded with a 10-bit analogue-digital converter and controlled via USB

via a PC. On the programming side, the developed FLU sensor has the option of varying the amount of light entering the detector by setting the exposure time. Test measurements showed that exposure times of the detector of 1 ms, 10 ms, 100 ms and 1 s are well suited for measuring relevant fuel samples. Up to 4 measurements are therefore carried out during a measurement cycle and the associated measurement data are saved. If the measured light intensity of a measurement falls below a threshold value, the exposure time of the FLU detector is increased step by step. On the one hand, this procedure prevents the detector from being overdriven in the case of strongly fluorescent samples and at the same time ensures the highest possible measurement accuracy for weakly fluorescent samples. It should be noted here that measurement data should only be compared with one another if the exposure time of the detector corresponds.

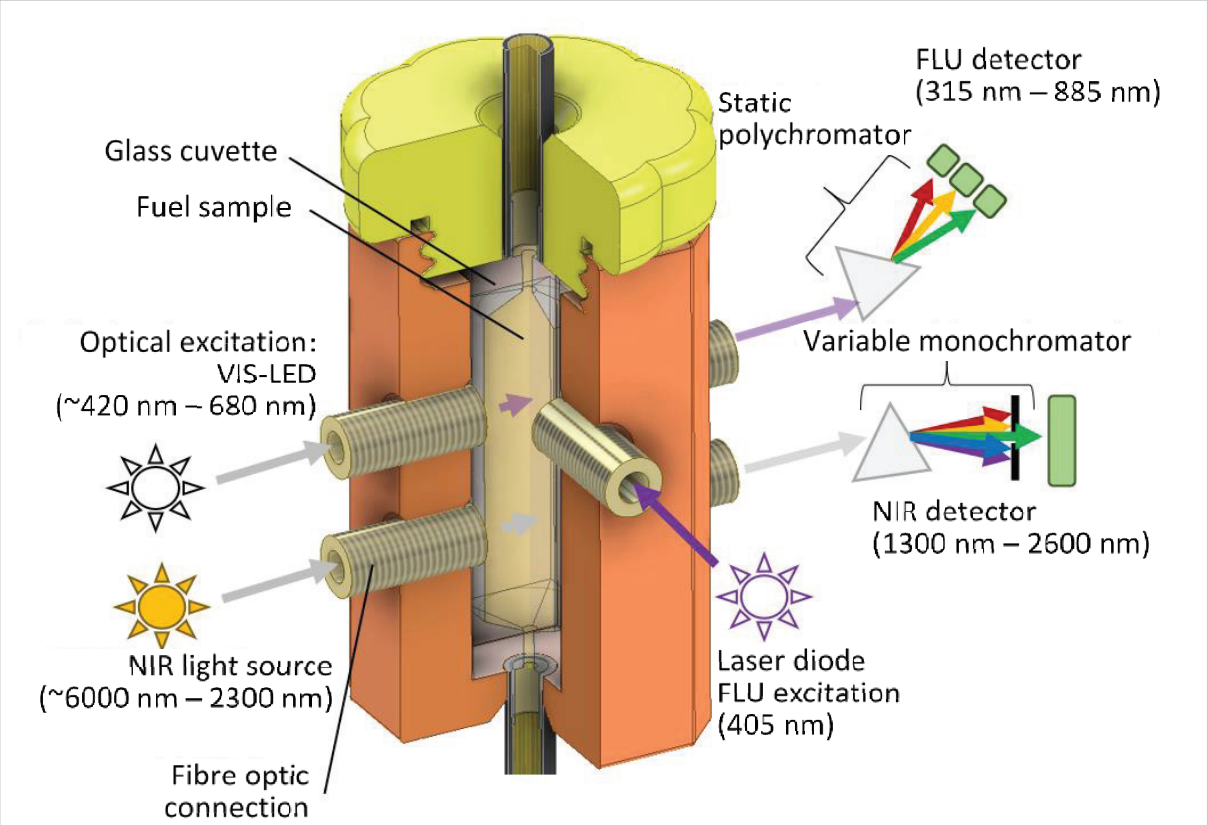

Figure 14: Functional diagram of the optical sensor.

Optionally, the fluorescence detector can also be used in combination with an LED excitation built into the measuring unit to record an absorption spectrum at wavelengths from around 440 nm to around 620 nm. Such a transmission measurement can provide additional information content about samples which have an absorbance in the range of the visible light spectrum, but no fluorescence (e.g. turbidity of fuel). Corresponding to the fluorescence measurements, up to four exposure times (of 1 ms, 10 ms, 50 ms, 100 ms) per measurement cycle are also used in these absorption measurements.

In the lower part of the optical sensor (Figure 14) there are two light guide connections for near infrared spectroscopy (NIR). Here the fuel sample is irradiated with a broadband halogen lamp as a light source. Within the sample, the energy of the incident radiation can excite molecules into different oscillation states, which can lead to spectral absorptions. The radiation emerging on the opposite side of the sensor thus contains indirect information about absorbing molecules within the sample. The NIR detector (neospectra mini spectrometer) connected there splits the incident radiation sequentially with the help of a monochromator and measures the intensity of the individual spectral components

of the light with a wavelength of 1300 nm to 2600 nm one after the other with a resolution of 8 nm. By comparing the measured intensity spectrum with a measurement of the empty cuvette, the absorption caused by the fuel can be calculated.

5 Evaluation of the mass spectrometric investigations

5.2 Chromatographic separation

For the mass spectrometric analysis of the ageing products, the aged fuel (Rancimat) is first separated by chromatography. The chromatogram obtained from RME aged 18 hours is shown in Figure 15. Due to the high-resolution mass-to-charge ratio, the sum formula of the eluted molecule can be determined for the respective peaks. In each case, the connections with the highest intensity are given. A complete separation is not possible with the large number of ageing products. However, several molecules can easily be measured side by side. The influences of the molecular structure depending on the solvent mixture used and the chromatography column can be determined from the retention times of the assigned main products in Figure 15. The polarity of the solvent decreases over the duration of the separation. A higher proportion of oxygen and more double bonds lead to a reduction in the retention time, while the retention time is increased as the chain length of the compounds increases. With an increasing proportion of oxygen and increasing chain length, both effects have an effect on the retention time, which results in the chromatogram in Figure 15, in which long-chain molecules with a low proportion of oxygen have the greatest retention times. Short-chain products with a high proportion of oxygen and many double bonds, on the other hand, have short retention times. The factors influencing the retention time of the molecules are summarised in Figure 16.

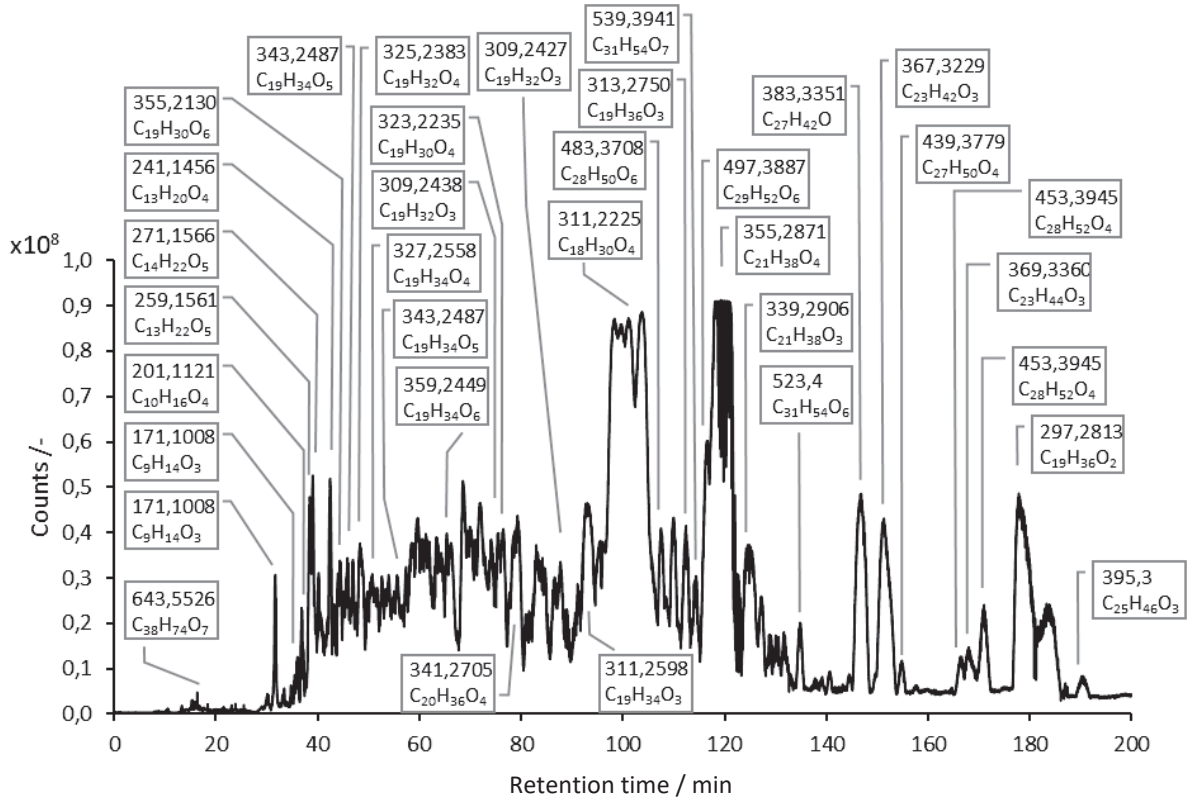

Figure 15: Chromatogram of RME (Rancimat) aged 18 hours with an assigned molecular formula for the respective measured mass-to-charge ratios. The specified mass-to-charge ratios represent those with the highest intensity for the respective retention time.

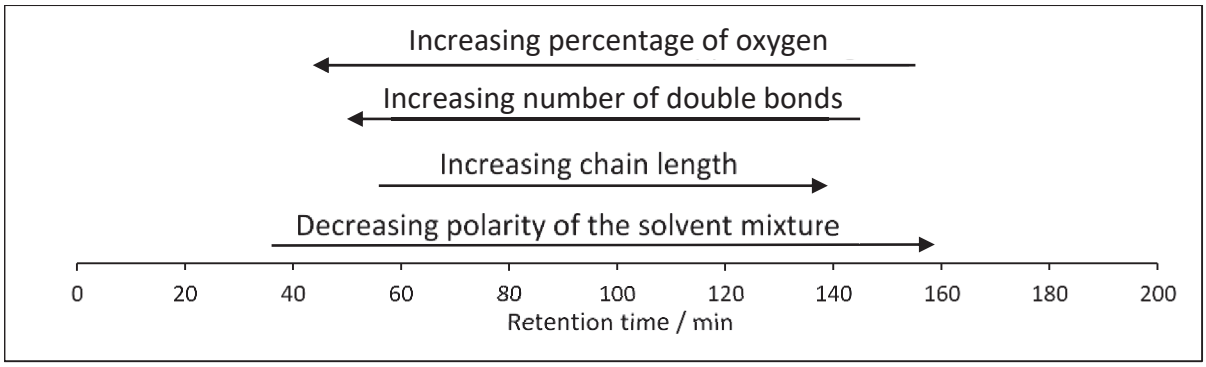

Figure 16: Factors influencing the chromatographic separation.

Chromatographic separation is essential for two reasons. By separating the compounds, cross-influences during the ionisation of different compounds are reduced and, on the other hand, constitutional isomers can be distinguished from one another. Constitutional isomers are compounds with the same empirical formula but different structural structures. For structure elucidation in the MS/MS experiment, it must be ensured that the respective constitutional isomers are eluted separately from one another, because otherwise the different fragmentation of two compounds would overlap. The constitutional isomers can be separated from one another by means of an optimised chromatographic separation of aged RME, as shown in Figure 15. The chromatographic separation is checked to determine whether the constitutional isomers are separated from one another by means of so-called base peak chromatograms. With the help of the basic peak chromatograms, the intensity of a single mass is extracted from the chromatogram in Figure 15. If there are no overlaid peaks in the basic peak chromatogram, structure elucidation can be carried out with the aid of MS/MS experiments. The compounds with the mass-to-charge ratio m/z = 311 are an example in which the separation of the constitutional isomers can already be seen from the chromatogram. In the range of 90 to 110 min retention time, two compounds elute with two different exact masses (m/z = 311.2598 with the empirical formula $C_{19}H_{34}O_3$ and m/z = 311.2225 with the empirical formula $C_{18}H_{30}O_4$). In addition, through the high-resolution mass and the comparison of the fragmentation patterns, the statement can also be made that at m/z = 311.2225 there are four conformational isomeric compounds, since the same fragmentation pattern is present in each case. With the chromatographic separation in Figure 15, the basis is created so that the structures can be elucidated in the second step by means of MS/MS experiments. The combination of MS/MS experiments and the information from the chromatographic separation form the basis of the investigations discussed in the results section.

5.3 Structure elucidation of the ageing products with MS/MS fragmentation pattern

Tandem mass spectrometry is used to elucidate the structure of the ageing products of RME. The gentle ionisation by means of chemical ionisation at atomic pressure (APCI) generates ions with an even number of electrons, which typically have a low internal energy. Due to the low internal energy, little or no fragmentation is caused during ionisation.[40] The mass-to-charge ratios thus found in the mass spectrum represent the molecular ions of the respective compounds under the selected conditions.[46] In the positive ionisation mode, the individual molecular ions $[M+H]^+$ in the collision cell of the Q-TOF can be targeted to collide with inert gas molecules, causing fragmentation.[40] The evaluation method used is described in detail below using the example of the mass-to-charge ratio m/z = 327.2535 and is used in this form for all compounds found. Due to the high-resolution mass spectrometry, a sum formula can be assigned to each mass-to-charge ratio. For m/z = 327.2535 the empirical formula is $C_{19}H_{35}O_4$. With the formula

$$DBA = \frac{2c - h + 2}{2} \tag{11}$$

the double bond equivalents (DBÄ) for the sum formulas $C_cH_hO_o$ can be calculated with DBA = 3. For further structural information, the molecular ion in the collision cell is excited to fragment with an energy of 20 eV. The MS/MS mass spectrum obtained is shown in Figure 17. The blue point in the mass spectrum (Figure 17) marks the molecular ion. All other mass-to-charge ratios represent fragments of the molecular ion. Due to the high-resolution mass spectrometry, a sum formula can also be assigned to the individual mass-to-charge ratios in the MS/MS spectrum.[40] A key role in the structure elucidation by means of fragmentation patterns in the MS/MS mass spectrum is a certain knowledge of the expected structure of the precursor molecules (molecular ions that are fragmented in the collision cell), which considerably simplifies the evaluation. As can be seen from the MS/MS spectrum in Figure 17, a large number of fragment ions are produced during fragmentation. Basically, the fragmentation is based on the classic electron impact ionisation (EI) reactions, charge migration reactions and charge retention reactions. These fragmentation reactions can take place with a loss of neutral particles, which enable a statement to be made about functional groups in the molecule.[46]

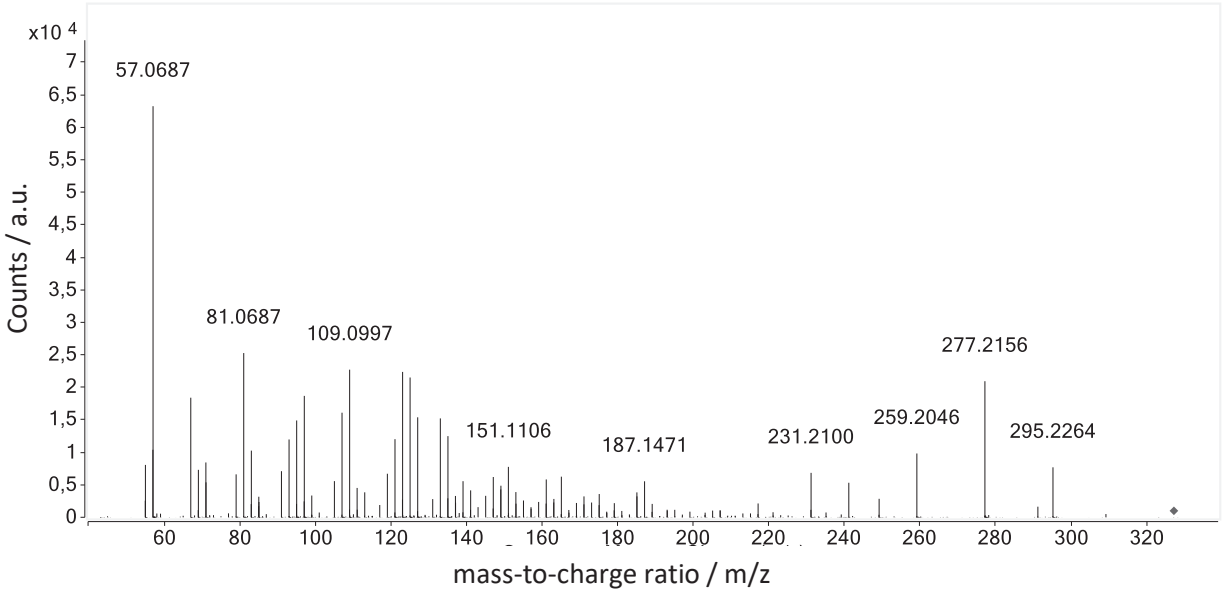

Figure 17: MS/MS mass spectrum at 20 eV of m/z = 327.2535. The blue point in the mass spectrum marks the precursor molecule.

In Figure 18 the fragment ions are arranged in a decay scheme. The corresponding sum formula is assigned to the individual mass-to-charge ratios. In the case of selected fragment ions, the proposed structure is shown for better traceability. The fragmentation begins with the molecular ion [M+H]+ and proceeds along corresponding routes to increasingly smaller fragment ions. In the example shown here, there is a loss of neutral particles of methanol (CH3-OH) with the formation of the fragment ion m/z = 295.2264 ($C_{18}H_{31}O_3$), which indicates the methyl ester function in the precursor molecule. In the oxidised fatty acid methyl esters examined here, the initial fragmentation is primarily based on the bond cleavage in the α position (on the same carbon to which the oxygen atom is bonded) to an oxygen atom. By eliminating H_20 as neutral particles and the observed fragmentation in the area of the two carbons of both epoxides, these can be identified as functional groups (m/z = 71.0842; m/z = 169.1217; m/z = 155.1053; m/z = 153.1257; m/z = 99.0788). The position of the epoxides in the carbon chain can be localised through the molecular formula of the fragments. Starting from these fragment ions, the fragment ions are further fragmented, whereas fragments without oxygen atoms are formed through further loss of neutral particles (CH_3-OH, H_2O, CO). Due to the loss of neutral particles of H_2O during

the fragmentation, polyunsaturated compounds are formed in the course of the fragmentation, which can be assigned to the respective fragmentation routes. Different fragmentation routes can lead to the formation of the same fragment ion.

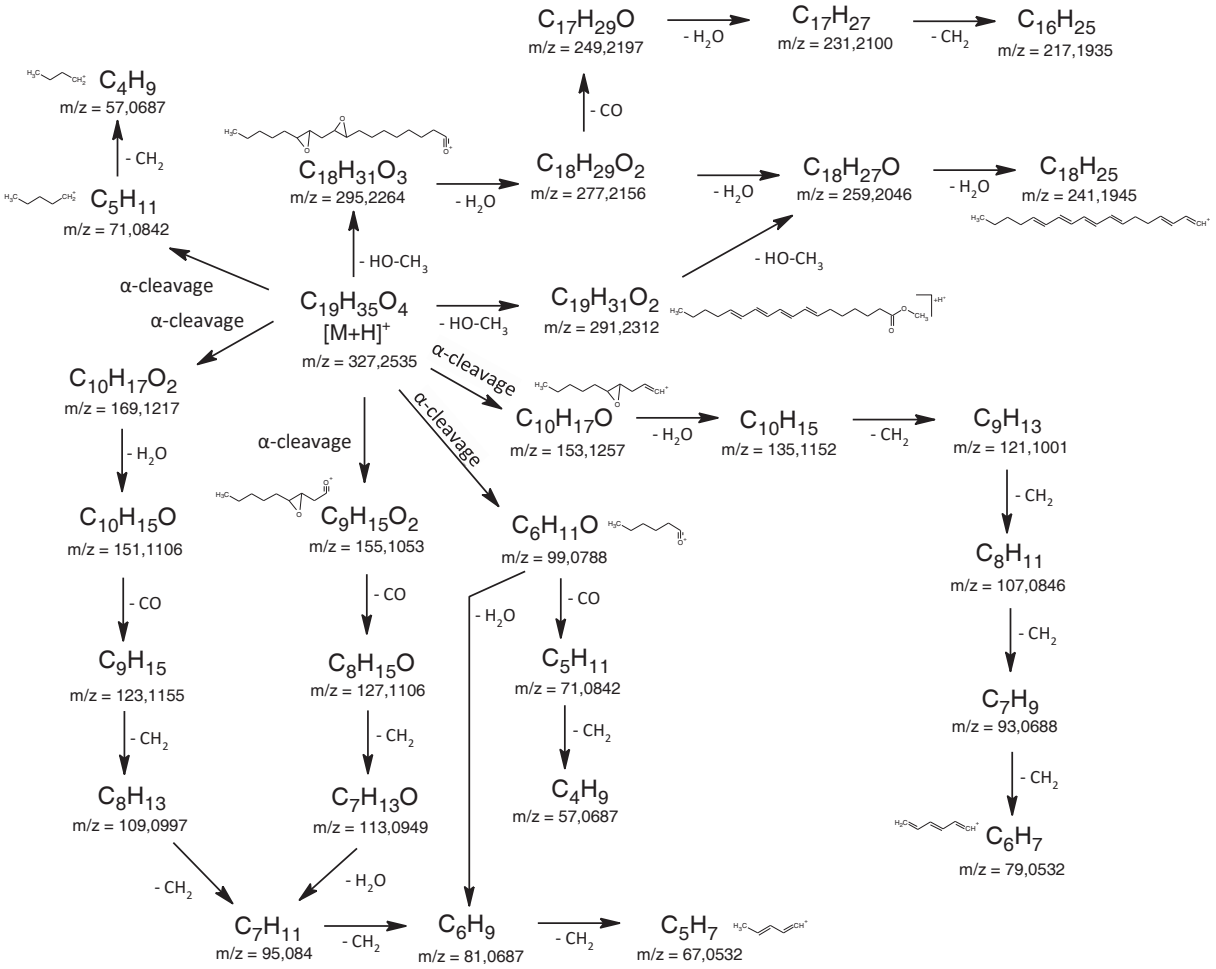

Figure 18: Decay scheme with the fragments from the MS/MS spectrum of m/z = 327.2535.

However, the individual fragmentation reactions may differ considerably in terms of their probability, which results in the respective intensities of the fragment ions. With the sum of the information from Figure 18, a structural proposal can be made for the connection with the mass-to-charge ratio m/z = 327.2535, which is shown in Figure 19. To illustrate how the individual fragment ions are used for the structure elucidation, the fragments in the molecular structure are marked in Figure 19. The numbers indicate the mass-to-charge ratio and the vertical lines mark the bond cleavage that occurs, which leads to the fragments.

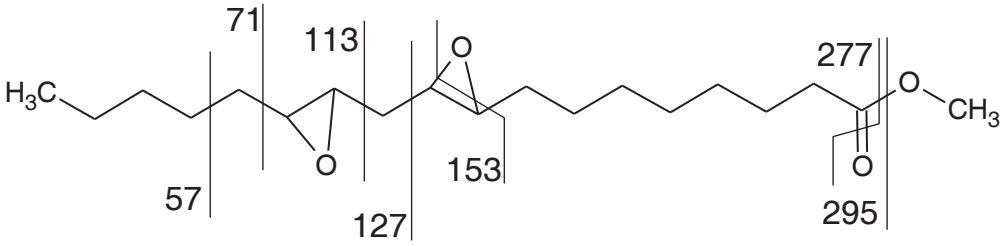

Figure 19: Suggested structure for m/z = 327.2535 based on the fragment ions of the MS/MS spectrum.

In this way, the compound can be determined as a twofold oxidised product of methyl linoleic acid. The fragmentation pattern of the MS/MS spectrum confirms the presence of the oxidation as two epoxide groups. All other compounds in the mass spectrum of RME are identified with the same method and are discussed in detail below as the basis of the ageing mechanism of FAME.

6 Ageing tests by RME

6.1 Overview of the ageing test

The investigation of the ageing products of biodiesel is a very complex system due to the different FAMEs with single, double, triple unsaturated and saturated fatty acids and the resulting large number of different oxidation products. For a better overview, the different categories of the products that can be identified by mass spectrometric examinations are presented at the beginning (Figure 20).

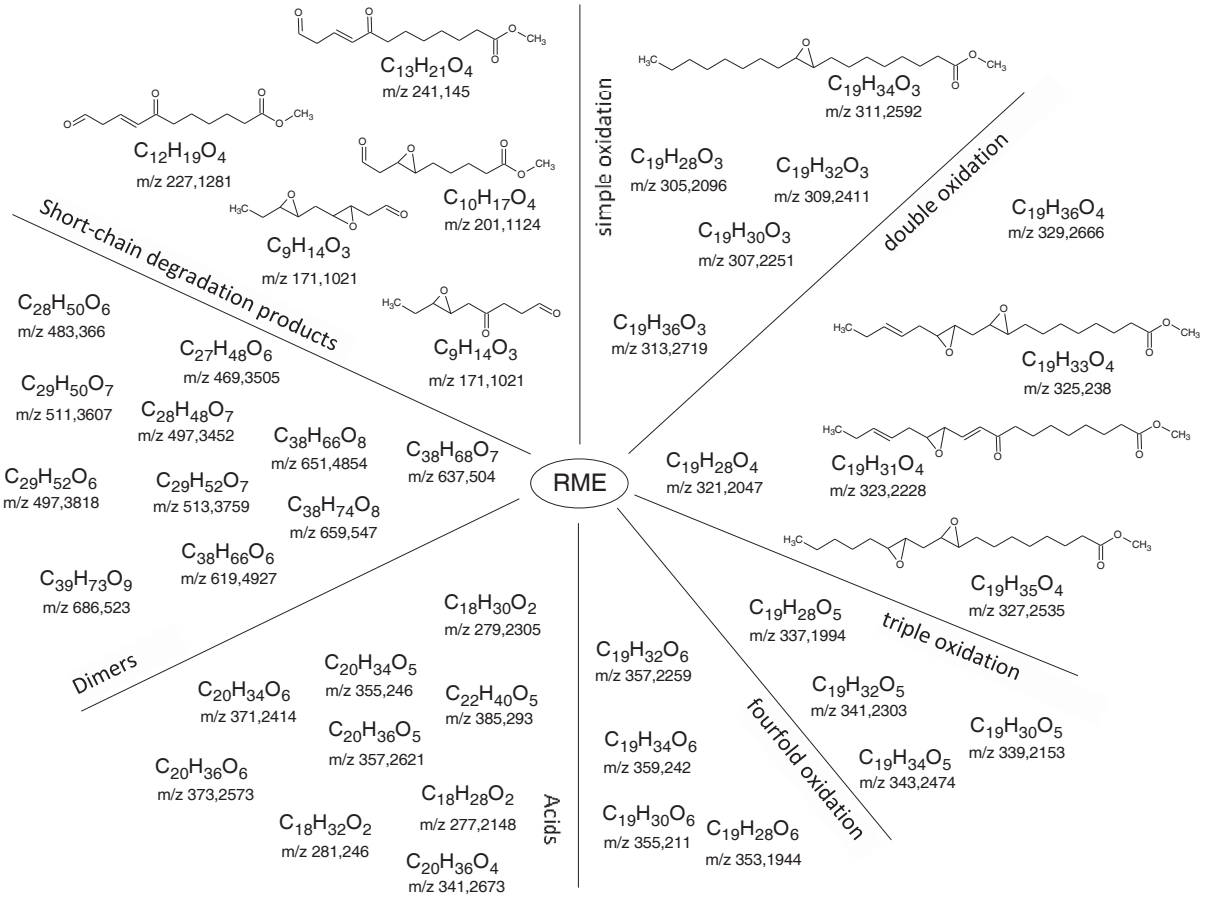

Figure 20: Overview of the identified categories of ageing products from RME.

As shown in Figure 20, the ageing products are divided into four different degrees of oxidation. One to fourfold oxidation products can be identified. The different degrees of oxidation result on the one hand from the number of double bonds in the molecule and on the other hand from the progress of the oxidation. Molecules with several double bonds can more easily undergo multiple oxidation, which results from the mesomeric-stabilised radical formation through the participation of the double bonds.[29] During the measurements, a limit of the oxidation can be determined in the case of a fourfold oxidation. This limit relates to the unchanged chain length of the fatty acids. Due to the reaction of the

molecules with one another, compounds can also be found which have a higher number of oxygen atoms. Since FAME (RME) in the unaged state already have two oxygen atoms in the molecule due to the ester group, a simple oxidation means the presence of three oxygen atoms. Consequently, a fourfold oxidation has six oxygen atoms. Another category of ageing products are acids that are formed by ester hydrolysis. Since all naturally occurring fatty acids have an even number of carbons and a carbon is added through the esterification of methanol to form the methyl ester, all of the starting materials from RME have an uneven number of carbons. Methanol is split off by hydrolysis of the ester group, which reduces the number of carbon atoms by one. In this way, acids formed during ageing can easily be identified by the even number of carbons. From the categories of degrees of oxidation and acids, the CC bond cleavage gives rise to the category of short-chain degradation products. These short-chain molecules are the fragments of CC cleavage that remain in the fuel. The smaller fragments are discharged in the Rancimat during ageing and lead to an increase in conductivity in the measuring cell (see Section 4.1.1). In addition, these short-chain molecules remaining in the fuel represent the starting products of the next category of dimers. The dimer category is based on two dimerization reactions. The majority of the dimers found are composed of the reaction of short-chain degradation products and oxidised fatty acid methyl esters. A smaller part of the dimers found results from a link between two oxidised FAME molecules (see Section 6.2.4). Details on the individual categories and the underlying mechanisms are discussed in detail below.

6.2 Identified ageing products and statements about the underlying mechanisms

The identification of a large number of ageing products under the same conditions enables FAME ageing to be described in its entirety. The individual categories into which the ageing products can be divided are already presented under 5.1. The individual reaction steps of ageing are shown and discussed in accordance with these categories. In order to be able to describe an overall picture of ageing, the results of the ageing product identification are supplemented below with suggestions on reaction mechanisms that have already been discussed in the literature[29][30][31]. Based on the data available here, those that most plausibly explain the ageing products found can be identified from the numerous hypotheses on fuel ageing. In the area of the oligomerisation of FAME, a mechanism for the formation of long-chain ageing products can be presented for the first time through the structure determination of the products.

6.2.1 Simple oxidation products

The first category of ageing products are simply oxidised products. Only those products are to be considered here that cannot be classified into the categories of acids, short-chain degradation products and dimers through further reactions. To identify the simple oxidation products of the starting materials C18:1 ME, C18:2 ME and C18:3 ME, the three associated masses to charge ratios m/z = 309.243; m/z = 311.2592 and m/z = 313.2742 are examined in the mass spectrum. Due to the compounds differing by one double bond, the m/z each have a difference of m/z equal to two (two hydrogens). Since in simple oxidation the mass increases by 16 through the incorporation of an oxygen atom, the corresponding reagent (C18:1 ME, C18:2 ME and C18:3 ME) can be added to the three masses with charge ratios (m/z = 309.243; m/z = 311.2592 and m/z = 313.2742). However, each of these mass-to-charge ratios can be assigned to several structures (see constitutional isomers, Section 5.2).

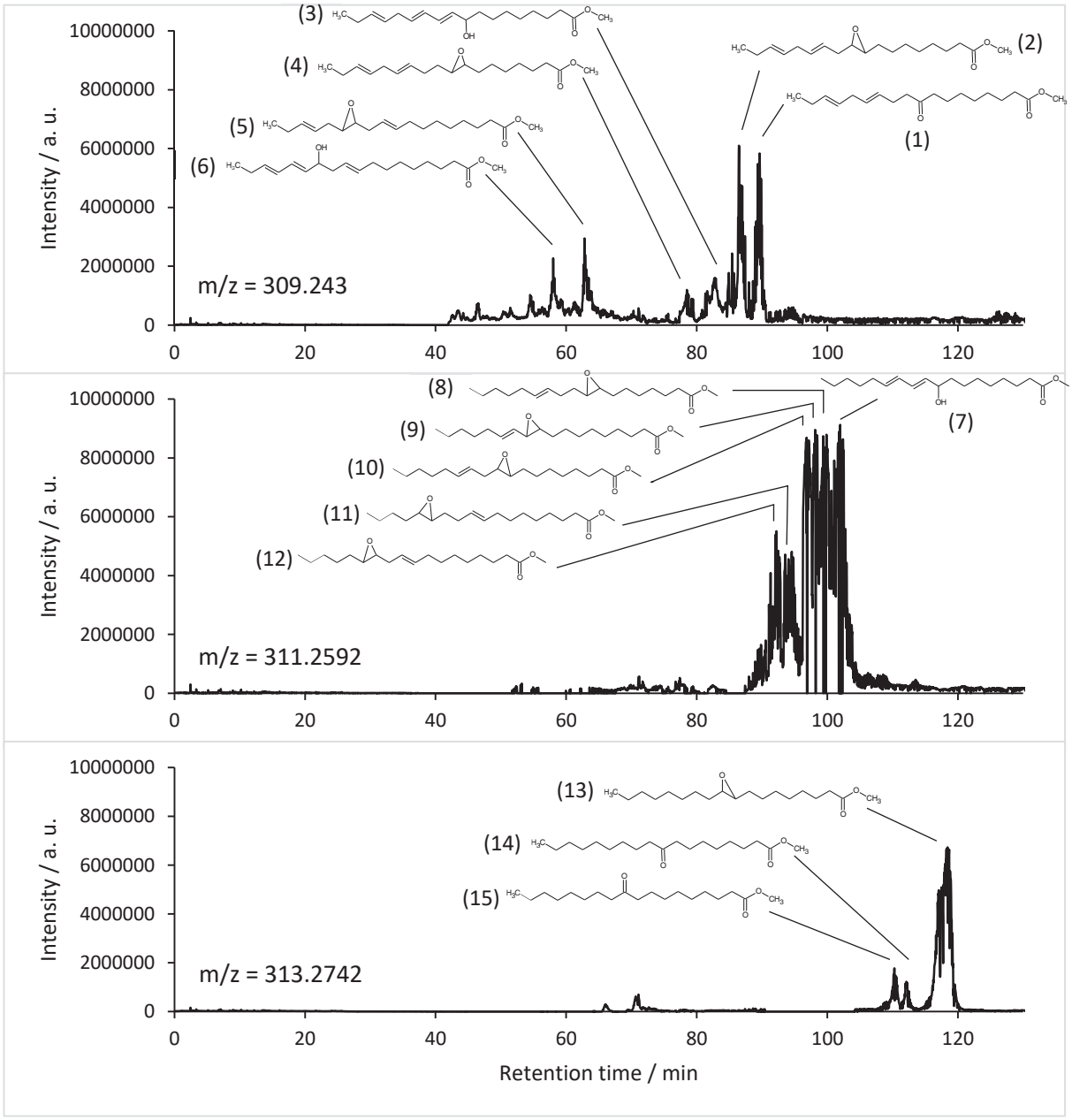

Figure 21: Base peak chromatogram from the MS spectrum of RME aged 18 hours with mass-to-charge ratios m/z = 309.243 (top), m/z = 311.2592 (middle) and m/z = 313.2742 (bottom).

Chromatographic separation enables the different compounds with the same empirical formula to be identified using MS/MS mass spectra. The base peak chromatograms of the three masses to charge ratios m/z = 309.243, m/z = 311.2592 and m/z = 313.2742 are shown in Figure 21. The base peak chromatogram enables a specific mass-to-charge ratio to be extracted from the measured mass spectrum. In this way, the isomeric compounds can be shown with good chromatographic separation. The molecular formula $C_{19}H_{33}O_3$, which corresponds to the $[M+H]^+$ molecular peak, can be assigned to the mass-to-charge ratio m/z = 309.243 (Figure 21 top). The chromatographic separation for m/z = 309.243 makes clear that there are a number of different compounds. Six of these compounds are identified by means of MS/MS evaluation (compounds 1 to 6). The slightly different geometry of the molecules depending on the position of the epoxy group, alcohol group or ketone results in a different equilibrium between the stationary and liquid phase. The equilibrium is influenced on the one hand by the angled geometry of the double bonds, epoxy and ketone groups and on the other

hand by the increasing polarity caused by the oxidation. Epoxides, alcohols and ketones have different permanent dipole moments, which means that they have different retention times. The strongly angled geometry of compounds 1 to 6 results in a globular structure that results in fewer interactions with the non-angled C18 alkane chains of the stationary phase (see Section 3.1). The retention times of the compounds 1-6 are below 90 minutes. Compared to the compounds 1-6, the compounds 7-12 have a less strongly angled geometry. The compounds 7-12 with a mass-to-charge ratio of m/z = 311.2592 are based on C18:2 ME as reagent. The compounds with m/z = 311.2592 consequently have one less double bond, which causes a retention time shift. Compounds 7-12 have retention times of 90 to 110 minutes. Compounds 13-15 (Figure 21 below) are based on the mass-to-charge ratio of m/z = 313.2742 and are based on C18:1 ME as the reagent. Compared to compounds 1-12, compounds 13-15 are significantly less globular. The angled structure at the carbons 9 and 10 in the middle of the molecule results in a stretched area that has a greater interaction with the stationary phase. The retention times of compounds 13-15 are 110-120 minutes. Figure 21 generally shows that the number of compounds is reduced from m/z = 309.243 via m/z = 311.2592 to m/z = 313.2742. In addition, the window of retention times is reduced (50 min at m/z = 309.243; 20 min at m/z = 311.2592 and 10 min at m/z = 313.2742). The number of double bonds in the reagent is the cause of the increase in possible ageing products. The ageing products of simple oxidation differ, on the one hand, in the type of functional group. Alcohols, ketones and epoxides can be determined for the single oxidised compounds 1-15. On the other hand, the positions at which the oxidation occurs differ. A special feature is the position relative to the position of the double bond in the starting materials C18:1 ME, C18:2 ME and C18:3 ME. The position of the oxidation becomes clear using the example of the epoxides found. In compounds 2, 5, 10, 12, 13 the epoxides are in the place of the original double bonds. In compounds 4, 8, 9, 11 the epoxides are shifted by one carbon relative to the position of the original double bond. Based on this identification of the type and location of the oxidation, the underlying mechanism can be checked for plausibility. The compounds 1 to 15 form the basis for the discussion of the reaction mechanisms that are described in the literature. The mechanism of the autoxidation of fatty acids is discussed in the literature in a large number of publications. The influence of double bonds, the formation of hydroperoxides and the formation of epoxides are generally accepted.[29] However, the underlying reaction mechanisms have not been finally clarified. The generally accepted state of research is described in Section 2.4 and is assumed here as the basis for further discussion. In the following, three mechanisms from the literature for the plausible formation of the compounds 1 to 15 are discussed.

In Figure 21 below, only compound 13 can be identified as epoxide for the single oxidation products for C18:1 ME. In the case of compound 13, the epoxy sits at the point where the double bond was originally in the reagent. A selective formation of this epoxide cannot be explained by a radical mechanism (Figure 22), in which hydrogen abstraction takes place in the α-position to the double bond (Figure 22). The dissociation energy of the C-H bond, which is a measure of the stability of the radical formed, and the radical stabilisation energy, which is defined by the energy gain through delocalisation of the radical. [22] Taking into account the radical stability and the delocalisation of the allyl radical that occurs at C18:1 ME, a radical mechanism would result in a specific theoretical product ratio. Due to the two α-positions to the double bond, a total of four resonance structures can be formulated. From these four resonance structures of the radicals, three possible epoxides follow, which are conceivable from C18:1 ME (Figure 22). Since two resonance structures result in the formation of the epoxide at the original location, the product ratio of the three epoxides is 1:2:1 (see Figure 22).

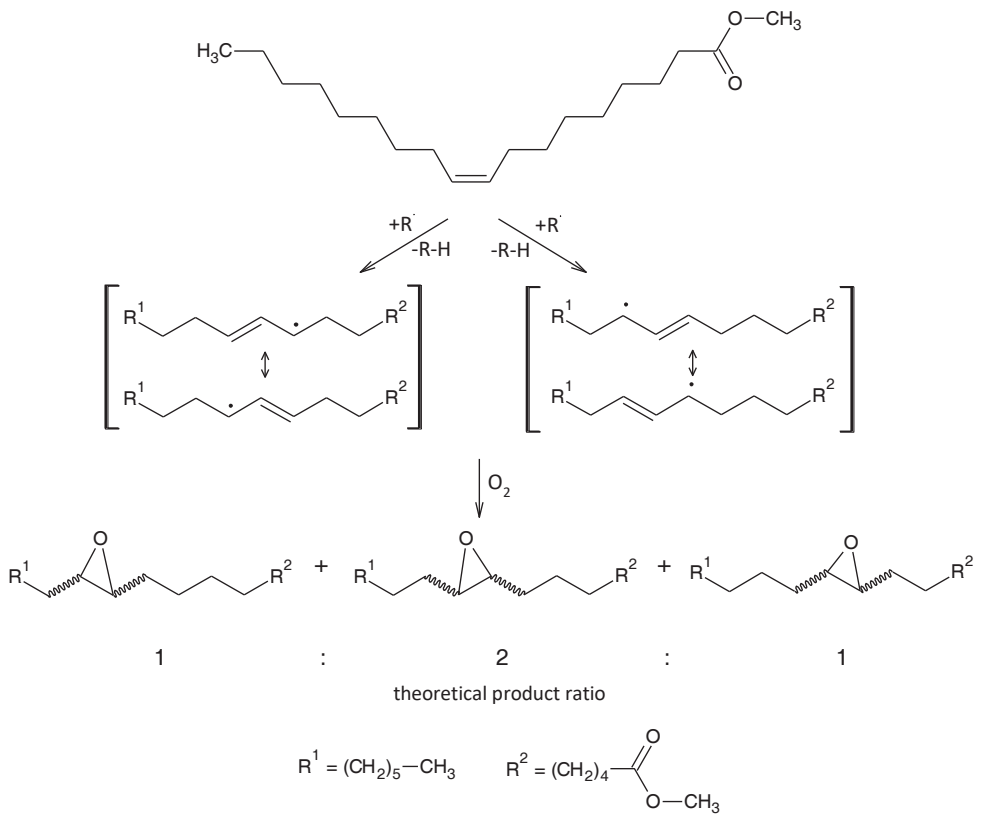

Figure 22: Possible mechanism of epoxide formation at C18:1 ME.

However, the actual product ratio found is 0:1:0. Only the epoxy can be found at the original double bond position (see Figure 21 below). Accordingly, epoxide formation cannot be explained solely through a radical mechanism. Another reaction mechanism must be present to explain the product ratio found. In connection with the oxidation products of 13-cis-retinoic acid, a mechanism has been postulated in the literature which would explain the epoxide formation at the original position of the double bond.

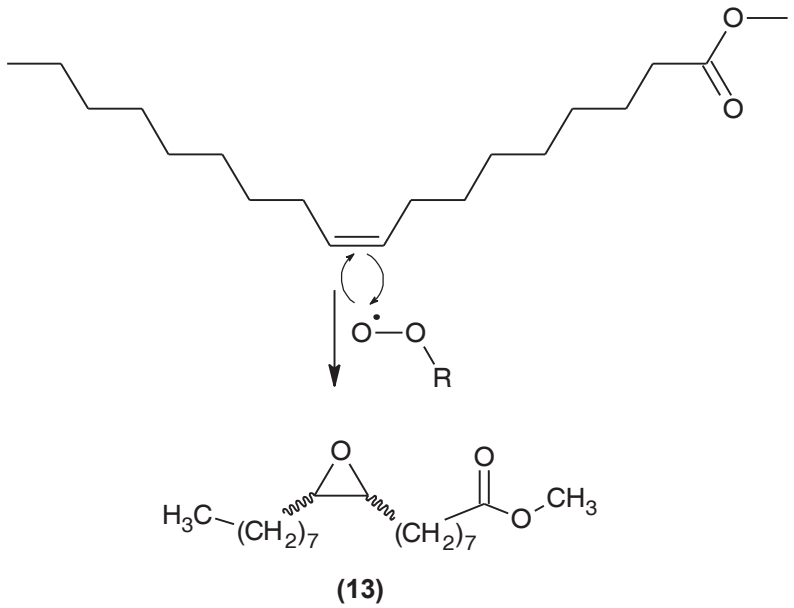

(13)

Figure 23: Mechanism in which the double bond is directly involved in epoxide formation. The mechanism is based on studies in the literature [30] and has been transferred to FAME here.

The mechanism carried over to C18:1 ME is shown in Figure 23. Peroxide radicals are formed by hydrogen abstraction and subsequent reaction of the radical with molecular oxygen. These peroxide radicals react with the double bond to split off alkoxy radicals. This bimolecular reaction mechanism with the direct participation of the double bond can explain the selective epoxide formation at the double bond position. However, a mechanism with the direct involvement of the double bonds alone cannot explain the identified compounds.

For the oxidation products of C18:2 ME and C18:3 ME, in contrast to C18:1 ME, epoxides can also be identified whose position is shifted by one carbon to the position of the double bond. This means that the general reaction mechanism from Section 2.4 plausibly explains the identified products. Figure 24 shows the reaction pathways that lead to the identified products using the reaction mechanism from Section 2.4. A plausible explanation is provided by considering the radical stability. While resonance-stabilised radicals can be formed with C18:1 ME with allyl radicals, their stability is considerably below that which is possible with C18:2 ME and C18:3 ME. By splitting off hydrogen at the bisallyic position at C18:2 ME and C18:3 ME, delocalised radicals with high stability are formed over five carbons (Figure 24 square brackets). By delocalising the radical over five carbons, three resonance structures can be formulated (Figure 24 below). By reaction of the middle resonance structure in Figure 24 with molecular oxygen, epoxides can be formed via the radical mechanism starting from the bisallylic position offset by one carbon to form the double bond (compound 9). The other two resonance structures with terminally located radicals lead to an alkoxy radical and a hydroxy radical via the reaction with molecular oxygen and the formation of the hydroperoxide and its decomposition. The alkoxy radical reacts in an intramolecular reaction with the neighbouring π-electron of the double bond. The radical resulting from the further π-electron reacts by hydrogen abstraction and compounds 12 and 10 are formed.[29] The formation of compounds 8 and 11 (Figure 24 top) can only be explained meaningfully by the hydrogen abstraction of the allylic position. However, the appearance of compounds 8 and 11 in the oxidation of C18:2 ME raises the question of why this reaction with formation of an ally radical cannot be observed at C18:1 ME. The allyl radicals of C18:1 ME, C18:2 ME and C18:3 ME do not differ in their radical stabilisation energy, which means that the probability of formation should not differ significantly. For a possible explanation, the geometry of the molecules must be taken into account in the bimolecular reaction at C18:1 ME. As can already be seen in the chromatographic separation, the retention times differ depending on the number of double bonds and the associated angled structure. As a result, C18:2 ME and C18:3 ME have a more globular structure than C18:1 ME. Since the mechanism with a direct reaction of the double bond is a bimolecular reaction and the participation of a radical means a diffusion-controlled reaction, a globular structure can lead to steric shielding of the double bond. At C18:1 ME, the double bond is significantly more exposed (Figure 23). The mechanism from Figure 24 based on bisallylic and allylic radical formation also explains the occurrence of alcohols in the oxidation products.[29]

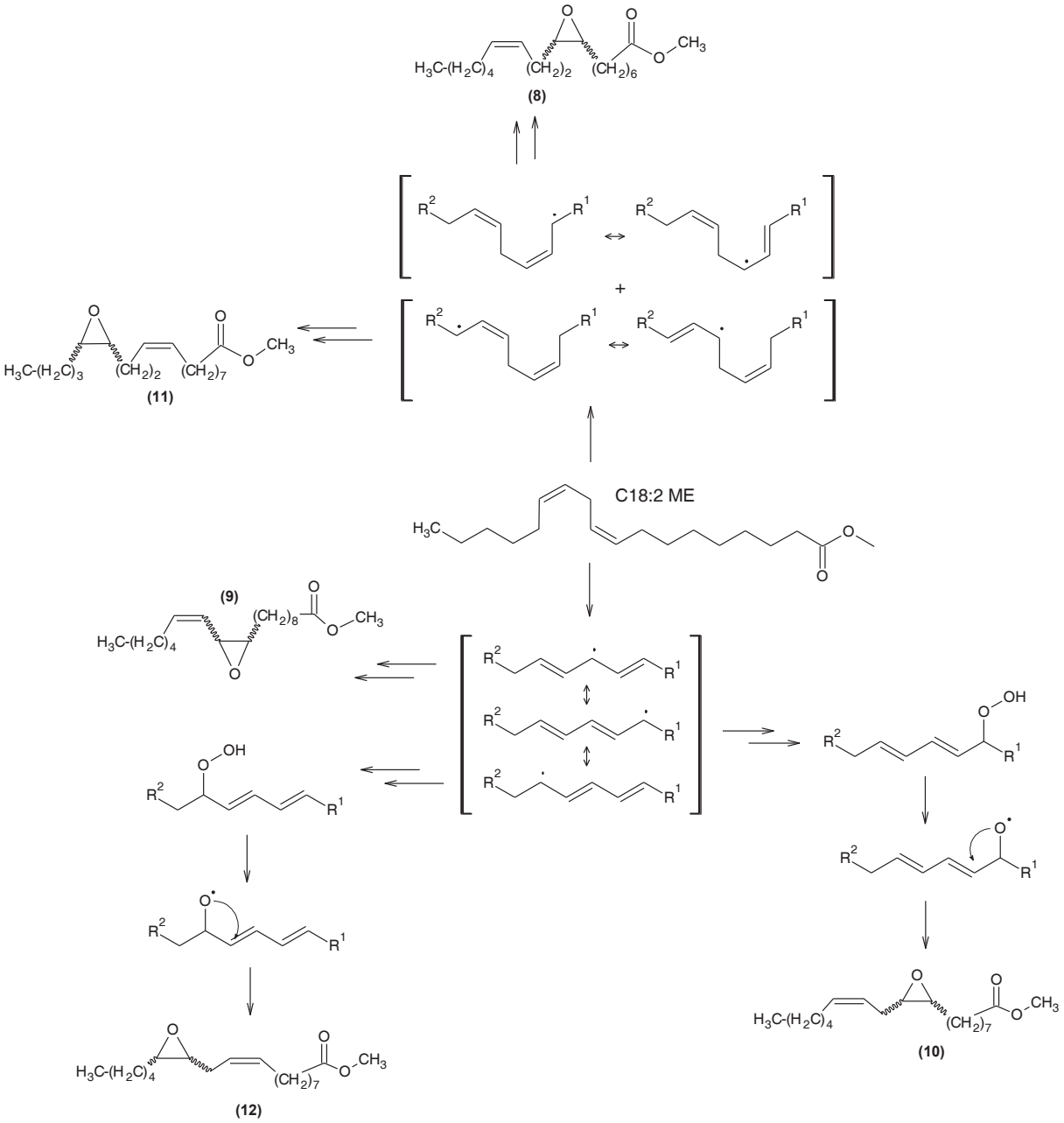

Figure 24: Reaction diagram for the formation of simple oxidation products (8 to 12) starting from C18:2 ME.

In Figure 25, the first step of the reaction that leads to the formation of hydroperoxides is explained in more detail (this first step is the base of the double arrows in Figure 24). The second step in Figure 25 represents the decomposition of the hydroperoxide into an alkoxy radical and a hydroxy radical. Up to this point the reaction mechanism corresponds to that of radical epoxide formation. At this point, two reaction paths can be taken. The epoxide is formed in an intramolecular reaction (Figure 24 below) in which an alcohol group can be formed from the alkoxy radical by hydrogen abstraction (Figure 25). Hydrogen abstraction leads to compound 7. There are several influencing factors that affect the likelihood of reactions. Epoxide formation is an intramolecular reaction that is generally orders of magnitude more likely than bimolecular reactions.[47] This statement is confirmed by the ratio between epoxides and alcohols in the identified compounds 1 to 15. Due to the fact that alcohol groups can be further oxidised to ketones under the oxidative ageing conditions, the product ratio and thus the probability of the two routes cannot be definitively derived from the product distribution.

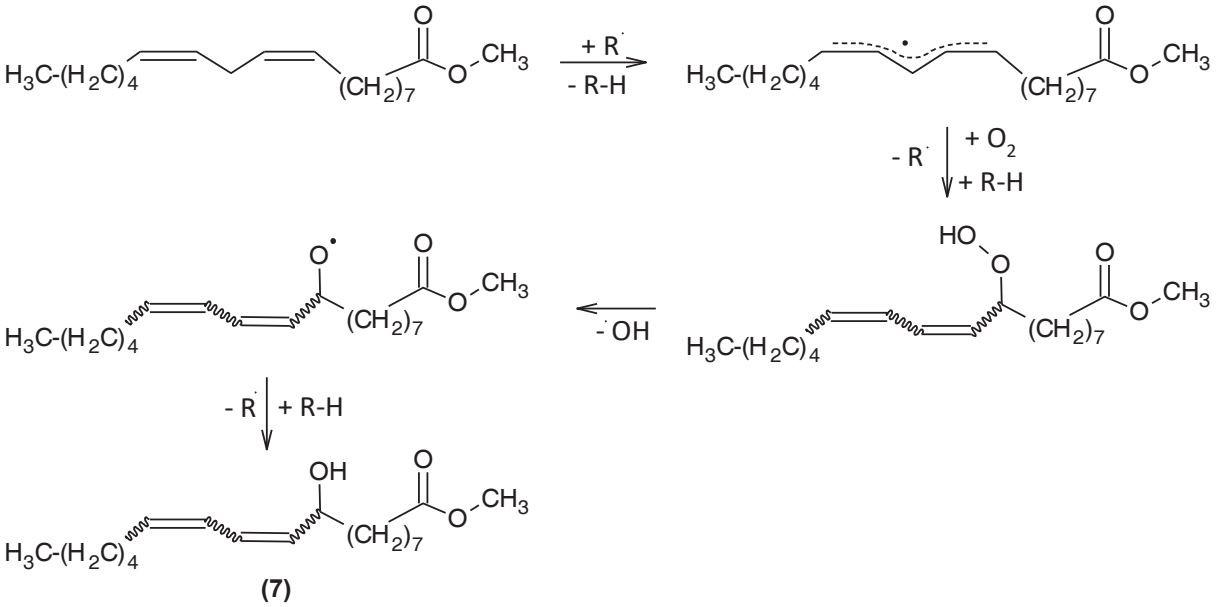

Figure 25: Reaction mechanism explaining the formation of alcohol groups during ageing.

In addition to the direct mechanism that leads to the formation of the epoxide, the oxidation products of C18:1 ME (Figure 23) have another special feature. Two further compounds can be identified in the chromatogram (compound 14 and 15). These two compounds are ketones, each of which is located on one of the carbons on which the double bond was originally present in the reagent. A radical mechanism, as in epoxide formation, would lead to a product ratio where ketones would have to exist in the α-position to the double bond. For this selective formation of compounds 14 and 15, a mechanism has been found in the literature that can plausibly explain the formation (Figure 26). This mechanism has been investigated for a large number of epoxides with different residues by Winstein and Henderson in literature[31] and is used here as an explanation. The reaction generally takes place under Lewis acid catalysis or the heat of reaction alone, which means that the reaction can occur under the ageing conditions (110 °C and 10 L per hour of air flow). During the reaction, the hydrogen migrates from one epoxy carbon to the other and the ketone is formed when the CO bond is opened. Since both residues are hydrogen atoms, the direction of the epoxide opening is equally likely in both cases, which plausibly explains the product ratio of the ketones (compounds 15 and 16) found.

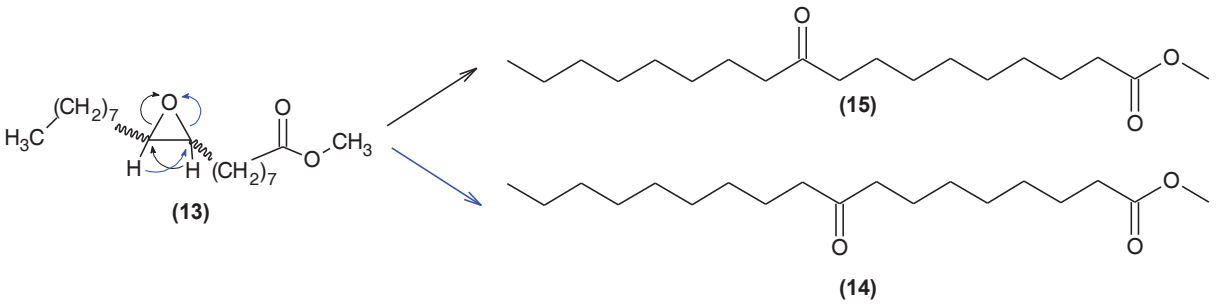

Figure 26: Hydrogen rearrangement and epoxide ring opening with the formation of ketones.[31]

6.2.2 Multiple oxidation products

The discussed mechanisms for the formation of the simple oxidation products are preceded as the first step by the reaction of an allylic or bisallylic radical with molecular oxygen. In the previous section, this is assumed as a prerequisite for the mechanisms and is proven in the discussion of the multiple oxidation products with the identification of hydroperoxides among the oxidation products. Analogous

to the identified epoxides, alcohols and ketones, the hydroperoxides have a large variety of products due to the multiple C-H bonds with low dissociation energy and the delocalisation of the radicals over, in some cases, several carbons. The actual number of mass-to-charge ratios remains manageable due to constitutional isomerism. When examining the ageing products, it was possible to observe an upper limit of oxygen atoms that the monomeric oxidation products can form. Even after 400 hours of artificial ageing, no monomers with more than six oxygen atoms can be found in the Rancimat. Since two of these oxygen atoms are already present in the FAME educts, the maximum observed oxidation is four. This limits the maximum number of hydroperoxide groups per monomer to two. That a double hydroperoxide formation takes place is possible through the identification of compound 16 (Figure 27).

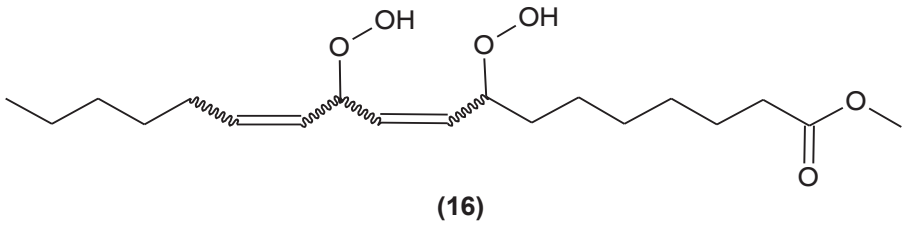

(16)

Figure 27: Structural formula of methyl 8,11-bishydroperoxyoctadeca-9,12-dienoate (16).

Assuming that the first radical formation takes place at the bisallylic position corresponding to the lower dissociation energy, the precursor compound contains two allylic positions, in which one of them reacts with another oxygen molecule to form the double hydroperoxide. As mentioned at the beginning, compound 16 is only one hydroperoxide compound among many that are formed during ageing. Hydroperoxides have a low bond dissociation energy at the O-O bond. In radical polymerisation, hydroperoxides are used, among other things, as radical initiators, since they can form radicals under the influence of heat or light.[48] Thus, hydroperoxides are not thermodynamically stable products of FAME ageing, but act as intermediates in the formation of secondary ageing products. A possible way is shown in Figure 28 which describes the further reaction of hydroperoxides.

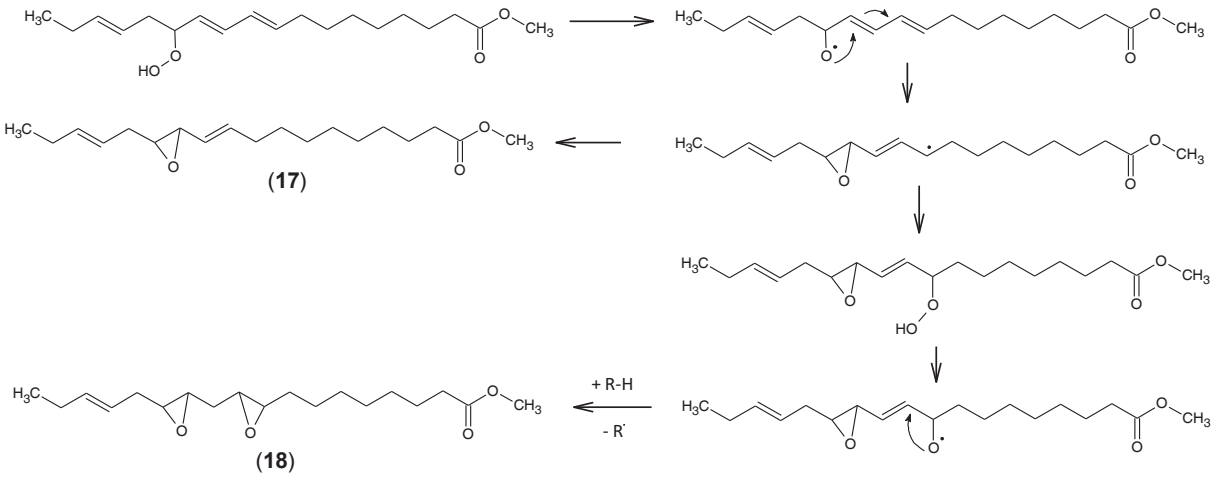

Figure 28: Reaction mechanism of epoxide formation.

Due to the low dissociation energy, the hydroperoxide breaks down into a hydroxy radical and an alkoxy radical, which leads to the formation of epoxides in an intramolecular reaction. During epoxide formation, the neighbouring double bond creates a stabilised allyl radical that can react further through two reactions. The first route involves hydrogen abstraction and leads to the formation of compound 17. In the second option, a further reaction with molecular oxygen takes place and leads to compound 18 via renewed dissociation of the hydroperoxide and an intramolecular reaction.

Further identified multiple oxidation products of RME are shown in Figure 29. From the compounds 19 to 25 shown, it can be concluded that the oxidation can proceed with retention of the double bond or with dissolution of the double bond. Compounds 19 and 22 each have a double bond isolated between two epoxy or ketone groups. This reduces the number of C-H bonds in the α-position to the double bond. In the case of a neighbouring ketone, there is no C-H bond in the α position on the side of the ketone. A direct oxidation of the double bond by a peroxide radical is sterically prevented by the globular structure, resulting from the angled structure at the four positions of the epoxides (the ketone and the double bond). This makes further oxidation more difficult and the presence of a double bond in the event of multiple oxidation of the molecule is understandable. The mechanisms described in the previous section, in combination with the structure of C18:3 ME, lead to a theoretical limitation in the number of oxidations that occur in connection with a double bond.

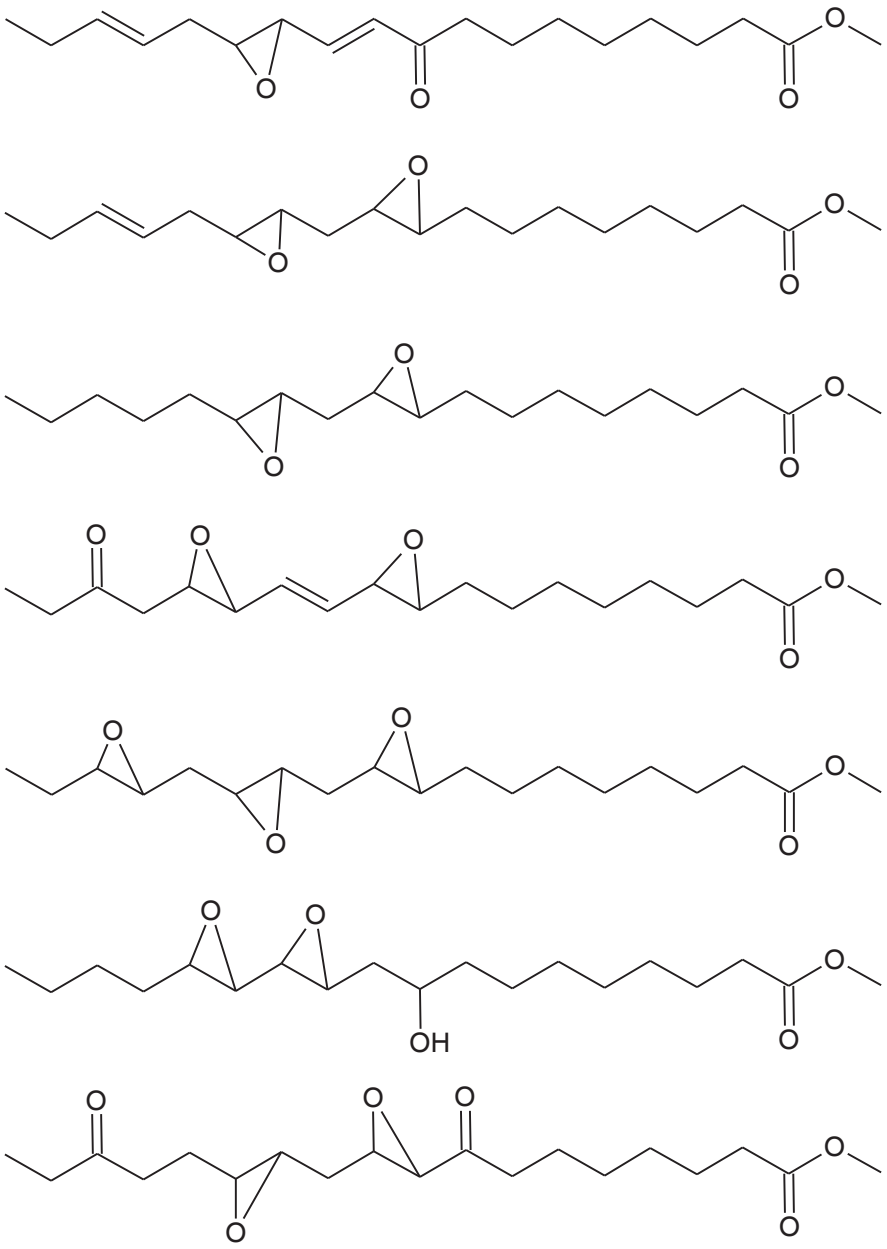

Figure 29: Identified multiple oxidation products of RME.

In practice, within the framework of the underlying investigations, the upper limit of the oxidation of monomers can be numbered at four. Based on the fact that epoxides are the most common oxidation

in the compounds identified here and the mechanism is based on an intramolecular reaction, the probability of epoxide formation is higher than that of the other functional groups. The epoxide formation takes place inevitably by dissolving the double bond. As a result, a maximum of three epoxides can be formed in the C18:3 ME. Further oxidation can therefore only result from an alcohol group or a ketone. The formation of an alcohol group is based on the same mechanism as the epoxide formation.[29] Only the last step is different (Figure 25), whereby the formation of the alcohol group as not occurring intramolecularly has a lower probability (Figure 25 and Figure 28). A fivefold oxidation can theoretically only be realised with the formation of two alcohol groups. A fivefold oxidation is theoretically possible by doubling the process, but is considered unlikely.

6.2.3 Short-chain degradation products

The oxidation of the fatty acid methyl esters not only leads to an increase in the oxygen content in the molecules, but also causes them to break down into short-chain molecules. The process of splitting oxidised molecules leads to two cleavage products per molecule. A cleavage of the C18 ME takes place at the point of oxidation. The position of the oxidation is given by the position of the double bonds in the C18 ME. The double bond at carbon 15 (see Figure 7) can result in shorter cleavage products from C18:3 ME than is the case with C18:2 ME and C18:1 ME. The size of the fission product and the associated boiling point influence further ageing.[29] Highly volatile small fission products are discharged from the fuel and are used in the Rancimat ageing method to determine the onset of ageing. The larger fission products remain in the fuel and undergo further reactions. The degradation products remaining in the fuel can be measured and identified using high-resolution mass spectrometry. A selection of three short-chain breakdown products that remained in the fuel are shown in Figure 30.

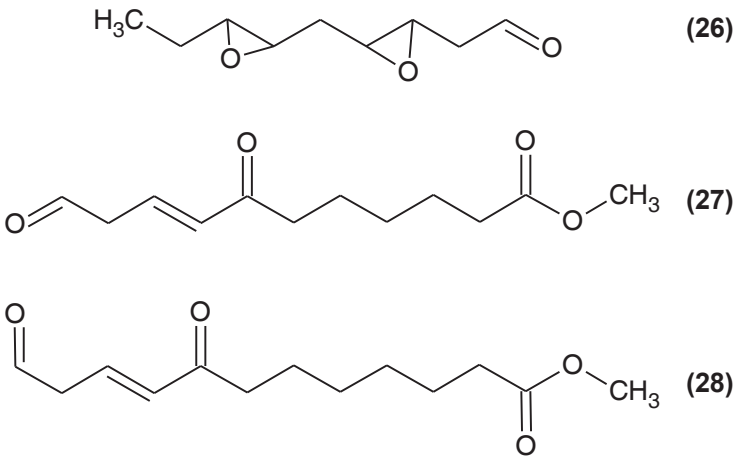

Figure 30: Identified short-chain degradation products of RME.

In principle, the two cleavage products formed can be distinguished into the part with the methyl ester function (compound 27 and 28) and the part without (compound 26). The more terminal the bond cleavage position in the molecule, the lower the boiling point, which makes it more likely to be discharged from the fuel. For this reason, it is mainly the breakdown products with a methyl ester function that remain in the fuel. In the case of fuel ageing, it has so far been shown that a large number of different compounds arise. The process of oxidation can result in different functional groups (epoxides, alcohols, ketones) and their position in the molecule can occupy several positions in the molecule due to the delocalisation of the radicals involved.[29] The short-chain degradation products are just as diverse as the oxidation products resulting from oxidation. The connections 26, 27 and 28

identified here all have one thing in common. All compounds have an aldehyde group at the end. Under the oxidative ageing conditions, the aldehyde groups can easily be further oxidised to the carboxylic acid (Figure 31). This finding plays a decisive role in the investigation of dimer formation in the following section.

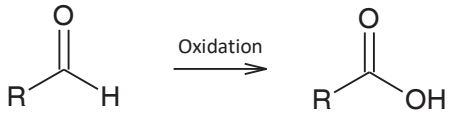

Figure 31: Oxidation of aldehydes to carboxylic acid.

6.2.4 Dimerization

One effect of fuel ageing that has not yet been adequately researched is oligomerisation. Oligomerisation is the formation of long-chain molecules that are formed from two or more monomers.[49] Investigations with high-resolution mass spectrometry provide new insights in this area. An oligomerisation, as it is inferred from GPC measurements in literature, can only be partially confirmed with the data available here. The mass spectrum of RME aged 400 hours is shown in Figure 32. The mass spectrum shows that the measured mass-to-charge ratios are divided into three areas. The formation of long-chain molecules is mainly limited to the formation of compounds with a mass of up to 727 g/mol. In addition, traces of larger molecules can be measured which are in the range of a trimerization, but which are no longer relevant for the composition of aged RME (Figure 32). The clustering that can be observed in Figure 32 is an indication of the oligomerisation. Oligomerisation is the reaction of monomer units with one another. Depending on the size of the monomer units, there are only certain masses that are added up from the masses of the monomers. In the case of RME ageing, there are educts (C18:1 ME, C18:2 ME, ...), oxidised educts and short-chain degradation products. The starting materials have an average molar mass of approx. 300 g/mol.

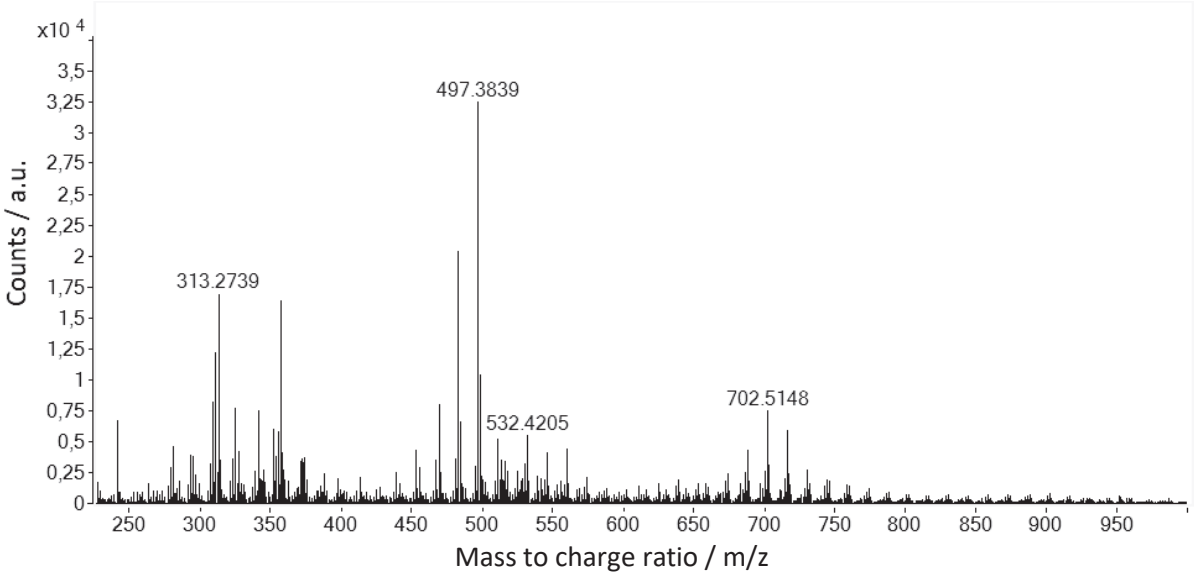

Figure 32: High resolution mass spectrum from RME aged 400 hours.

The oxidised starting materials are in the range between approx. 310 g/mol and 360 g/mol. The short-chain degradation products have an average mass of 200 g/mol. Based on the molar masses of the compounds identified so far, the three areas can be assigned to the corresponding underlying

monomer units. The rough assignment made here is further specified and verified by the structure elucidation of the masses.The first range in the mass spectrum in Figure 32 encompasses the starting materials and oxidation products with a range from 300 to 400 g/mol. The second range from 450 to 550 g/mol results from the dimerization of C18 ME with short-chain cleavage products. The third range around 700 g/mol comprises dimers from two C18 ME or even more strongly oxidised compounds from the second range.

For a more detailed composition, the carbon number is plotted against the number of oxygen atoms in Figure 33. The dimers have the same diversity as the monomeric starting compounds. Behind every mass there is a series of constitutional isomers, which can easily result in several hundred ageing products. According to the number of carbons, the masses found can be classified according to their monomers. The greatest intensities include the range of dimerization with short-chain degradation products and also shows the greatest number of different masses (range from 24 to 31 carbons in Figure 33) in the mass spectrum. When RME ages, mainly two dimers with 28 and 29 carbons are formed. This corresponds to a dimerization of a C19 and a C9 or C10 degradation product. C9 or C10 fragments result from cleavage by oxidation at the double bond between carbon 9 and 10 in the fatty acid methyl esters. Since this position of the double bond is at C18:1 ME, C18:2 ME and C18:3 ME, cleavage products are more likely to occur at this point.

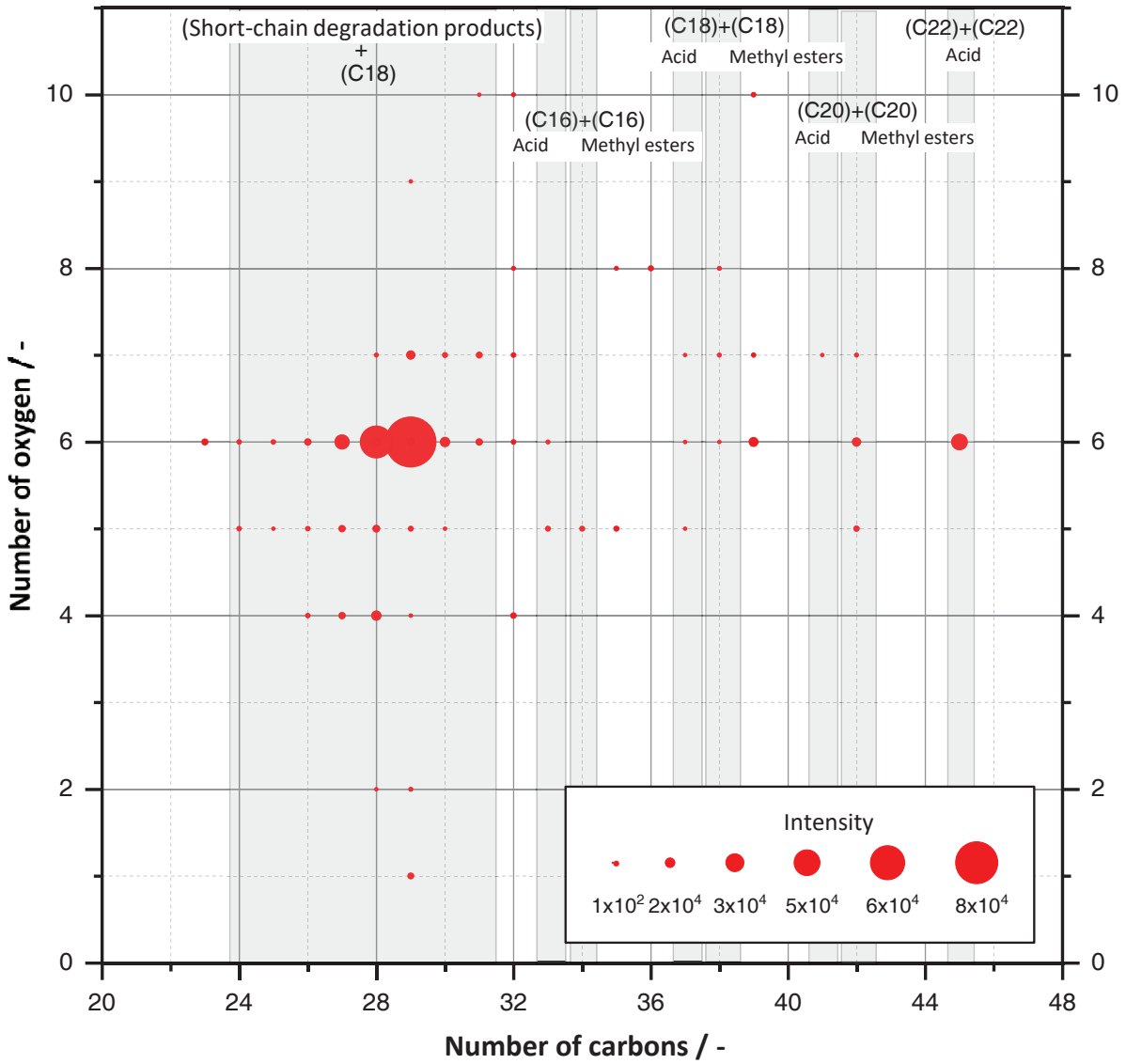

Figure 33: Long-chain ageing products, shown as a function of the number of oxygen and carbon atoms.

The degree of oxidation that is necessary for dimerization can be derived from the number of oxygen atoms. The main dimers present have a number of six oxygen atoms. If one considers that the short-chain degradation products predominantly have the methyl ester function, there are four oxygen atoms that are already contained in the molecule before ageing. The oxidation of the fatty acid residue is relatively low with two oxygen atoms in the main products.

Structural proposals for five dimers can be made from the MS/MS mass spectra (Figure 34). Including the two main products (compound 30 and 29) with m/z = 497.3869 and m/z = 483.3743 from Figure 32 and correspondingly C28 and C29 from Figure 33.

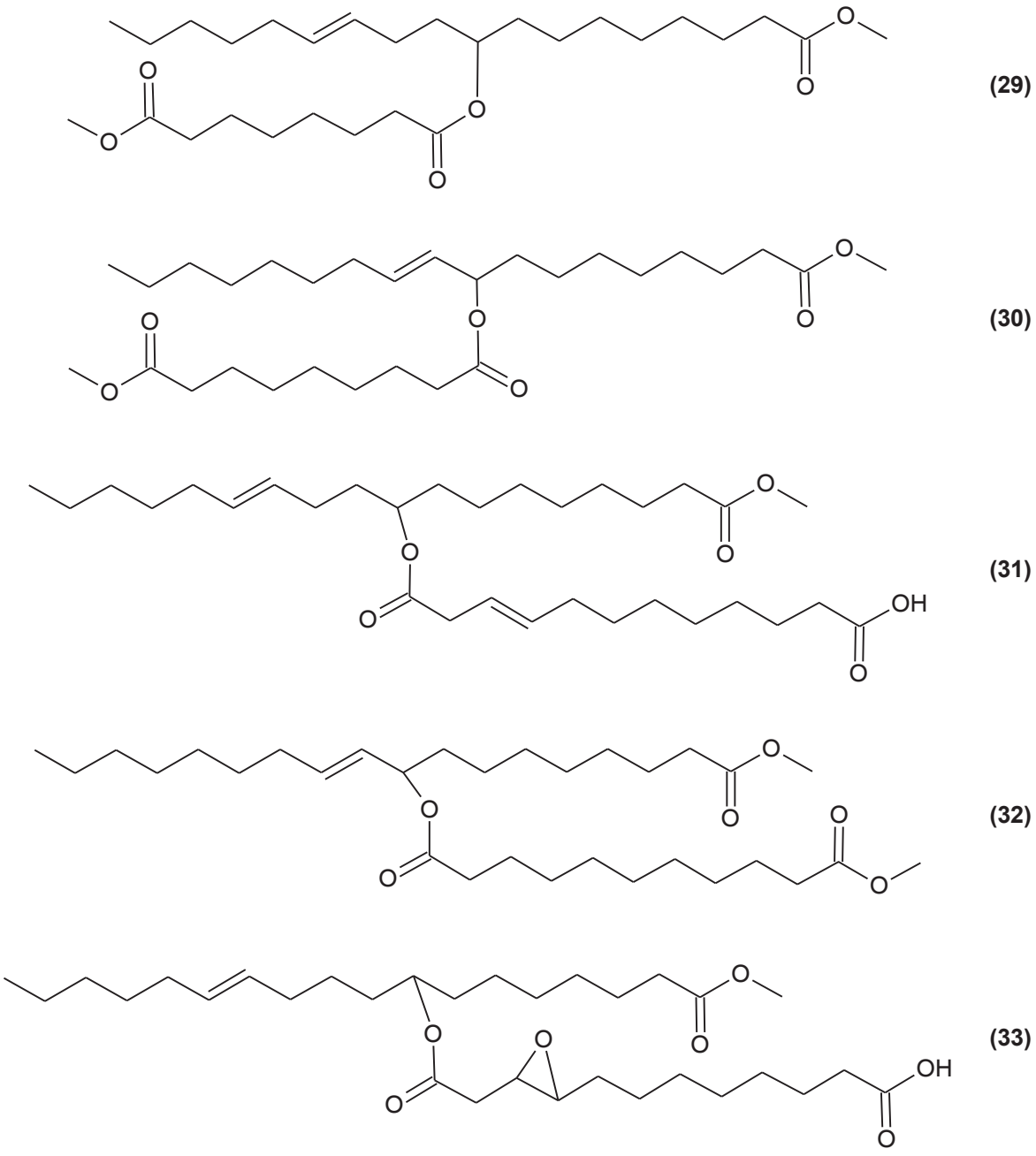

Figure 34: Structural formulas of the identified dimers based on the MS/MS evaluation.

The identified dimers are composed of C18 ME and short-chain degradation products with C9, C10 and C12. What all five dimers have in common is the ester group, which links the two monomer units with one another. The short-chain monomer units either have two carboxylic acid groups or one carboxylic acid group and one methyl ester group. With the knowledge of the structures behind the oligomerisation, the ageing products can be confirmed with another measuring method. The carbonyl groups of the dimers from Figure 34 can be detected and confirmed by Fourier transform infrared spectroscopy (FTIR). The FTIR spectra for different ageing times of RME are shown in Figure 35. Unaged fatty acid methyl esters show an intense vibration band at ν = 1740 cm^{-1} (C=O stretching vibration). Ageing leads to band broadening and an increase in intensity. The examinations carried out on the ageing products (Figure 20) can confirm the presence of ketones and acids. In each of the identified dimers there are three carbonyl groups that have a different chemical environment. In combination with an increasing loss of mass over the ageing period, this leads to an increase in intensity and a broadening of the carbonyl band in the FTIR spectrum (Figure 35).

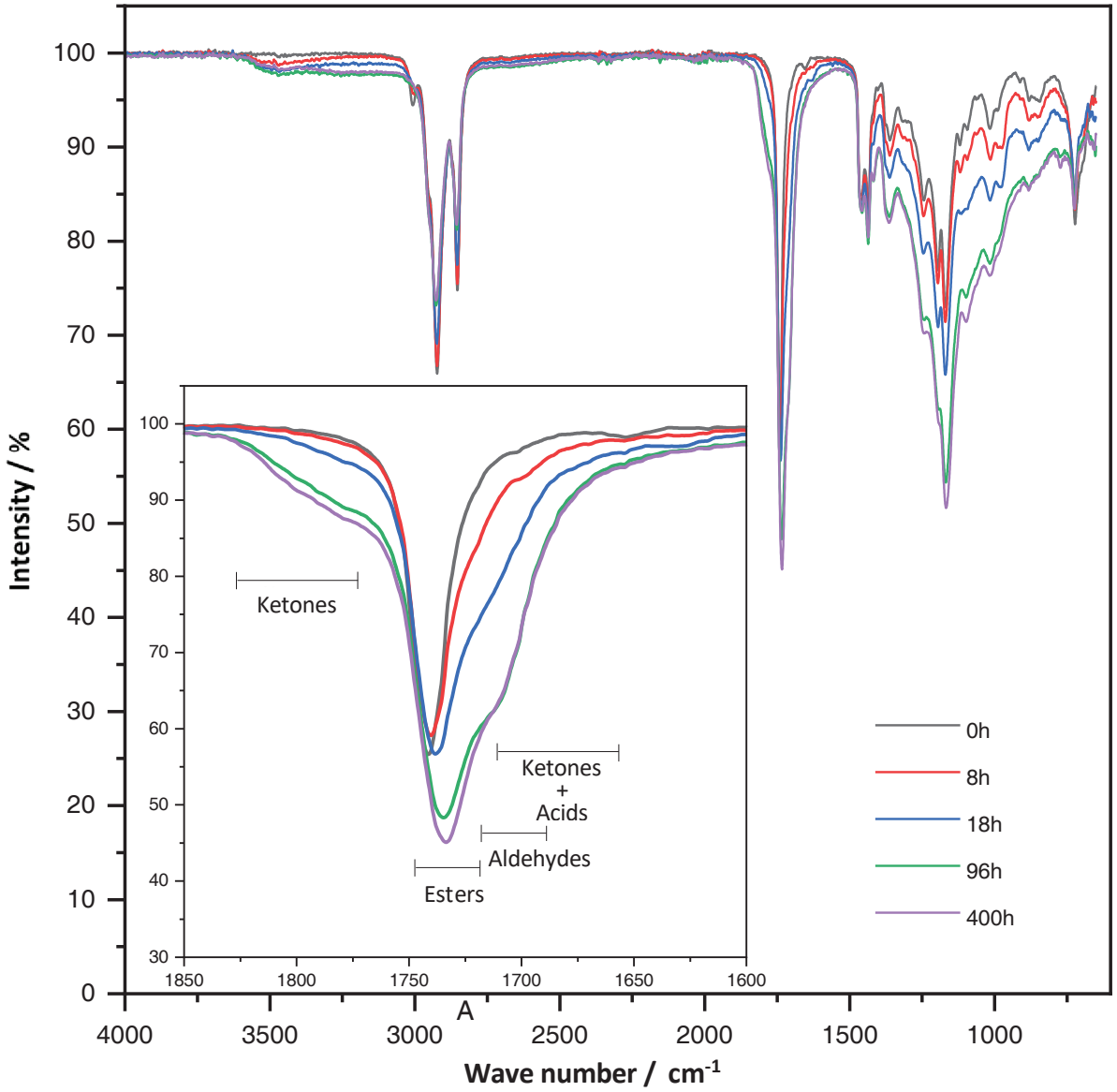

Figure 35: Infrared spectrum for RME with different ages.

The change in the carbonyl band is made up of four influences (aldehydes, ketones, acids and esters). The effects of the individual functional groups on the carbonyl vibration band are given in Figure 35.

The superposition of the vibration bands of the ketones, aldehydes and acids with the carbonyl vibration of the esters results in the formation of the shoulder at approx. v = 1720 cm^{-1}. The influence of the ketones is also shown by the broadening of the vibration band at the base of the peak. By identifying the structure of the dimers, the increase in intensity and the associated increase in the full width at half maximum can be used to describe the carbonyl band, along with the influences of the other functional ones. The sudden increase in the carbonyl band between 18 h and 96 h and the course over time are discussed in more detail in Section 6.3 for the time behaviour of ageing.

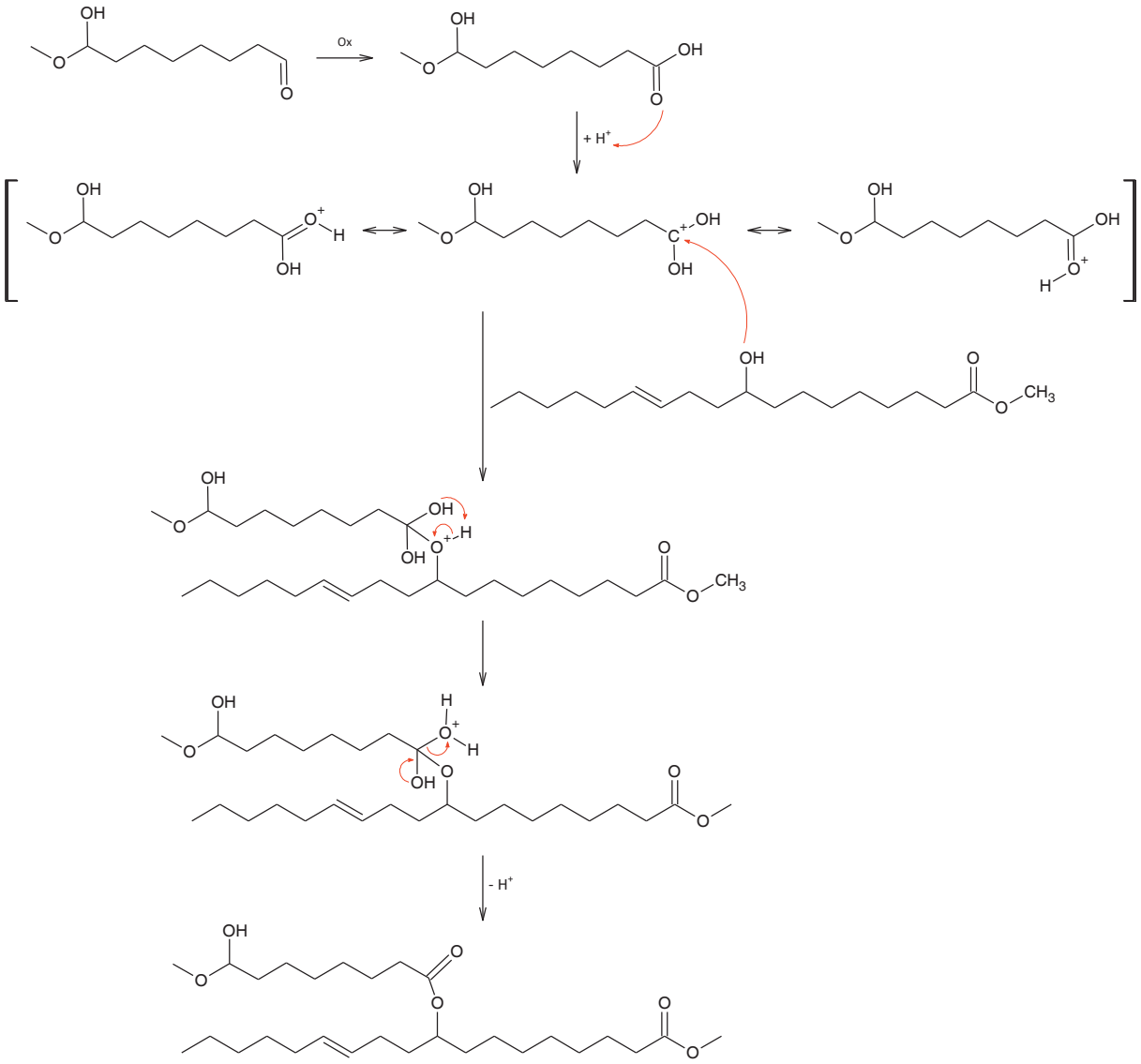

Figure 36: Reaction mechanism of the esterification of short-chain degradation products with oxidation products of RME.

The C18 ME monomer unit is not further oxidised in the identified products, apart from the linking ester group. There are two aspects to consider for the underlying mechanism. On the one hand, when identifying the short-chain degradation products, the terminal aldehyde group was noticed as a common feature. Under the oxidative conditions, this can easily be oxidised to the carboxylic acid. On the other hand, when RME ages, esterification can only result from one carboxylic acid group and one alcohol. Both prerequisites for an esterification are given by the results shown so far (Figure 21 and Figure 31). The reaction mechanism of the esterification that leads to the formation of the dimers is

shown in Figure 36. The esterification described in Figure 36 specifies as a prerequisite that the molecule in the C18 ME monomer units must be functionalised with an alcohol group through primary oxidation. The short-chain ageing products are initially oxidised to the carboxylic acid. Under acid catalysis, the lone pair of electrons in an alcohol group can attack nucleophilically on the partially positive carbon of the carboxylic acid. By forming an intramolecular hydrogen bond, the hydrogen atom can rearrange with one of the oxygen atoms of the carboxy group. By splitting off water and deprotonation, the ester is formed in the last step.

The formation of oligomers can be discussed in more detail from the mechanism of esterification. The measurements and evaluations show that predominantly dimerization occurs. At this point the question arises why only traces of trimers, for example, are found. According to the mechanism of esterification in the formation of long-chain molecules, the formation of tri- or tetramers is possible. However, corresponding requirements must be met for this, which reduce the likelihood of trimerization. For a trimerization a monomer must have two functional groups (alcohol group and acid group). These so-called linker molecules can be detected during ageing, but are only present in low concentrations. For the esterification, these are on the one hand dialcohols and on the other hand monomers with a carboxylic acid group and an alcohol group or dicarboxylic acids. Compounds 31 and 33 are identified dimers which, through their carboxylic acid group, can each undergo further esterification to give trimers. With each further chain extension, however, additional reactions must take place on the molecule, which reduces the probability accordingly. In addition, it must be taken into account that the ester hydrolysis, which is responsible for the formation of some of the acids during ageing, can also take place in the oligomers. The ester hydrolysis is the reverse reaction of the esterification, in which the dimers break down again into two monomers. Taking into account both aspects, the product distribution found for the long-chain ageing products is a logical consequence of the underlying reactions.

6.2.5 Acids

Carboxylic acids represent a category of ageing products that can be easily identified by the molecular formula. The formation of acid proceeds in two ways. On the one hand, the fatty acid methyl esters can be hydrolysed during ageing. Free fatty acids are created. On the other hand, the short-chain degradation products found can be oxidised to carboxylic acids by the terminal aldehyde groups. Since the short-chain degradation products also produce compounds with an even carbon number, depending on the position of the cleavage, easy identification only applies to hydrolysed fatty acid methyl esters. The reason is that the even carbon number after hydrolysis under the ageing conditions can only arise through ester hydrolysis. In the case of the mass-to-charge ratios with an even number of carbon atoms in the assigned empirical formula, all constitutional isomers are also carboxylic acids. The variety of C18 acids formed can be shown by appropriate extraction of base peak chromatograms (Figure 37). The carboxylic acids differ from the other oxidation products in that they have shorter retention times. Due to the decrease in polarity or the elution strength over the separation time of 200 min, polar products elute first. The carboxylate anion is formed by deprotonation and dissolves better in polar solvents. However, the retention time is also influenced by the geometry of the molecules, which means that retention differences occur according to the number of double bonds or the degree of oxidation.[50] Figure 37 shows the influence of the double bonds and the oxidation on the short retention times of the carboxylic acids from a number of four oxygen atoms and the longer retention times of the hydrolysis products with the empirical formulas $C_{18}H_{30}O_2$ (C18:3), $C_{18}H_{32}O_2$ (C18:2) and $C_{18}H_{34}O_2$ (C18:1). The other acids shown are the corresponding single or multiple oxidation products. The lowest variety of acids can be found at C18:1.

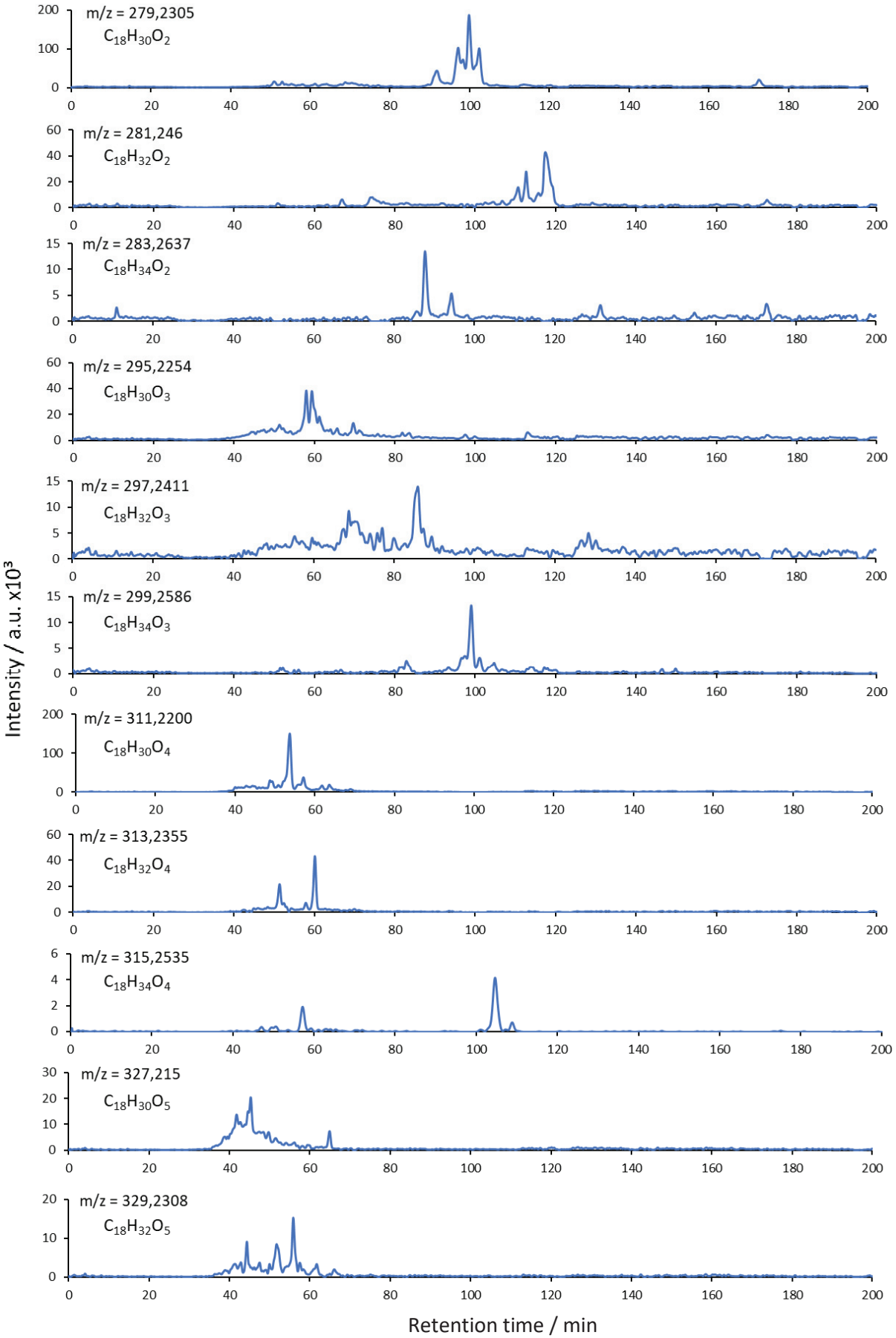

Figure 37: Base peak chromatograms of the carboxylic acid compounds in RME aged for 24 hours.

Regardless of the number of oxidations, a main product can be found in the respective chromatograms for m/z = 283.2637, m/z = 299.2586 and m/z = 315.235. This corresponds to the product distribution found for the simple oxidation products in Figure 21. Due to the greater number of double bonds and the associated greater variety of oxidation options, the C18:2 and C18:3 acids have a greater number of constitutional isomers. In addition, a decrease in the intensities towards greater oxidation can generally be observed. Since the oxidation products are formed first in the course of ageing, the non-oxidised compounds have more time to hydrolyse compared to the oxidised compounds, which means that their proportion must be greater. From the available data, no differences in acid formation can be identified that cannot be attributed to the different proportions of C18:1 ME, C18:2 ME and C18:3 ME in the RME.

6.3 Time course of RME ageing

The investigations of the ageing products with structure elucidation and mechanistic consideration represent the first step towards understanding RME ageing. The second step is to investigate the kinetics of RME ageing. The kinetic investigation is based on tracking the chemical changes over the course of ageing over time. For this purpose, fuel samples in the Rancimat RME are aged between 1 and 400 hours. The ageing products of all samples that have been aged for different periods of time are measured using mass spectrometry. This means that individual masses can be tracked over the ageing period of 400 hours. The time course obtained is shown in Figure 38. The categories correspond to the categories introduced and discussed in Section 6.1. Based on the subdivision of the categories, the results are discussed individually for each of the categories in Figure 38. Figure 38 shows the intensities of individual masses as a function of ageing time In the case of the starting products, only the C18 ME and the resulting compounds are considered for the RME ageing. Without a reference measurement of the respective compounds, the intensities shown do not allow any direct correlation with the actually present concentration. This is due to the different ionisation of the compounds. The qualitative consideration without direct correlation of the concentration, considering the onset of education and the time course, already enables the analysis of the ageing dynamics. The time courses shown in Figure 38 are discussed separately for each category below.

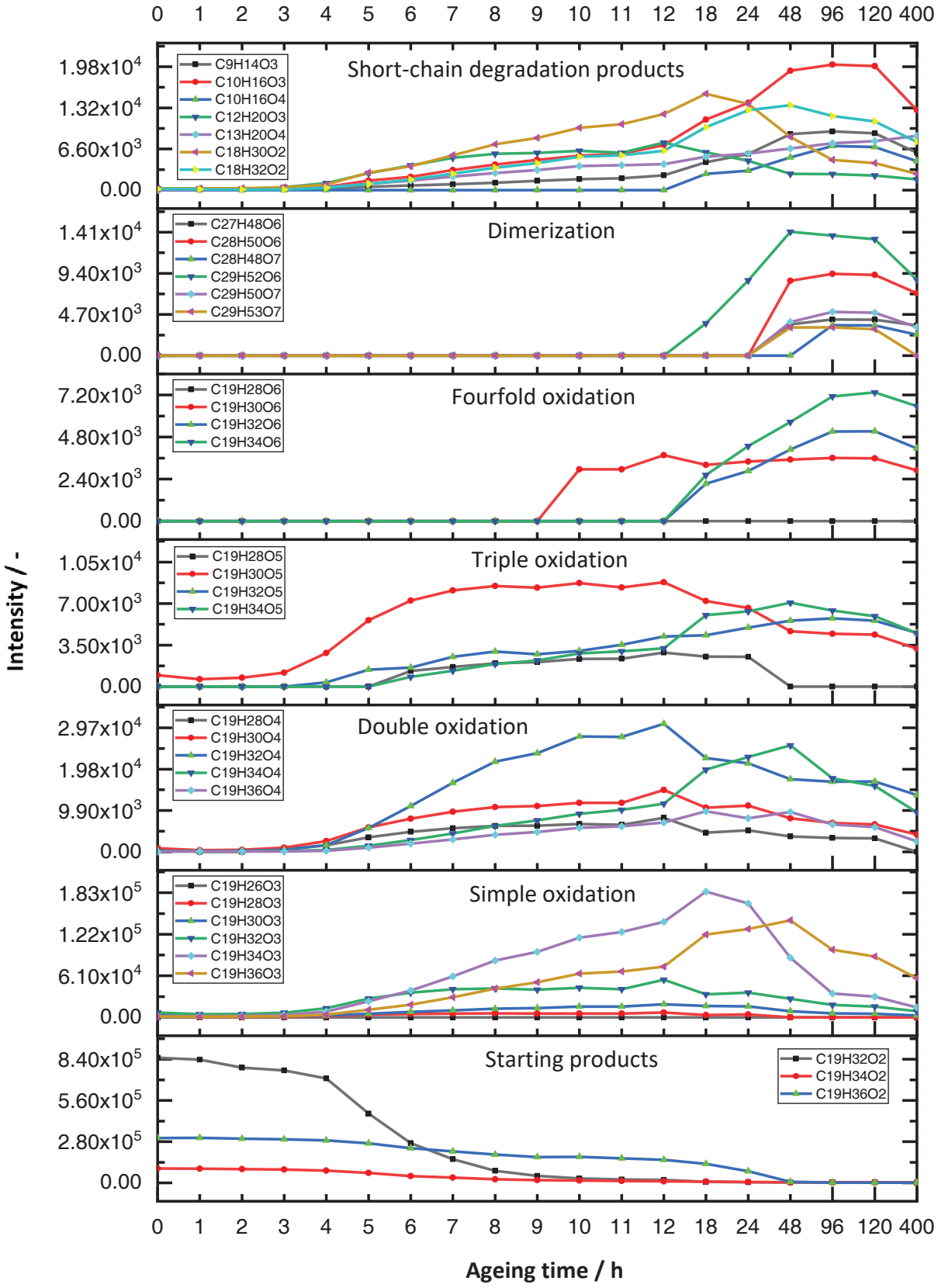

Figure 38: Time course of ageing of RME.

6.3.1 Starting products

When looking at the starting products, the different ionisation becomes clearly visible. C18:3 ME occurs in the RME in far lower concentrations than C18:2 ME or C18:1 ME.[33] The intensity of C18:3 ME is orders of magnitude higher than that of C18:2 ME and C18:1 ME. As shown, this strictly applies to the starting products with their low polarity. An approximate distinction can be considered for the oxidation products. This is due to the increasing polarity of the ageing products, which means that they are in the optimal application range of the APCI. Nevertheless, an exact comparison of concentrations is not possible without a reference determination of the respective compounds. The relative decrease with time exhibited by C18:3 ME in Figure 38 confirms the easier oxidation of the bisallylic positions. The RME used in the Rancimat has an induction time of four hours. Due to the two bisallylic positions in C18:3 ME, however, a slight decrease occurs within the induction time, which reflects the high susceptibility to oxidation. After an ageing period of four hours, there is a sudden increase in the breakdown of C18:3 ME and the onset of the breakdown of C18:2 ME and C18:1 ME. C18:1 ME with the allylic position in the molecule decreases continuously after the induction time has elapsed. The presence of C18:1 ME can be read off up to 48 hours of ageing from Figure 38. Due to the large scale of the intensity, the course is no longer resolved in the range between 48 and 400 hours. However, unoxidized C18:1 ME can be detected up to 400 hours of ageing.

6.3.2 Simple oxidation products

When considering the oxidation products, there is one special feature that will be worked out in more detail in the course of the discussion. Due to certain primary oxidation of C18 ME, further oxidation can take place by orders of magnitude more easily than in principle (see Figure 40). For this reason, the beginning of the simple oxidation does not reflect the degradation of C18:3 ME in the starting products, which already begins after 1 hour. The general formation of simple oxidation products begins after an ageing period of three hours. That means even during the induction period. Since the concentration of natural antioxidants decreases in the course of the induction period, the likelihood of oxidation increases within the induction period and an increase in the oxidation products can be observed during the induction period. The simple oxidation products of C18:1 ME ($C_{19}H_{36}O_3$), C18:2 ME ($C_{19}H_{34}O_3$) and C18:3 ME ($C_{19}H_{32}O_3$) accumulate over the ageing period until they reach a maximum at 48 h, 18 h and 12 h respectively. After that, the proportion decreases accordingly. After 400 hours of ageing, only significant amounts of $C_{19}H_{36}O_3$ remain. Since the simple oxidation products of C18:2 ME and C18:3 ME can be more easily oxidised several times (bisallylic and allylic positions present), the course corresponds to the expectations. In addition to the oxidation products, which react while maintaining the double bond equivalents, compounds with the empirical formula $C_{19}H_{30}O_3$ are also formed, where the double bond equivalents are increased by one through oxidation. These are compounds in which oxidation has led to the formation of a keto group and the three double bonds are retained.

6.3.3 Twofold oxidation products

The twofold oxidation products are formed from their corresponding simple oxidation products. This results in a correlation of the time courses, which on the one hand has to do with the reaction mechanism described in Figure 28 and on the other hand can be explained by the number of bisallylic and allylic positions. The time course of $C_{19}H_{36}O_4$ (C18:1) roughly follows the course of $C_{19}H_{36}O_3$. Since further oxidation takes place without the influence of the double bond, the intensity is correspondingly lower. After an ageing period of 48 hours, the intensity decreases again in a manner analogous to simple oxidation. The decrease in intensities is due to the subsequent reactions that occur in all categories. The starting products are consumed over the ageing period. As a result, fewer and fewer simple oxidation products are formed. Since the simple oxidation products are in turn consumed by

further oxidation, cleavage into short-chain degradation products or dimerization, the maximum marks the equilibrium of both influences. When the fourfold oxidation is reached, the further consumption is reduced to the formation of short-chain degradation products and dimers. The short-chain degradation products can react further through dimerization. The dimers formed can break down again into the monomers either by trimer formation or by ester hydrolysis. This results in a dynamic system in the ageing of fatty acid methyl esters, which does not reach a stable state even after 400 hours of ageing. The double oxidation of C18:2 ME ($C_{19}H_{34}O_4$) shows the decreasing reactivity of the allylic position compared to the bisallylic position, which is primarily attacked in the single oxidation. The slope of the curve is therefore significantly smaller with the double oxidation. The course of the curve for $C_{19}H_{34}O_4$ also shows that the maximum is shifted from 18 h for the single oxidation to 48 h for the double oxidation. Consequently, the further reactions lose weight when equilibrium is established, since both double bonds are consumed with the formation of epoxides (functional groups resulting from the oxidation and the double bond equivalents).

6.3.4 Triple oxidation

Due to the larger number of double bonds, the triple oxidation takes place preferably at C18:2 ME and C18:3 ME. Due to the multiple oxidation, special conditions arise in connection with the primary oxidation, which strongly influence the course of the reaction of some compounds. Compared to the other triple oxidation products, the compounds with the empirical formula $C_{19}H_{30}O_5$ show an early onset of formation and a higher intensity. However, the early onset and in particular the intensity are well below the single and double oxidation (different y-axes). For the interpretation of this clearly different course for $C_{19}H_{30}O_5$, the individual constitutional isomers must be taken into account. Figure 39 shows the basic peak chromatogram for m/z = 339.2153, which makes the constitutional isomers visible through different retention times. Two main products can be identified for $C_{19}H_{30}O_5$. During the oxidation to compounds 34 and 35, a ketone group and a hydroperoxide are each formed. The compounds 34 and 35 differ in the position of the oxidation and the position of the double bonds. Compound 34 is responsible for the early formation and the higher intensity, which can be seen from the observation of the base peak chromatogram over time. To answer the question why this compound 34 in particular has a comparatively higher probability of formation, the radical stabilities must be examined more closely.

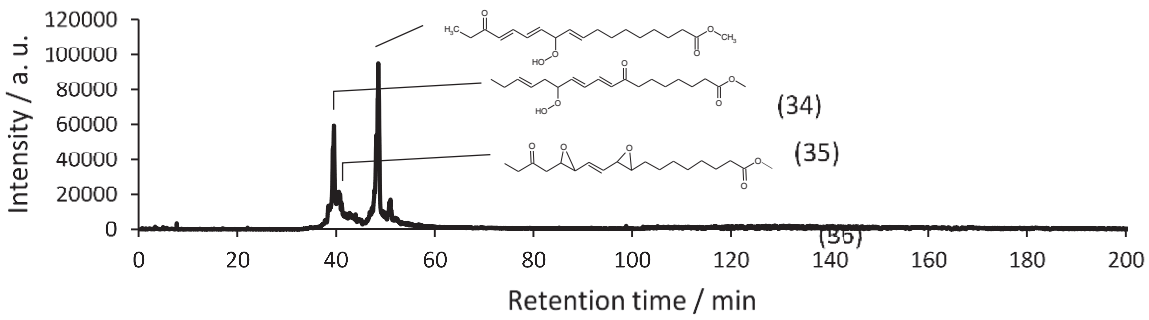

Figure 39: Base peak chromatogram for m/z = 339.2153 of the RME sample aged 18 hours.

The time course and the higher intensity of compound 34 can be plausibly explained by the reaction path illustrated in Figure 40. A special feature in the course of the oxidation leads to the increased formation of compound 34. The underlying reaction is shown in Figure 40. The starting compound in Figure 40 is formed by the primary oxidation of C18:3 ME at the bisallylic position at which the

preferred elimination of hydrogen occurs at the beginning. By reaction with molecular oxygen, the formation of the hydroperoxide and the subsequent decomposition into the alkoxy radical, an alcohol group can be formed by hydrogen abstraction. [29] Due to the oxidative reaction conditions of ageing, the alcohol group oxidises further to the ketone. Because of the special arrangement of the ketone relative to the double bonds, the C-H bond marked in Figure 40 has a lower dissociation energy than is the case with the bisallylic position, which is already very reactive. This is due to the mesomeric stabilisation over eight carbons and the carbonyl oxygen. The delocalisation of the unpaired electron over such an extensive π system means a strong stabilisation of the radical, which results in the increased tendency to form. The delocalised radical shown with the five mesomeric boundary structures in Figure 40, considering all theoretical combinations of the three double bonds and the oxidation, is the theoretically most stable radical that can arise with C18:3 ME during ageing. However, the selective formation of compound 34 raises a further question, why the hydroperoxide group does not take place at other positions in accordance with the possible delocalisation of the radical. It must be considered that with hydroperoxides, the O-O bond can easily be cleaved under thermal or photochemical conditions. The cleavage depends on the dissociation energy of the O-O bond, which is reduced by a larger conjugated system. If the oxidation takes place at the end of the delocalised system with formation of hydroperoxide, the mesomer stabilisation is greater than with compound 34. Due to the lower resulting dissociation energy, the peroxide cleavage becomes more likely and the alkoxy radical formed is more stable. There is no accumulation of this compound in the course of ageing. The higher stability also increases the likelihood that subsequent reactions will take place that form short-chain degradation products through C-C cleavage. The other three-fold oxidation products with the empirical formulas $C_{19}H_{34}O_5$, $C_{19}H_{32}O_5$ and $C_{19}H_{28}O_5$ show a similar time sequence to each other, with $C_{19}H_{28}O_5$ reaching the maximum intensity after 24 hours and subsequent reactions dominating so strongly that the intensity drops suddenly.

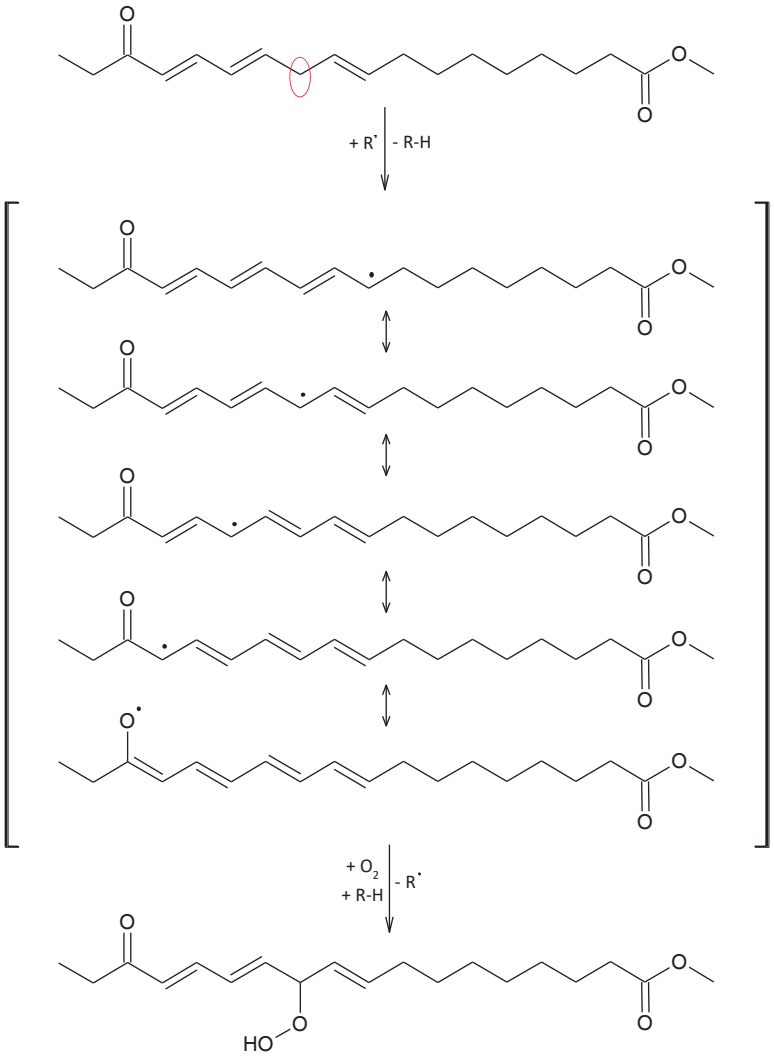

Figure 40: Oxidation of compound 34.

6.3.5 Fourfold oxidation

With increasing oxidation, the intensity of the oxidation products generally continues to decrease. Compared to the one to three-fold oxidation, the four-fold oxidation only sets in with a time delay at 9 or 12 hours. The compounds with the empirical formula $C_{19}H_{30}O_6$ arise after an ageing period of 9 hours. The earlier start of formation compared to $C_{19}H_{32}O_6$ and $C_{19}H_{34}O_6$ is probably due to the same better mesomer stabilisation of some compounds, with $C_{19}H_{30}O_5$ probably being precursor compounds. $C_{19}H_{32}O_6$ and $C_{19}H_{34}O_6$ as quadruple oxidation products of C18:2 ME and C18:3 ME are formed after about 12 hours of ageing, with a slight decrease after 120 hours.

6.3.6 Short-chain degradation products

All compounds with fewer than 19 carbons are listed under short-chain ageing products. These include acids that arise from ester hydrolysis and have one carbon less. Other short-chain breakdown products are decomposition products of oxidised compounds and have a carbon number between nine and thirteen. The short-chain degradation products arise after the induction time of 4 hours and accumulate in the course of ageing. Depending on the product, a decrease in intensity occurs in all compounds after a certain ageing period, which can be observed in some cases after 12 hours or only after 120 hours of ageing. The formation of the short-chain ageing products is related to the formation of the dimers, since these represent the preliminary stage.

6.3.7 Dimer formation

Further oxidation of the short-chain breakdown products to carboxylic acids can lead to dimerization through esterification (see Section 6.2.4). Like the fourfold oxidation, the dimerization does not occur until after the induction time. Depending on the compound, the beginning of the formation is between 12 and 24 hours. The delayed formation of the dimers can be explained plausibly for two reasons. On the one hand, all compounds show a different tendency towards oxidation. [51] A distinction must be made between the oxidation of double bonds, alcohols and aldehydes, which can take place with different degrees of ease. On the other hand, the monomers of the dimerization must be present and reproduced in sufficient concentration. On the one hand, the aldehydes of the short-chain degradation products can easily be oxidised to the carboxylic acid. The alcohols of the C18 ME monomer are strongly influenced by the diffusion-controlled hydrogen abstraction in competition with the intramolecular epoxide formation. On the other hand, the alcohol groups can be further oxidised to ketones under the oxidative conditions. Consequently, an equilibrium must be established in which there are sufficient monomers for dimerization, which results in the delayed formation.

The decrease in the dimers, as well as the other oxidation products after an ageing time of approx. 120 hours, results in a fuel that is already highly viscous at this point in time, but which continues to change dynamically. This dynamic results from the reversibility of the dimerization, which means that the composition will change continuously. By contrast, the process of oxidation and the associated cleavage of the oxidation products run an irreversible process that continuously breaks down the fuel into smaller degradation products as it ages. There is a loss of mass due to the discharge of volatile compounds. With increasing ageing, the increasing concentration of monomers with possibly even two functional groups (alcohol, carboxylic acid) leads to tri- or tetramerization, but above all to increasing oxidation of the molecules.

6.4 Influence of the fuel composition on the ageing behaviour

In addition to the ageing of RME as a pure component, the influence of blend components on the ageing behaviour of RME is of particular interest, since biodiesel is also used on the market with an admixture of up to 7%. The focus of the investigations is not the current formulation of the fuels, but rather a future application. For this reason, RME is tested for ageing with two other regenerative fuels, hydrogenated vegetable oil (HVO) and polyoxymethylene dimethyl ether (OME), in the form of binary and ternary mixtures. HVO and RME are already established regenerative fuels and are therefore of great interest for future fuel formulations. Binary and ternary mixtures of RME, OME and HVO are also interesting because of the polarity differences between HVO and OME or RME. HVO and OME still form homogeneous mixtures at room temperature, but already form a miscibility gap at 20 °C. If RME is added to HVO/OME mixtures, phase separation can be prevented from an admixture of 20%. The aim of the investigations is to discuss the influence of miscibility on the ageing of RME. The respective aged compositions for this are marked as dots in Figure 41. The entire experiment is designed in the simplex lattice design and contains binary mixtures on the triangle sides and ternary mixtures on the triangle surface. In the simplex diagram, each side of the triangle represents the respective admixture of the component from 0 to 100 vol%. The corners of the triangle represent the pure fuels. The midpoint of the simplex corresponds to a composition of 33.3% RME, 33.3% OME and 33.3% HVO. The individual samples are mixed in percent by volume and aged using the petrooxy method. The petrooxy method is chosen here because of the volatility of OME. In the Rancimat, the premature removal of the OME portion would result in a continuous decrease in the OME portion over the ageing period. To avoid this, the samples are aged using the Petroxy method at 130 °C and up to a pressure drop of 20%.

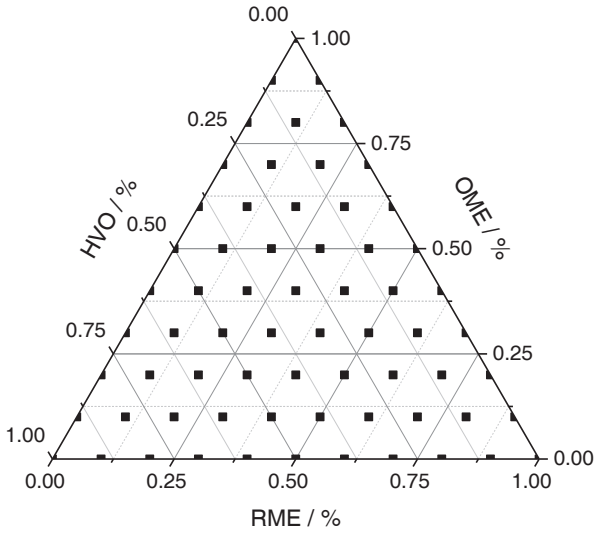

Figure 41: Overview of the aged fuel compositions. Admixture of fuels in percent by volume.

First, the miscibility in the unaged and aged state is considered and in the second step the ageing of RME is examined with high-resolution mass spectrometry and discussed with the miscibility. The miscibility before and after ageing is shown in Figure 42. The colour-coded temperature scale indicates the temperature at which a phase separation occurs. In the unaged state, the binary mixtures of OME and HVO show a phase separation from 20 °C. As the RME proportion increases, the temperature at which the phase separation begins is shifted to lower temperatures. With 10% RME the phase separation temperature is between 0 °C and -5 °C. With 20% RME admixture, a phase-stable mixture is guaranteed down to -20 °C. Depending on the composition, the RME, OME and HVO systems contain temperature-stable mixtures (green area). The ageing of the fuel mixtures changes their miscibility. In general terms, oxidation changes the polarity of the fuel. The three fuel components RME, OME and HVO each have different oxidation speeds. This can be determined by the time it takes for the pressure drop in the Petrooxy to reach 20%. The susceptibility to oxidation decreases from RME (14.31 min) via OME (87.96 min) to HVO (240.13 min). Due to the different oxidation stability of RME, OME and HVO, RME ages preferentially. This can plausibly explain the miscibility in the aged state. The polarity differences between RME, OME and HVO can be illustrated by measuring the permittivity in numbers. HVO has a relative permittivity of ε_r = 2.05, RME of ε_r = 3.27 and OME ε_r = 4.09. The miscibility is improved by adding RME to OME and HVO (phase separation temperature drops to lower temperatures). This is due on the one hand to the polarity between HVO and OME and on the other hand to the amphiphilic structure of RME. This means that RME has a polar ester group and a non-polar alkyl radical. This makes RME the solution mediator between OME and HVO. However, ageing primarily oxidises RME. Oxidation means an increase in polarity, which means that the role of solubilising agent is no longer given with increasing age. As a result, the red area in Figure 42 on the right expands compared to the unaged fuels (left).

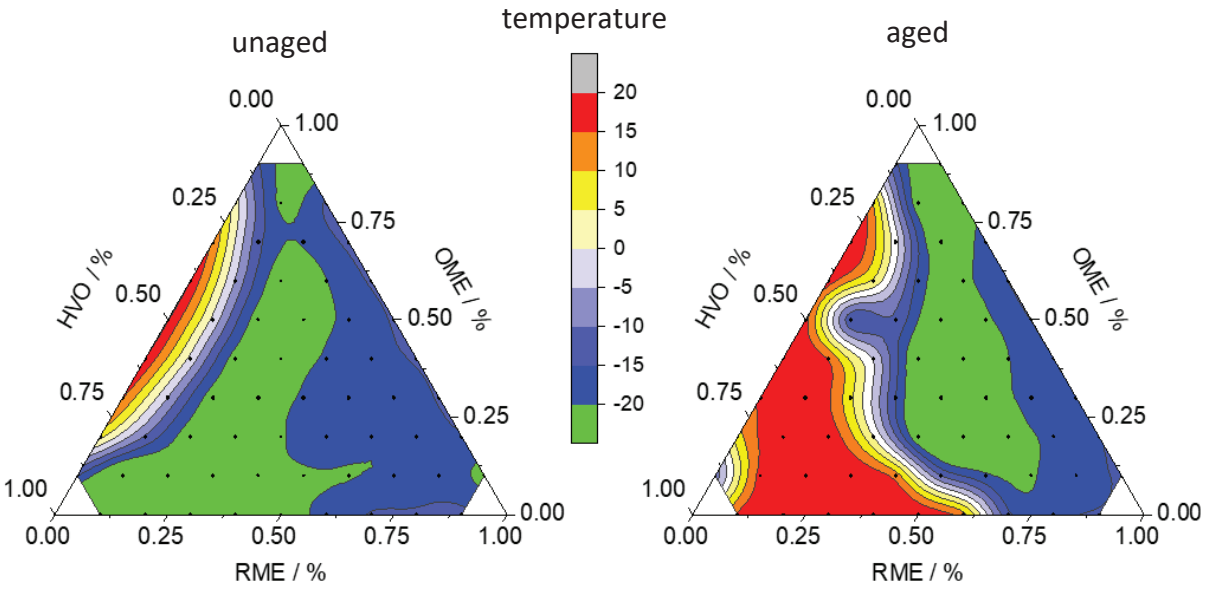

Figure 42: Temperature-dependent phase separation of unaged and aged mixtures of RME/OME/HVO.

The same cause is also present with the binary mixtures of HVO and RME. If the proportion of HVO is high, the polarity of the fuel mixture is relatively low (HVO is non-polar). The oxidation products formed during ageing have a higher polarity. The polarity difference between non-polar HVO and the polar oxidation products leads to a phase separation analogous to HVO/OME mixtures. This general interpretation is deepened in the following by a more detailed consideration of the ageing products. For this purpose, the aged samples are examined using high-resolution mass spectrometry. The investigation specifically relates to the formation of oxidation products from RME. The individual categories of oxidation products are discussed separately. From section 6.3.7 it is known that in the course of the ageing of RME dimer formation only occurs after a certain time. Ageing at 130 °C and a pressure decrease of 20% in the Petrooxy do not yet lead to the formation of longer-chain ageing products. Therefore, only the 1 to 4-fold oxidation products, the formation of short-chain ageing products and the formation of acids are discussed in the following.

6.4.1 Simple oxidation

For the simple oxidation products, four masses with the empirical formulas $C_{19}H_{30}O_3$, $C_{19}H_{32}O_3$, $C_{19}H_{34}O_3$ and $C_{19}H_{36}O_3$ are shown in Figure 43 in four simplex diagrams depending on the composition. The individual empirical formulas describe several compounds (constitutional isomers). This is due to the fact that the oxidation can take place at different positions in the molecule due to multiple double bonds. The precursor compound (C18:1 ME, C18:2 ME or C18:3 ME) can be determined from the sum formulas according to the number of double bond equivalents. $C_{19}H_{36}O_3$ are the oxidation products of C18:1 ME, $C_{19}H_{34}O_3$ of C18:2 ME and $C_{19}H_{32}O_3$ or $C_{19}H_{30}O_3$ of C18:3 ME. The compounds of the empirical formula $C_{19}H_{30}O_3$ differ from $C_{19}H_{32}O_3$ in that the oxidation did not occur with the dissolution of the double bond. Through the targeted investigation of the oxidation products of C18:1 ME, C8:2 ME and C18:3 ME, the formation of the oxidation products can be linked to the solubility.

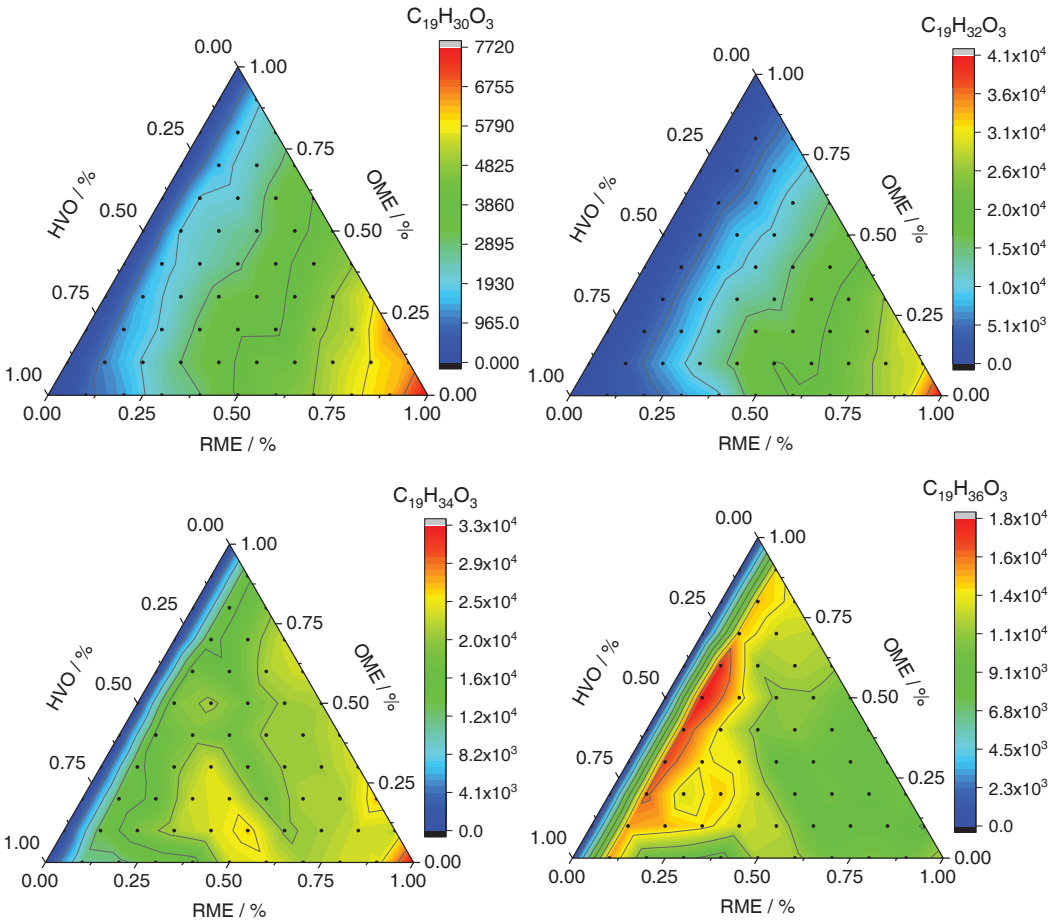

Figure 43: Mixture-dependent intensity profile of the simple oxidation products $C_{19}H_{30}O_3$, $C_{19}H_{32}O_3$, $C_{19}H_{34}O_3$ and $C_{19}H_{36}O_3$.

The fatty acid methyl esters differ in their geometry through the number of double bonds and the resulting different intermolecular interactions. The intramolecular interactions affect the melting points of the individual fatty acid methyl esters. The melting point decreases with an increasing number of double bonds. The double bonds lead to an angled structure, which means that the individual molecules can form fewer interactions with one another. In the mixture with OME, the π bonds lead to a better interaction with polar components. Figure 43 shows the colour-coded intensity as a contour diagram. The representation is selected for each simplex in such a way that the highest intensity is marked with red and the lowest intensity with blue. The intensity scales are different for all simplexes, so the colour gradient only describes the tendency within a simplex. The numerical values given in the legend must be used for the intensity comparison. For $C_{19}H_{30}O_3$ there is a continuous colour gradient in Figure 43 corresponding to the increase in RME. The more RME there is in the sample, the more $C_{19}H_{30}O_3$ is formed. However, this trend decreases as the number of double bonds decreases. $C_{19}H_{30}O_3$ and $C_{19}H_{32}O_3$ each with three double bonds (the difference is only in the form in which the oxygen atom is bound in the molecule) have a similar colour gradient. In the case of $C_{19}H_{34}O_3$ with two double bonds, a more inhomogeneous course with island formation develops. In the case of $C_{19}H_{36}O_3$, the maximum, which was previously 100% RME, is shifted to an admixture of RME of 10%. In the case of the simple oxidation products in Figure 43, the influence of miscibility primarily affects the oxidation products of C18:1 ME. Here the intensity curve clearly shows the miscibility gap from Figure 42. In addition, a clear island formation occurs around the sample with 20% RME/60% HVO/20% OME, which corresponds to the red area shown in Figure 42. This means that an increased solubility-dependent oxidation occurs at C18:1 ME.

6.4.2 Double oxidation

In the case of the double oxidation products (Figure 44), an increasingly inhomogeneous course with stronger island formation can be observed. Only $C_{19}H_{30}O_3$ continues to show a course following the increasing RME share. A dependency on the fuel composition can already be observed with $C_{19}H_{32}O_4$. Because in the double oxidation the reagent has a higher polarity than the non-oxidised fatty acid methyl esters as a result of the first oxidation, the inhomogeneous course is shifted towards the more unsaturated fatty acid methyl esters. Island formation at $C_{19}H_{32}O_4$ roughly follows the phase separation temperature range of below -20 °C in Figure 42 (green area). In the case of $C_{19}H_{34}O_3$, the area around 10% RME admixture is evident in the intensity distribution. Compared to $C_{19}H_{36}O_3$, the range of maximum intensity is shifted towards smaller HVO admixtures and more restricted to a small range of 20 to 40% HVO admixture. Compared to the first oxidation ($C_{19}H_{36}O_3$), $C_{19}H_{36}O_4$ shows an increasingly homogeneous course. The maximum is at 100% RME. With 10% RME admixture, only a local maximum is formed at 10% RME/50% OME/40% HVO. The measurements of the double oxidation products show that ageing has different effects on the different masses. In addition, the primary oxidation already influences the further oxidation behaviour.

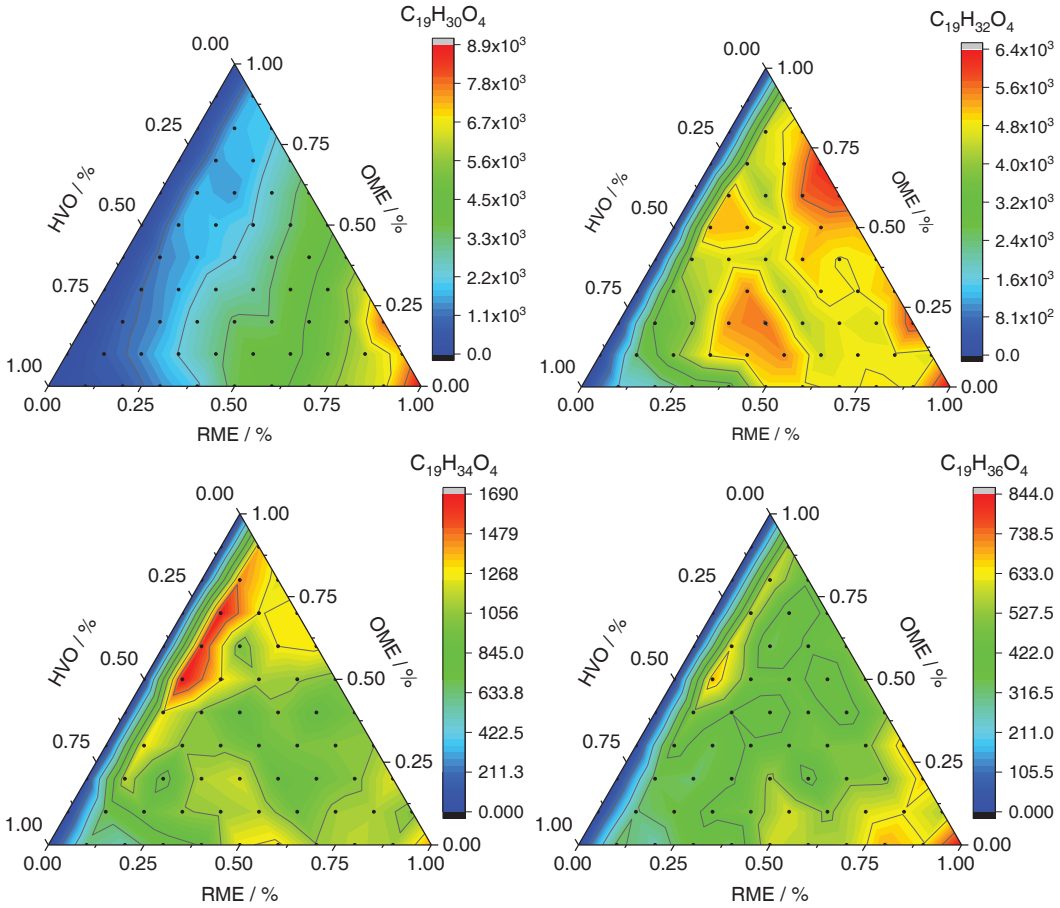

Figure 44: Mixture-dependent intensity profile of the double oxidation products $C_{19}H_{30}O_4$, $C_{19}H_{32}O_4$, $C_{19}H_{34}O_4$ and $C_{19}H_{36}O_4$.

6.4.3 Triple oxidation

In the case of triple oxidation, the consideration is limited to three empirical formulas, since for C18:1 ME a triple oxidation can no longer be observed during this ageing process (Figure 45). $C_{19}H_{30}O_5$ still shows a homogeneous course according to the RME share. The radical stability offers a conceivable explanation for this constant course. For $C_{19}H_{30}O_5$, the time courses shown in Section 6.3 show that

formation began much earlier and that the intensity was generally higher. The mesomeric stabilisation occurring over several carbons and one oxygen atom in the double oxidation is given as an explanation. Due to the greater stability, the reactivity decreases, as a result of which this oxidation is no longer so strongly diffusion-controlled. Any influence of the hydration shell and the associated diffusion of molecular oxygen to the molecule would therefore have less of an influence on the oxidation. This assumption is supported by the fact that the formation of the hydration shell depends on the solvent composition (fuel composition). In the case of $C_{19}H_{32}O_5$, a clearly pronounced island formation can be observed, which can no longer be explained by the miscibility. The same also applies to $C_{19}H_{34}O_5$, whereby the maximum here is 40% RME/60% OME. However, due to the low intensity, a deeper discussion is difficult.

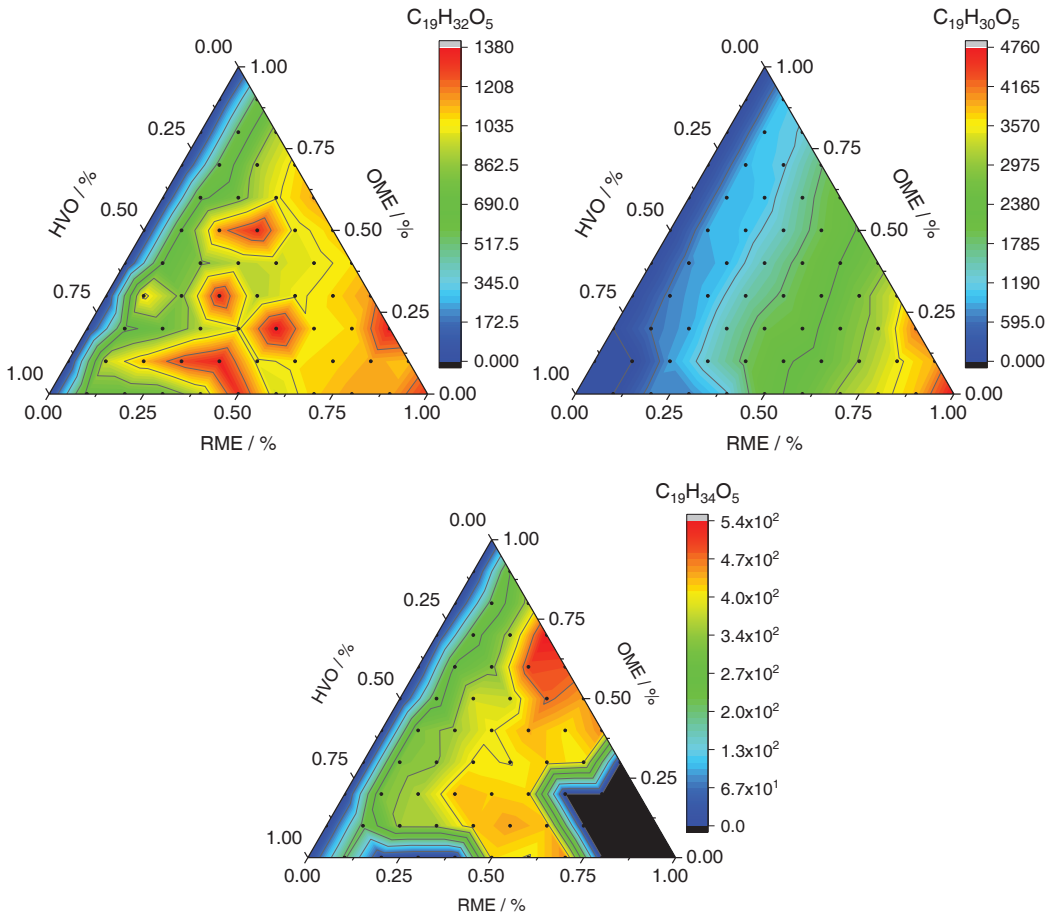

Figure 45: Mixture-dependent intensity profile of the triple oxidation products $C_{19}H_{32}O_5$, $C_{19}H_{34}O_5$ and $C_{19}H_{36}O_5$.

6.4.4 Fourfold oxidation

The fourfold oxidation (Figure 46) only occurs with the oxidation products starting from C18:3 ME. Therefore, the fourfold oxidation is reduced to the empirical formulas $C_{19}H_{28}O_6$ and $C_{19}H_{30}O_6$. In the case of $C_{19}H_{28}O_6$ and $C_{19}H_{30}O_6$, there is again an increasing dependence on the phase stability of the samples. In the red area of the aged fuels in Figure 42, where the samples are already cloudy at room temperature, no fourfold oxidation products are formed. With $C_{19}H_{28}O_6$ the maximum is 100% RME whereas with $C_{19}H_{30}O_6$ the maximum is shifted towards binary OME/RME. $C_{19}H_{28}O_6$ differs from $C_{19}H_{30}O_6$ by one double bond equivalent. This means that in the case of $C_{19}H_{28}O_6$ with fourfold oxidation there are more reactive positions at which the oxidation can occur. In the fourfold oxidation step, $C_{19}H_{28}O_6$ has two double bonds for easy oxidation and $C_{19}H_{30}O_6$ has only one. The effect of the double

bonds can also be seen in the intensity with which both compounds generally occur ($C_{19}H_{28}O_6$ > $C_{19}H_{30}O_6$). In the case of stable radicals, i.e. compounds that prefer to oxidise, the miscibility or the polarity of the fuel matrix has less of an effect on the oxidation. The result is a homogeneous curve that follows the RME component. If the radical stability is low and the reactivity is consequently high, the fuel matrix has an effect on the formation of the ageing products.

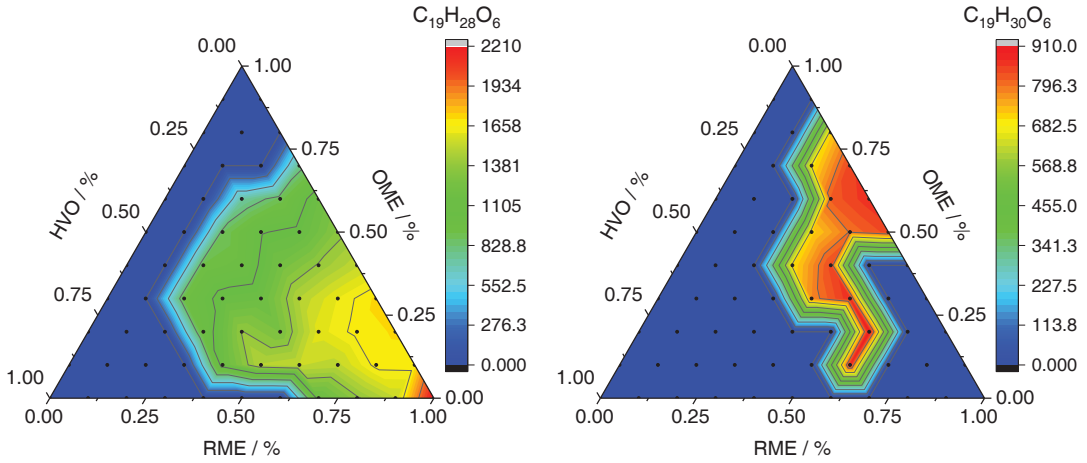

Figure 46: Mixture-dependent intensity profile of the fourfold oxidation products $C_{19}H_{28}O_6$ and $C_{19}H_{30}O_6$.

6.4.5 Short-chain degradation products and acids

The last category of ageing products are short-chain degradation products (Figure 47), which are composed of acids ($C_{18}H_{28}O_2$, $C_{18}H_{30}O_2$ and $C_{18}H_{32}O_2$) and breakdown products ($C_{13}H_{20}O_4$, $C_9H_{14}O_3$ and $C_{10}H_{16}O_3$). The formation of acids (ester hydrolysis) is another reaction in which the miscibility influences the formation. With $C_{18}H_{28}O_2$ (starting from C18:3 ME), as with $C_{18}H_{30}O_2$ (starting from C18:2 ME), there is a homogeneous course corresponding to the RME proportion. At C18:1 ME, the maximum of the intensity is again found at 10% RME with $C_{18}H_{32}O_2$. The same influence of miscibility can be seen as with simple oxidation. The investigations show that not only radical reactions that lead to oxidation, but also ester hydrolysis due to the polarity of monounsaturated fatty acid methyl esters has an effect. The formation of short-chain degradation products follows a homogeneous course, in which the formation increases with an increasing proportion of RME.

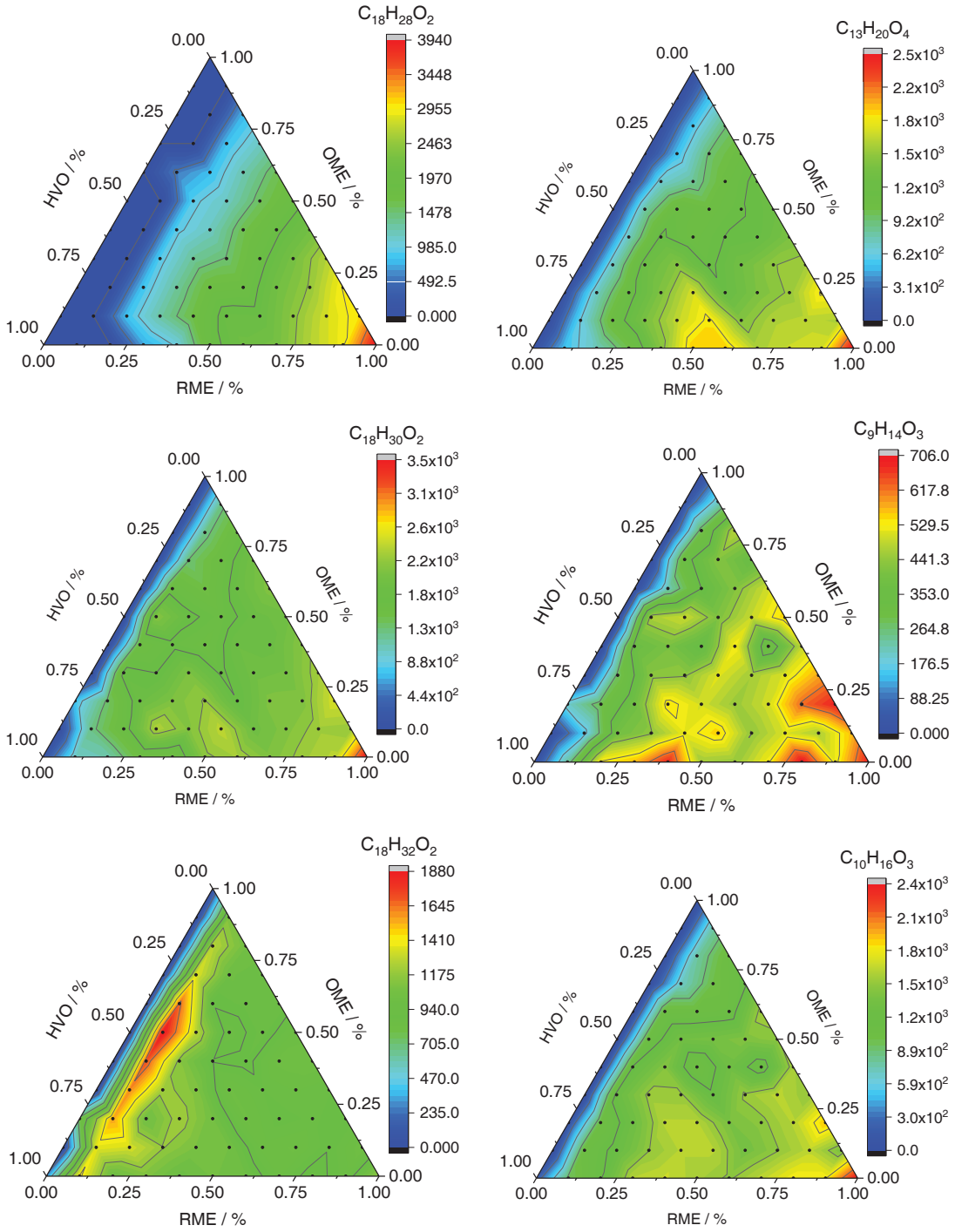

Figure 47: Mixture-dependent intensity profile of the short-chain degradation products (right) and acids (left).

6.4.6 Influence of the volume fraction of RME

With the mass-selective investigation of the RME ageing depending on the admixture components OME and HVO, it becomes clear that the miscibility has an influence on certain ageing products. With this selective consideration, the question arises as to how the miscibility in total affects the ageing behaviour. For this purpose, the sum of all examined masses is plotted in. The representation of the intensity scale is replaced by a standardised representation in Figure 48. The standardised representation enables a comparison between RME as pure fuel and the RME admixtures, in which the intensities are normalised to the value of pure RME. For easier traceability, the intensities, relative to

pure RME, are also given in percent. The sum of the ageing products shows an almost homogeneous course corresponding to the RME share. The inhomogeneous course of the oxidation ($C_{19}H_{36}O_3$) and the ester hydrolysis ($C_{18}H_{32}O_2$) of C18:1 ME only have a minimal effect on the course in Figure 48 due to the large number of other products. However, if the percentage course is included in the evaluation, it becomes apparent that disproportionate ageing occurs in the entire Simplex. With an admixture of 10 vol% RME, the specification of the ageing products gives a value of 25% RME. With an increasing RME share, the disproportionate ageing decreases accordingly. An exception is the range between 40 and 60% RME admixture, in which ageing between 50 and 60% can be observed over an admixture range of 20 vol%. The admixture of OME and HVO generally leads to stronger ageing per volume fraction of RME compared to pure RME. The effect of the miscibility on the ageing behaviour can be made visible from the sum of the ageing products in Figure 48 by a normalisation to the RME portion, which is shown in Figure 49. This means that the disproportionate percentage of ageing can be read off for all compositions in the Simplex.

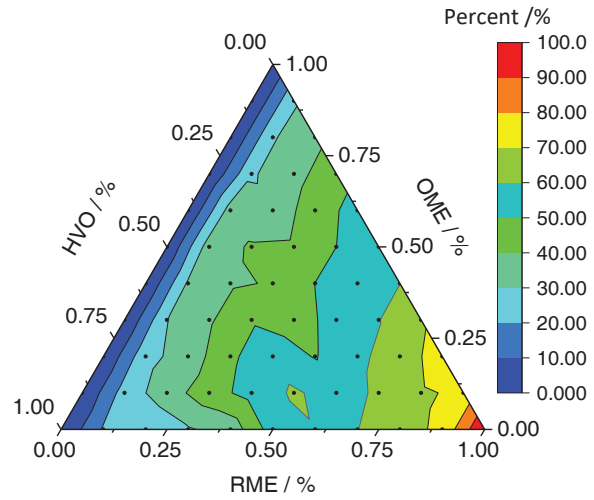

Figure 48: Mixture-dependent percentage intensity profile of the sum of the individual masses. Normalised to the ageing of pure RME.

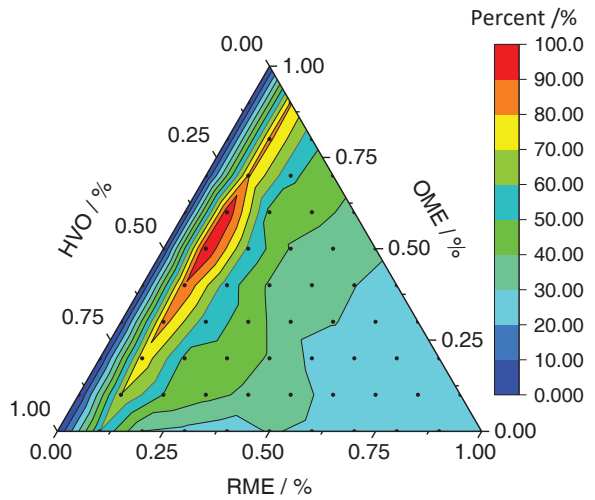

Figure 49: Mixture-dependent percentage intensity curve per 10% volume fraction RME. Representation in percent and normalisation to the maximum intensity value.

The curve in Figure 49 shows the disproportionate range of ageing. The ageing of 10 vol% RME is shown for each point in the simplex. The ageing per 10 vol% RME is standardised to the greatest disproportionate ageing that occurs. The representation in Figure 49 enables a simple assessment of the disproportionate influence, which has only a relative meaningfulness due to the further normalisation. The absolute disproportionate ageing must be taken from Figure 48. Due to the relative representation, however, small changes in the disproportionate ageing can also be represented. The relative representation in Figure 49 shows that with a composition of 10% RME and 50% OME /40% HVO or 60% OME /30% HVO, the disproportionate ageing is at the maximum. Within the 10% RME admixture, ageing decreases again starting from the maximum. The course with the maximum of ageing per volume fraction corresponds to the miscibility gap that forms at 10% RME starting from and 50% OME /40% HVO or 60% OME /30% HVO at low temperatures. On the basis of the phase separation studies in Figure 42, the composition at the maximum represents the compositions which have the worst miscibility. The simplex can be divided into two areas according to the course in Figure 49. The first area includes the region with 10 and 20% RME admixture, in which ageing occurs more intensely and the miscibility at low temperatures (down to -20 ° C) is not completely given. The second area comprises the high RME admixtures from 60% RME, in which the disproportionate ageing is the lowest.

Together with the influence of the phase separation from Figure 42, the optimum fuel composition can be specified with 60% RME /20% OME /20% HVO in the RME/OME/HVO system from Figure 49.

With the presented results of the mixture-dependent ageing it could be clearly shown that the fuel composition has an influence on the ageing. An optimised fuel formulation thus represents a concept for improving the ageing stability, which increases synergistically with an additive with antioxidants. If the composition minimises oxidation, the added antioxidants are also used up more slowly. With the addition of RME, however, it must be considered that with more RME, there is also more easily oxidisable fuel in the formulation. That means the induction time is shortened by more RME with the same additives. The influence of polarity on ageing is antagonistic to the induction time. If the RME proportion is reduced, the mixing stability decreases and the induction time increases with less RME. If the RME proportion is increased, the mixing stability increases, the induction time decreases, but there is an improved ageing stability per volume portion of RME. Especially for the mixtures of RME/OME/HVO, the stability of the mixture must primarily be considered due to the polarity differences of the components. In the context of a stable mixture, however, the ageing stability can then be optimised in a targeted manner. The RME/OME/HVO system offers enough degrees of freedom that fuel availability can also be considered when optimising.

7 additive tests

The investigations in Section 6 clearly show that fuel ageing at RME leads to a considerable chemical change, which in turn causes a change in physical parameters such as density and viscosity. For this reason, the addition of additives to fuels is of particular importance. The ageing stability of fuels is determined either with the Rancimat test or the Petrooxy test. The measurement parameter is the induction time, which indicates from which time the antioxidants are used up. In the search for new antioxidants, the acid formation that occurs during the ageing of fuels is used as a starting point. Many ongoing reactions can be catalysed by the addition of acids. [52] If the acid in the fuel is trapped by the addition of a basic antioxidant, the ageing reactions should slow down. This applies above all to fatty acid methyl esters, which can form so-called free fatty acids through ester hydrolysis. [53] This means that with FAME two reactions have to be considered. On the one hand ester hydrolysis, which can be accelerated by temperature and acid, and on the other hand oxidation by molecular oxygen. In the following, tributylamine (TBA) is examined as a basic compound for its antioxidant properties. In the first part, the influence of TBA on acid formation and oxidation is determined using high-resolution mass spectrometry. In the second part, TBA is examined for synergistic effects with six other commercially available additives.

To investigate the influence of acid formation and oxidation, a mixture of 80% RME and 20% OME is used as fuel. In the case of fuel mixtures of RME and OME, Section 6 shows that there is disproportionate ageing. Therefore, the mixture is ideally suited here to investigate the influence of TBA. The mixture of RME and OME is aged in the Petrooxy at 130 °C for 2 hours. The acid number is then determined for the aged fuel mixture of 80% RME and 20% OME. The amount of TBA that neutralises the aged sample is determined from the acid number determined. The determined amount of 195.9 mg TBA is added in a second ageing of the 80% RME and 20% OME fuel mixture and also aged for 2 hours. The studies with high-resolution mass spectrometry show that the addition of TBA reduces oxidation (Figure 50).

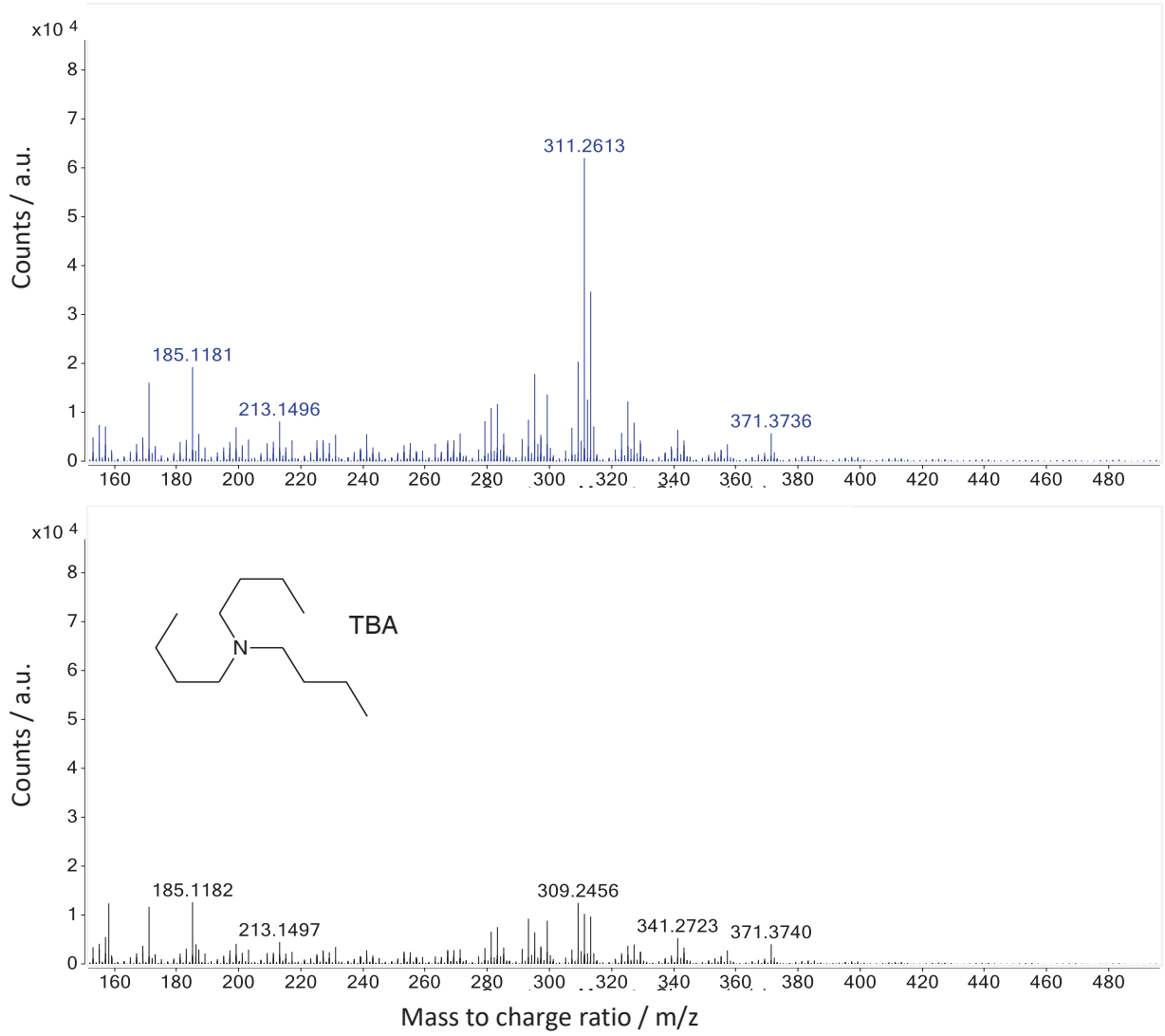

Figure 50: 2 hours mass spectra in the petrooxy aged fuel mixture of 80% RME and 20% OME. The mass spectrum shown above shows the ageing without additives. The mass spectrum shown below shows the ageing with the addition of tributylamine (TBA).

The formation of the simple oxidation product with a mass to landing ratio of m/z = 311.2613 is increased by a factor of 5 without TBA. In general, a reduction in the simple oxidation products can be observed in particular. The addition of TBA also has an impact on the formation of short-chain degradation products (for example: m/z = 185.1181 and m/z = 213.1496). The formation of multiple oxidation products is approximately 2 times below that of ageing without TBA. The mass spectrum of ageing with TBA can also be used to detect how TBA changes chemically as a result of oxidative stress. $C_8H_{18}NO$ can be identified as a breakdown product of TBA ($C_{12}H_{27}N$). It is the oxidised fragment of TBA. This means that the antioxidant effect is due to the oxidation of TBA, which competes with the fuel. In addition, acid formation during ageing with TBA can be compared with ageing without TBA. The acid number or the pH value of the ageing sample is not determined here, as this is not in the acidic range due to the addition of base. Rather, the dissociated acids of the free fatty acids are recorded. It can be determined that the formation of acid is less when TBA is added than when ageing without TBA. The formation of the selected acids is directly compared in Figure 51. With all acids, the intensity with the addition of TBA is below the ageing without TBA. All in all, it can be concluded that the neutralisation of acid formation and the competitive oxidation between TBA and fuel have a positive effect on acid formation and the formation of oxidation products.

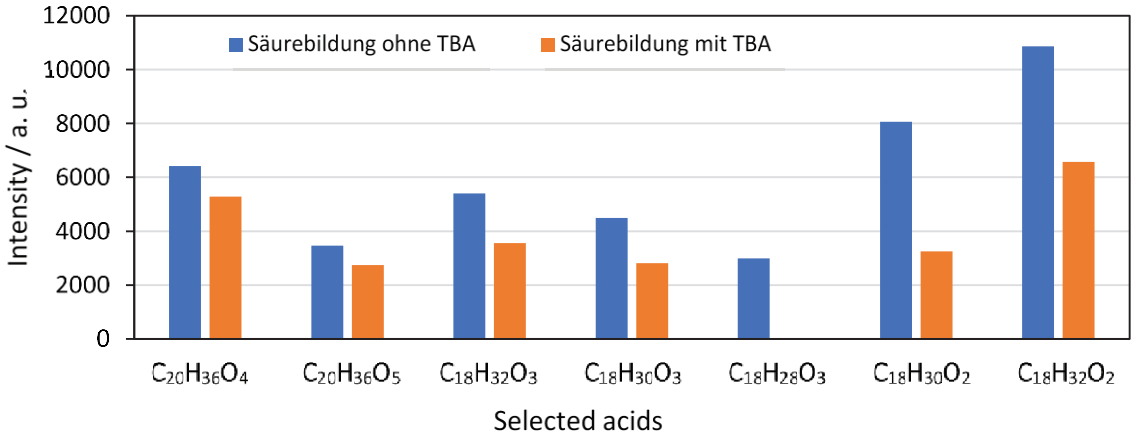

Figure 51: Selected acid formation during ageing of 80% RME and 20% OME with and without TBA.

The next step in studying TBA as a basic additive is to determine synergistic effects with other antioxidants. Synergistic effects exist when, due to the combination of two or more additives, the induction time of the combined additives is higher than the sum of the individual additives. For this reason, additive combinations consisting of three different additives are being investigated. Tributylamine (TBA) is used as a basic additive and combined with six other antioxidants (Figure 52).

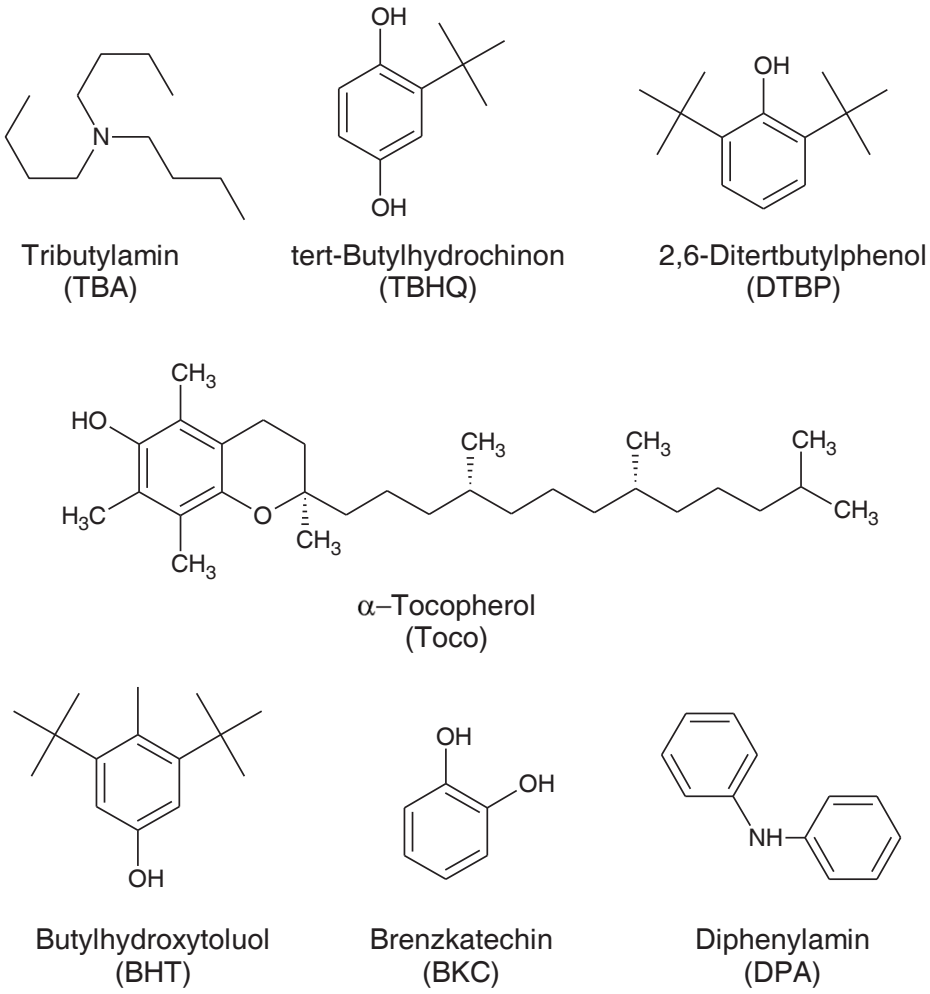

Figure 52: Structural formulas of the additives used in the investigation of the synergistic effects when combining different additives.

The selection includes commercially available antioxidants such as butyl hydroxyl toluene (BHT), tert-butyl hydroquinone (TBHQ), 2.6-di-tert-butylphenol (DTBP), catechol (BKC) and diphenylamine (DPA) as well as the natural antioxidant α-tocopherol (Toco). Because α-tocopherol is a naturally occurring antioxidant in the RME, a specially distilled RME that no longer contains any natural antioxidants is used for the investigations. The selection of α-tocopherol as the additive to be tested is of particular interest, since it occurs naturally in RME and therefore does not have to be added. Synergistic effects with α-tocopherol therefore represent a significant effect for economic reasons. The comparison of TBA with diphenylamine (DPA) is important for a further classification of the effectiveness of TBA. Since both compounds are based on nitrogen, the synergistic effects can possibly prove or disprove a similar mode of action.

To determine the synergistic effects of the seven compounds in Figure 52, the induction times of the pure substances and combinations of three are determined separately in the Rancimat test. For this purpose, 3 g RME are mixed with 1000 ppm additive and aged at 110 °C and 10 L air flow per hour. This means that when the additive is used in its pure form, 1000 ppm are added. In the case of the three combinations, 333 ppm of all three additives are mixed in. To determine the synergistic effect of the three combinations, each individual additive must also be tested once with 333 ppm. If you add the induction times of the three individual compounds of a combination of three and compare this with the ageing, in which 333 ppm of all three compounds are mixed in at the same time, the difference in the induction times represents the synergistic effect. The results of the investigations are shown in Figure 53. In Figure 53, the sum of the induction times of the individual compounds is plotted on the y-axis and the induction time of the three combinations when used simultaneously on the x-axis. If there are no synergistic and antagonistic effects, the results are exactly on the blue line. If the measuring point of the three-way combination is below the blue line, there are synergistic effects. If the measuring point is above the blue line, antagonistic effects occur. The pure substances are exactly on the blue line, since the sum here is equal to the determined induction time. Of the seven additives tested, TBA had the lowest induction time in the Rancimat test. Taking into account the mass spectrometric investigations, in which a reduced formation of oxidation products can be detected, it can be concluded that the decay products of TBA are discharged from the system and lead to an increase in conductivity. For this reason, the results must be interpreted with particular care. The competitive oxidation of TAB with the fuel leads to compounds that indicate ageing in the Rancimat test, but do not have the negative effects of aged fuel molecules (increase in viscosity, dimerization). For this reason, the most important interpretation lies in the occurrence of synergistic effects and not in the best induction time. DPA shows induction times similar to those of TBA in pure form. Therefore, the comparison between TBA and DPA, as an established antioxidant, is specifically discussed. In general, the great majority of the combinations show synergistic effects (measuring point below the blue line). The three-way combinations, in which TBA and DPA can be compared, are marked in colour in Figure 53 for the sake of simplicity. A comparison shows that TBA in combination with BHT and BKC or with TBHQ and Toco shows stronger synergistic effects than DPA. Conversely, DPA shows greater synergistic effects with TBHQ and BHT or TBHQ and BKC. From this it can be concluded that the use of TBA depends on the combined additives. This is of particular importance from two points of view. On the one hand, α-tocopherol occurs as a natural antioxidant in the RME, which results in a positive effect without additional additives. On the other hand, TBHQ has the largest induction time of the pure substances examined and also shows synergistic effects with α-tocopherol. The synergistic effects of TAB with α-tocopherol and TBHQ, together with the reduction in acidity during ageing, lead to long induction times and prevent secondary oxidation reactions due to the lack of acid catalysis. According to these investigations, TBA is a promising additive for RME.

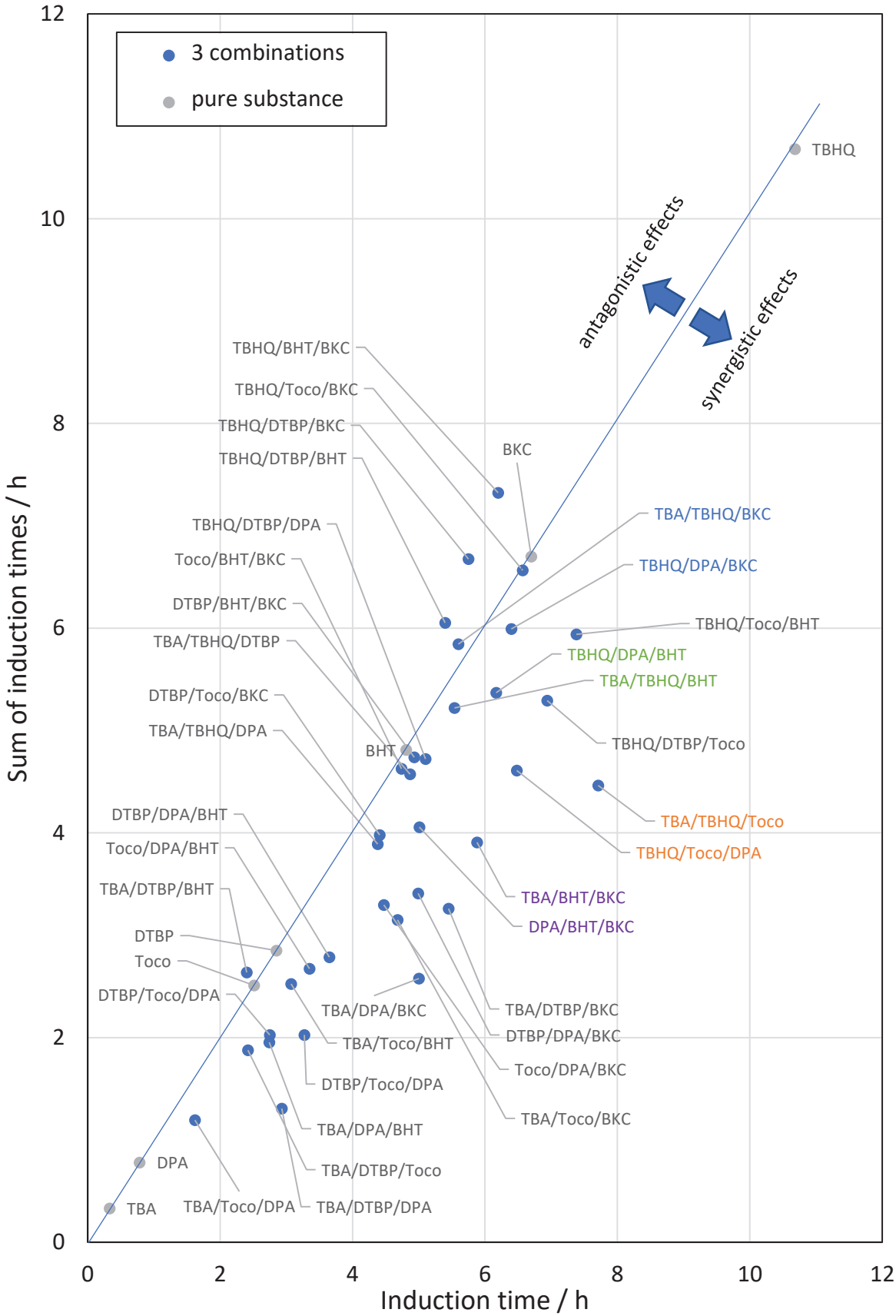

Figure 53: Investigation of the synergistic effects with three additive combinations. For this purpose, the induction time of the three combinations of additives is plotted against the sum of the induction times of the individually used additives (with the same concentration)

8 Developed fuel sensors

The developed fuel sensor system consists of a combination of a dielectric and an optical unit (see Figure 54). The dielectric unit measures the permittivity and optionally the conductivity of the filled fuel. The optical unit enables near infrared spectroscopy, fluorescence spectroscopy and, optionally, absorption spectroscopy in the visible light spectrum of the sample. The structure and functionality of the dielectric sensors (Figure 54 below) and the optical sensors (Figure 54 above) are described in Chapters 4.5.1 and 4.5.2. The advantages that result from the combination of the various measuring methods are discussed in more detail in Sections 8.2 and 8.3. Due to the modular structure, the two units can be installed and used both in combination in the same place and separately from each other.

The in-house developed measuring electronics are connected to the existing electrical connections, which communicate with a PC via USB and transfer the measured data. The miniaturised light sources and optical measuring devices for performing the optical measuring processes are connected to the five fibre optic connections.

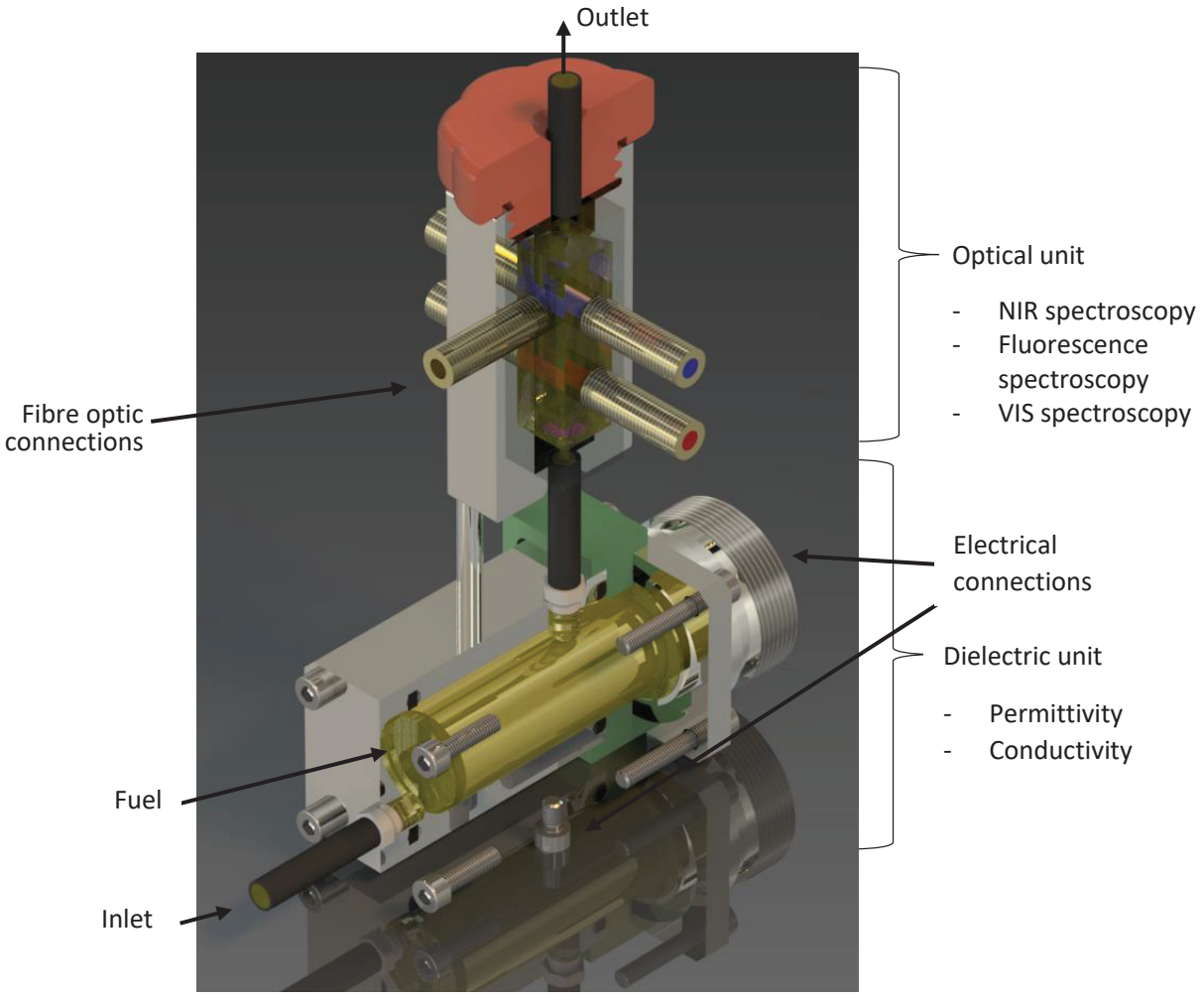

Figure 54: Partial section of fuel sensors (light sources and evaluation sensors not connected); above: optical unit (red-grey); below: dielectric unit (green-grey)

8.1 Empirical variance and measurement accuracy of the developed sensors

The following section deals with the measurement data of the different measurement principles integrated in the fuel sensor and their measurement uncertainty. First, the dielectric measurements of the permittivity at 100 kHz and the conductivity are analysed in Section 8.1.1 and then the optical measurements (NIR absorption spectroscopy, fluorescence spectroscopy and VIS absorption spectroscopy) in Section 8.1.2. The random measurement uncertainty of the measurement data is calculated from measurement series with n repetitions. The random measurement uncertainty (u_x) of the individual measurement (x_i) can be calculated under the assumption of a normal distribution of the measurement deviation using the Student's t-distribution, the empirical variance s_x and the expected value ($\bar{x}$) of a measurement series and given for a confidence interval of 95%:

$$\boldsymbol{s_x^2} = \frac{\boldsymbol{1}}{\boldsymbol{n-1}} \sum_{\boldsymbol{i=1}}^{\boldsymbol{n}} |\boldsymbol{x_i} - \boldsymbol{\bar{x}}|^2 \tag{11}$$

$$\boldsymbol{u_x = t_{95} \cdot s_x} \tag{12}$$

Based on the calculated uncertainties, a meaningful measuring range of the individual measuring methods of the sensor system can be specified and the significance of differences between two samples can be assessed.

8.1.1 Dielectric measurements (permittivity and conductivity)

In the following section, the data and the measurement uncertainty of the dielectric unit of the fuel sensor are analysed. The total measurement uncertainty of the dielectric measurements depends on the one hand on the measurement uncertainty of the measurement electronics, and on the other hand on the scattering of the measured variable within the sample, as well as the type of cleaning of the sensors.

The results of three different series of measurements (A to C) are plotted in Figure 55 in order to examine the influence of the different disturbance variables more closely. The permittivity ϵ_r' at 100 kHz is plotted on the x-axis and the conductivity σ of the fuel sample, measured with the dielectric sensor system, on the y-axis. The crosses correspond to the expected value of the sample and the error bars to the calculated random measurement uncertainty of a measurement for a confidence level of 95%. In the following, the various series of measurements A to C are first described and then the conclusions that can be drawn from the data are discussed.

In measurement series A, a rapeseed oil methyl ester (RME) is poured into the fuel sensor and a measured value is recorded a total of 50 times every 10 seconds. In measurement series B, the sensor is emptied and refilled with the same sample between the 10 individual measurements. Before the series of measurements, the sample is homogenised by shaking it, in order to avoid measurement deviations occurring during the individual measurements, especially with previously stored fuels due to the effects of deposits or phase formation. Measurement series C is analogous to measurement series B with the addition that the dielectric sensor (see section 4.5.1) is cleaned with acetone as the solvent between the individual measurements. The acetone dissolves any residues from the previous sample and rinses them out of the sensor. The solvent itself is then expelled from the sensor with the help of a stream of air. During the 3 series of measurements, the temperature of the sensor is kept constant at ±0.3 °C. However, the average temperature of the three different series of measurements varies between 20.4 and 21.6 °C.

The shift in the mean value of the measurement series A to C (see Figure 54) is caused on the one hand by this temperature difference and on the other hand by the scattering of the sample itself. Furthermore, in the measurement series B and C, the number of repeat measurements is reduced to n = 10 in order to reduce the time required. The effect of n on the measurement uncertainty is taken into account statistically in Student's t distribution.

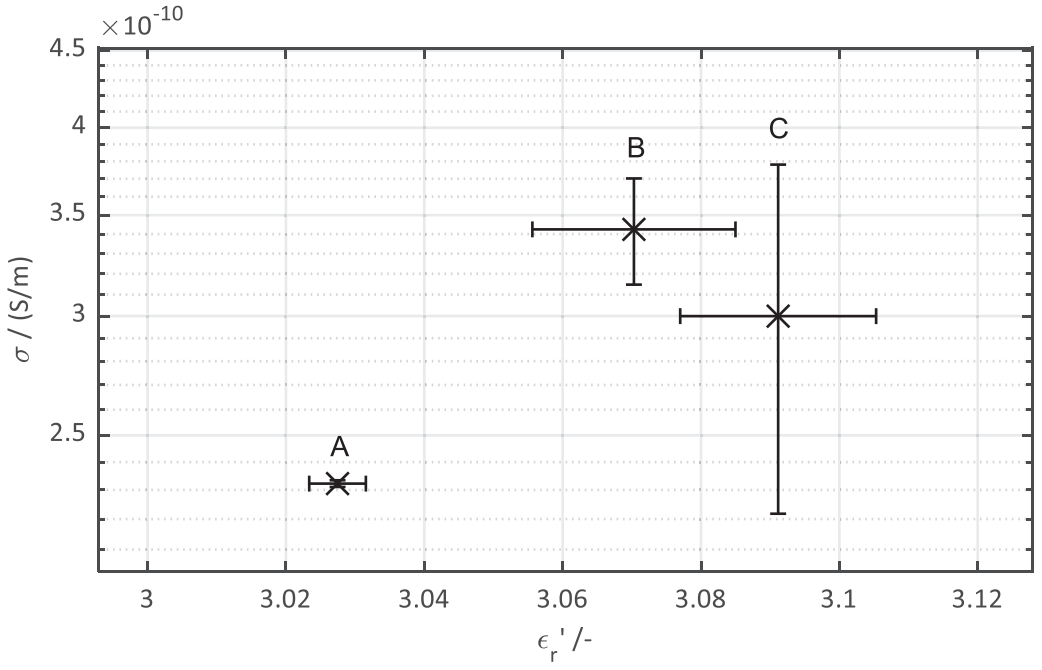

A: Measurement uncertainty of the measurement electronics (RME, n = 50)
B: Measurement uncertainty with refilling (RME, without sensor cleaning, n = 10)
C: Measurement uncertainty with new filling and acetone as solvent during cleaning (RME, n = 10)

Figure 55: Mean value and random measurement uncertainty of the conductivity and permittivity measurements of various measurement series based on n repetitions and a confidence level of 95%

Assuming that the sample does not change during measurement series A within the 500 seconds measurement time, the measurement uncertainty of A corresponds to that of the measurement electronics developed. For the confidence level of 95% there is a measurement uncertainty of:

$$u_{\varepsilon_r',meas} < \pm 0.005 \qquad and \qquad u_{\sigma,meas,rel} < \pm 1\ \%.$$

The measurement uncertainty of the conductivity measurement is given here in relative terms, as the electronics have four measuring ranges within the total measuring range from $10^{-13}\,\frac{S}{m}$ to $10^{-9}\,\frac{S}{m}$ between which it is automatically switched, and is valid in measuring range 2.

A comparison of the measurement uncertainty of A and B shows that the variance of the sample itself is many times greater than the measurement uncertainty of the electronics. The measurement uncertainty increases here to:

$$u_{\varepsilon_r',sample} \approx \pm 0.015 \qquad u_{\sigma,sample,rel} \approx \pm 8\ \%.$$

The cleaning process with acetone as the solvent, as used in measurement series C, does not affect the measurement accuracy of the permittivity measurement. Compared to most fuels, however, acetone has a high conductivity in the range of $10^{-8}\,\frac{S}{m}$, which is why even small amounts of acetone in the sensor can impair the conductivity measurement. This effect can be recognised by the increased

measurement uncertainty of the conductivity of measurement series C in Figure 55. When analysing fuels, however, the order of magnitude of the conductivity is usually sufficient. The advantages of the much faster and easier cleaning with solvents and the avoidance of old sample residues outweigh the disadvantages of the slightly increased measurement uncertainty in the conductivity measurement for the majority of the measurement tasks. If a higher accuracy is required for the conductivity measurements, a less conductive solvent such as cyclohexane can still be used.

In summary, the measuring accuracy of the developed measuring electronics u_{meas} clearly exceeds the variance of the measured values of the RME sample (u_{sample}). Therefore, when taking measurements, particular attention must be paid to sampling and sample handling in order to ensure a high level of measurement accuracy. Furthermore, a possible cleaning process with solvents has been validated, which enables an automated measuring process for the dielectric sensor unit.

8.1.2 Optical measurements (near infrared, fluorescence and VIS spectroscopy)

In the following section, the measurement uncertainty of the optical unit of the fuel sensor is analysed using sample measurements. First of all, the near infrared (NIR) measurements are discussed, then the fluorescence measurements and finally the absorption measurements in the visible light spectrum. The total measurement uncertainty of the optical measurements depends on the light source and detector used, but also on the sample itself. Fluctuations in the light source (thermal drift) in the NIR measurement can be significantly reduced by a sufficient preheating time of around 45 minutes (before the calibration measurement). The measurement uncertainty of the detectors can be achieved by optimising the light intensity that strikes the sensor. There is the possibility of changing the light path in the sample by using different cuvettes or changing the exposure time of the detector.

The analysis of the measurement uncertainty is carried out for each measurement principle using two series of measurements with n = 10 repetitions of a sample in the fresh state and the same sample after ageing for 48 hours according to the Rancimat method (see Section 4.1.1). This comparison illustrates, on the one hand, the change in the fuel with thermo-oxidative ageing and, on the other hand, the measurement uncertainty of the unitless quantities of absorbance and fluorescence can be better classified by comparing two similar samples. A conventional quartz cuvette with a light path of 10 mm in the sensor housing is used for each of the measurements.

The results of the series of measurements for each measurement principle are plotted against the wavelength in the following three graphs (Figure 56 to Figure 58). The black lines (dashed/solid) each describe the mean value of the (fresh/aged) sample. The grey lines (dashed/solid) show the upper and lower limits calculated from the respective measurement series for a confidence interval of 95%.

First, the measurement uncertainty of the NIR absorption spectroscopy of the fuel sensor is examined. The sensor structure is described in more detail in Section 4.5.2. Figure 56 shows the absorbance of a fresh and an aged sample over the wavelength λ. The main graph was scaled to the relevant area of the spectrum in order to be able to show the differences between the fresh and the aged sample as well as the areas of the 95% confidence level. If you compare the measured values of the fresh sample with those of the aged sample, considering the limits of the 95% confidence level, you can see that the NIR sensor unit used can measure significant differences between the aged and fresh sample. Several absorption bands can be seen in the spectrum, in which the two samples clearly differ from one another. The measurement data are not traced back to specific sample components at this point. The evaluation of the fuel composition using the sensor data is described in more detail in Section 8.2.

The entire measuring range of the detector from 1300 nm to 2600 nm is also shown at the bottom right in small in Figure 56. At wavelengths above 2300 nm, on the one hand, the light yield of the

halogen lamp, which is used as excitation in the NIR measurements (see Section 4.5.2), is too low and, on the other hand, the absorption of fuels is very high. The consequence of this is that the measurement uncertainty is significantly increased at longer wavelengths and should therefore not be included in the evaluation. Some fuels also have a high absorbance > 2.5 in the range from 1680 nm to 1780 nm, which can also increase the measurement uncertainty in this range.

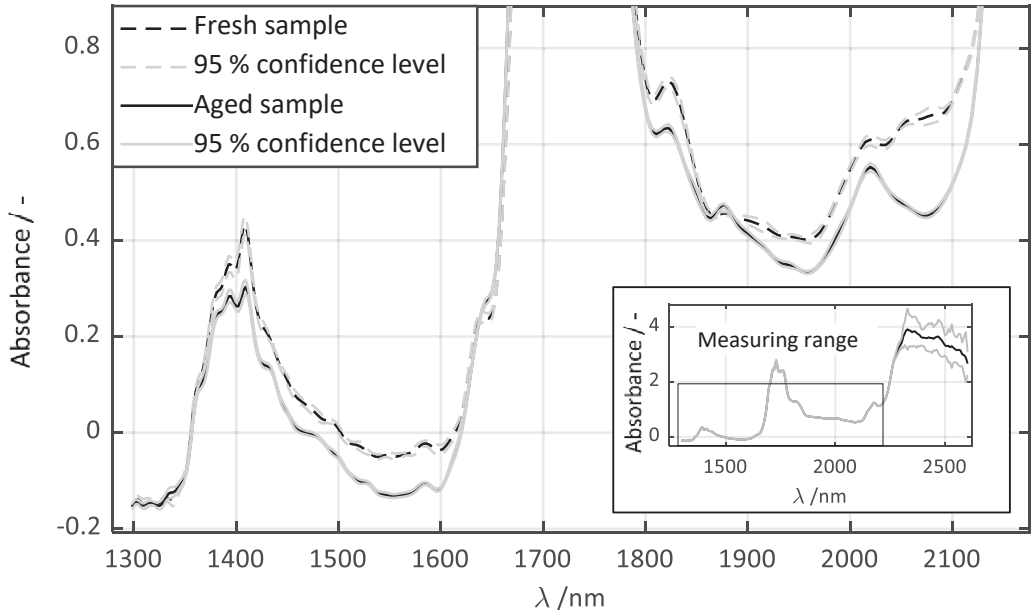

Figure 56: Exemplary measurement data and measurement uncertainty of the near-infrared absorption spectroscopy of the fuel sensor for a fresh and an aged fuel sample in a standard cuvette with a 10 mm light path

Figure 57 shows the measurement data of the fluorescence unit (see section 4.5.2) of the fuel sensor for a sample in the fresh and aged condition analogous to Figure 56. The fluorescence in counts (maximum 1024) is plotted on the y-axis of the graph and the wavelength λ is plotted on the x-axis. The detector exposure time of the two measurement series is 1s and the thermal noise of the detector is compensated by subtracting the measurement values of an empty cuvette from the sample measurement values. A significant difference in the measurement data between the fresh and the aged sample can also be determined with the fluorescence measurements. The fluorescence here has increased due to the ageing of the sample.

Finally, the measurement data of the optional absorption spectroscopy in the visible wavelength range of light are plotted in Figure 58 (see Section 4.5.2). Similar to NIR absorption spectroscopy, the spectrum of the detector must also be restricted for the VIS measurements due to the light source used. The fuel sensor automatically determines the maximum possible spectrum of the VIS measurements based on an empty measurement. For most samples, the built-in light emitting diode produces a measurable spectrum of around 420 nm to 680 nm. In the case of the two samples used here, the information content of the VIS measurements corresponds to that of the fluorescence measurement - absorption and fluorescence occur at similar wavelengths.

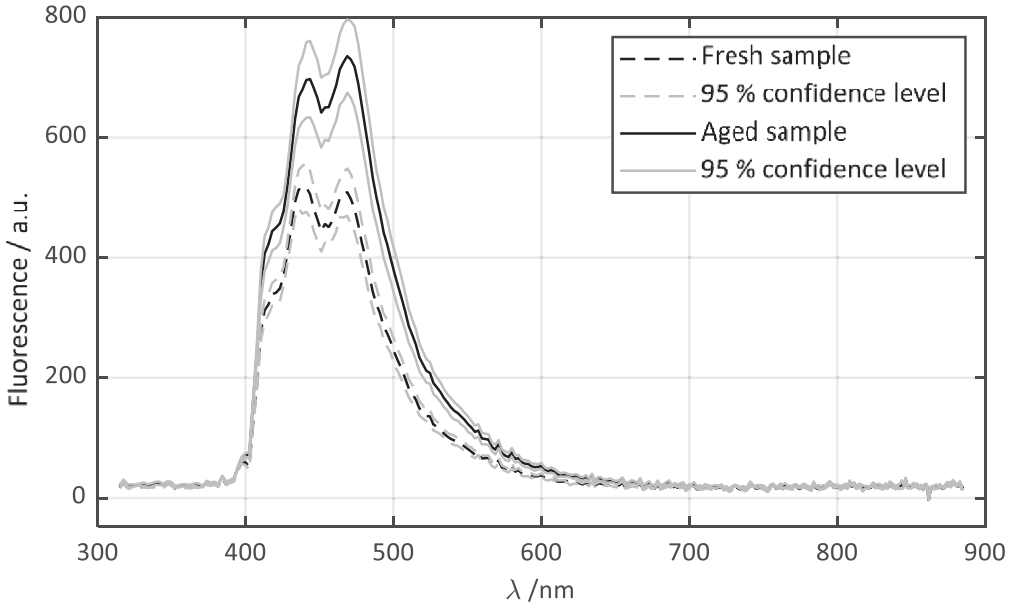

Figure 57: Exemplary measurement data and measurement uncertainty of the fluorescence spectroscopy of the fuel sensor for a fresh and an aged fuel sample in a standard cuvette with a 10 mm light path and 1 s detector exposure time

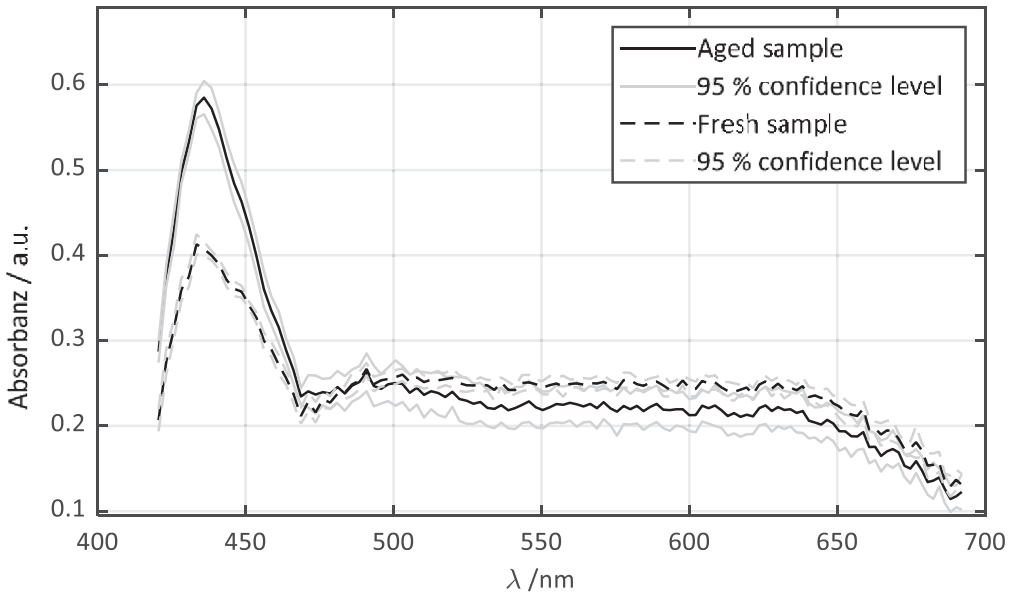

Figure 58: Exemplary measurement data and measurement uncertainty of the VIS absorption spectroscopy of the fuel sensor for a fresh and an aged fuel sample in a standard cuvette with a 10 mm light path and 50 ms detector exposure time.

8.2 Fluorescence measurement data

While the measurement results of the permittivity and the NIR absorption spectrum usually scale linearly with the constituents of a fuel sample and can therefore be used well for determining quantities and fuel constituents, the situation with fluorescence is often different, so that including the fluorescence data in the partial-least-square evaluation (see Section 8.3.4) only makes limited sense.

In the following, the measurement results of the fluorescence measurements of a selection of 9 example fuels are discussed on the basis of the three graphs in Figure 59. The samples of the three graphs in Figure 59 each show the fluorescence over the wavelength for different ageing states. The measurement results of the fresh samples are plotted above - in the middle those of the samples aged 24 hours according to the Rancimat method (see Section 4.1.1) and below those of the samples aged 48 hours.

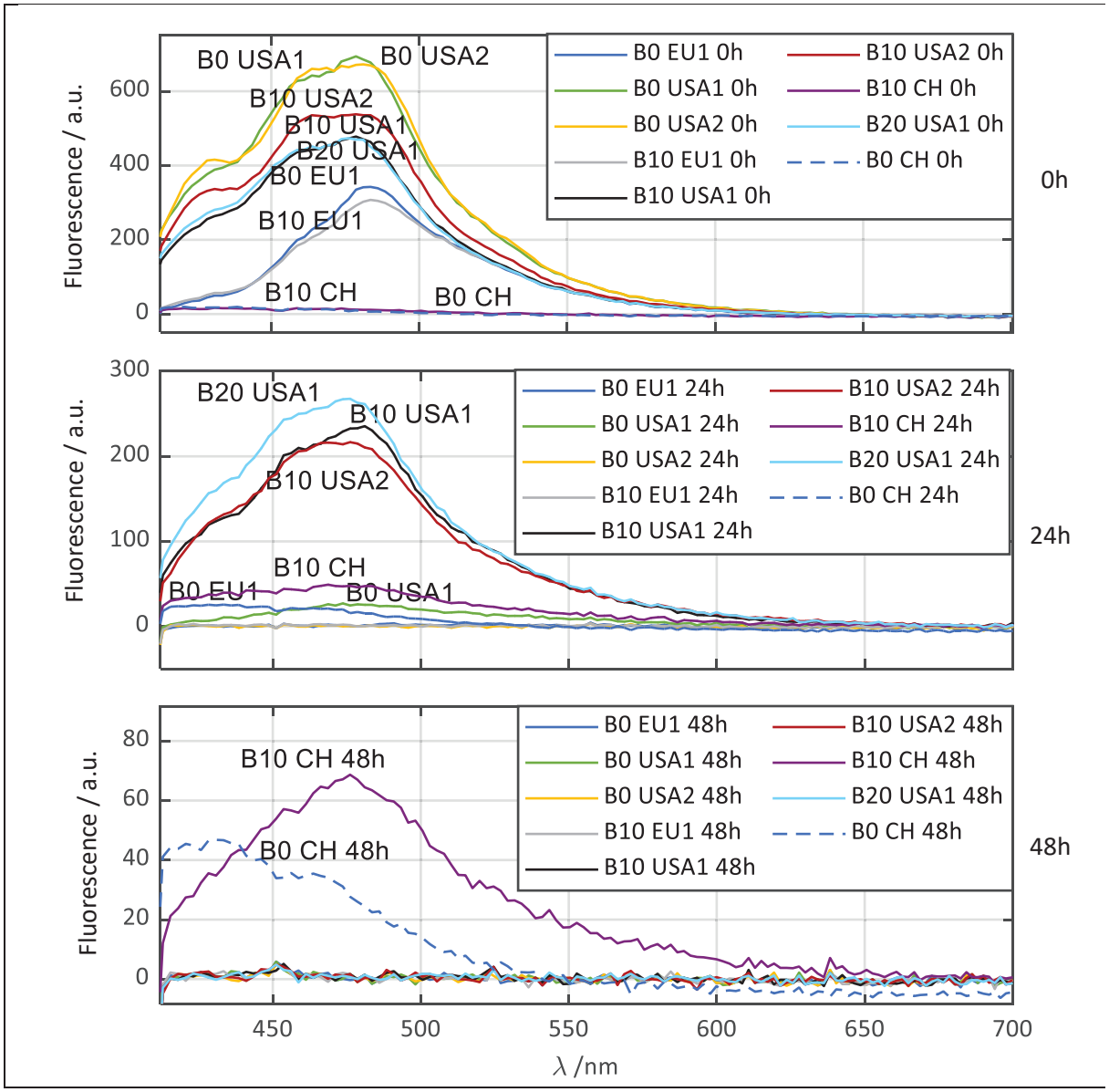

Figure 59: Measurement data of the fluorescence sensor for a selection of different fuels with a detector exposure time of 1s; Above: fresh samples, middle: Aged 24h, below: Aged 48h

If one looks at the measurement results of the fresh samples in Figure 59 above, several groups of two can be found, which show a similar course of the fluorescence over the wavelength. For example, the curves of B0 USA1 and B0 USA2, B20 USA1 and B10 USA1, B0 EU1 and B10 EU1, and B0 CH and B10 CH match very well. This can also be partly explained by the additive packages used. However, these similarities disappear when the fuels are thermo-oxidatively aged (see Figure 59 middle). While the fluorescence of most samples aged 24 hours has decreased compared to the fresh samples, it has even increased with the B10 CH. After an ageing time of 48 hours according to the Rancimat method, the fluorescence of the B10 CH increases further and the B0 CH also now shows fluorescence. In the case of all other fuels, however, the fluorescent component of the samples has completely degraded during the ageing process.

In summary, it can be stated that the fluorescence can be used to identify samples with certain matching and fluorescent components. However, due to the large number of fluorescent additives and fuel molecules used and the non-linearity of the fluorescence, it is generally difficult to draw quantitative conclusions about the sample components from the measurement data. The fluorescence sensor can, however, be used to recognise certain fuel samples and their origin. [54]

8.3 Determination of the fuel composition and the degree of ageing

The development of an on-board sensor system for measuring the fuel in the automobile is divided into two aspects. On the one hand, a suitable sensor system must be designed for data collection (Sections 4.5 and 8.1). On the other hand, the collected measurement data must be evaluated successfully. However, in addition to the sensor data, reference measurement data are also required for the data evaluation. First, with the reference data, a concept is developed as to how the measurement data can predict the required fuel parameters. The focus is on the determination of influencing factors and the methodology. In the second part, the sensor data are used to check whether the evaluation method can also be used with the partially lower-resolution measurement data from the sensor system. In both cases, the evaluation is based on the Partial Least Square (PLS) method.

8.3.1 Partial Least Square evaluation

For the Partial Least Square (PLS) evaluation, measurement data are correlated with defined parameters, so that the previously defined parameters can be predicted. For the PLS method, the parameters that are to be determined must be defined and recorded using measurement technology. In addition, the largest possible fuel dataset must be available with which the PLS is learned. The underlying concept is shown in Figure 60. The evaluation is based on a set of fuels with known parameters. These are correlated with the sensor data as a training matrix. The sensor signals of an unknown sample can be evaluated with the help of the training matrix and the parameters can be predicted. The fuel parameters collected this way can then be transmitted to the engine management system.

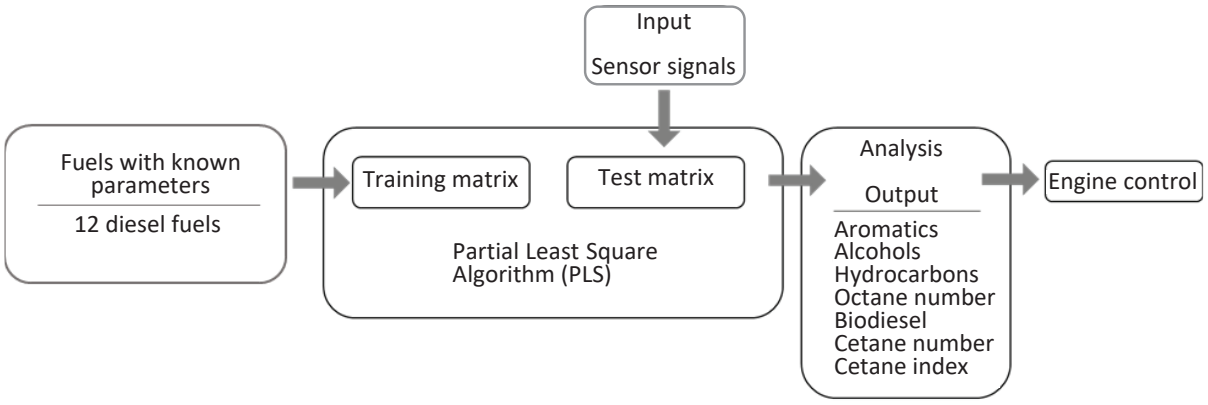

Figure 60: Overview of the partial least square evaluation for determining the fuel parameters.

8.3.2 Fuels used

The choice of fuels for teaching in the PLS evaluation is limited by the parameters to be examined. Only those fuels can be used for which all the desired parameters are fully available. 14 petrol and 35 diesel fuels and mixtures are used for the graphic evaluation in Figure 61. Since the complete fuel parameter data set is not available for all diesel fuels and mixtures, the PLS evaluations in the following will partly contain smaller data sets. The fuel parameters are determined primarily using the relative permittivity and near-infrared spectroscopy. Figure 61 is to illustrate at the beginning what information is contained in the measurement data.

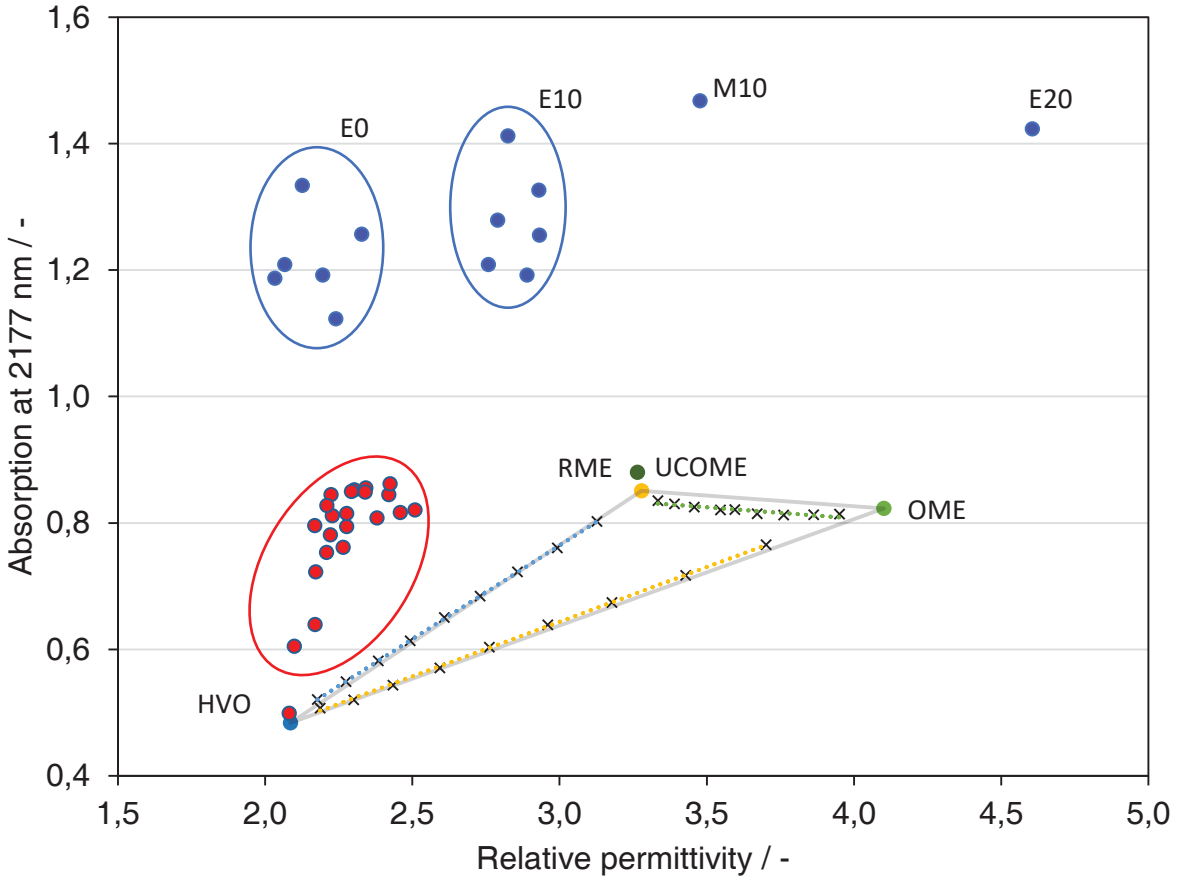

Figure 61: Visualisation of the information content by comparing the permittivity and the absorption of the 2177 nm wavelength of the near-infrared spectrum.

In this case, only one wavelength of the spectrum is used for the illustration of the fuel differences on the part of near-infrared spectroscopy shown in Figure 61. Even with this representation, a clear distinction can be made between gasoline, diesel and regenerative fuels. The petrol can also be classified according to the alcohol admixture. In the case of diesel fuels, the fuel parameters such as aromatics and biodiesel content lead to significantly smaller measurement differences. The difference in measurement between petrol and diesel fuels in Figure 61 lies in the polarity of ethanol and biodiesel. While biodiesel only has a slightly higher polarity than fossil fuel, the large polarity differences between ethanol and fossil petrol have a significant effect on the polarity-related permittivity. The variance of the fuels within the marked areas for diesel and petrol is due, for example, to the proportion of aromatics in the fuel. Mathematical methods such as the PLS used here must be used to predict the percentage of aromatics, for example, and to differentiate between unaged and aged fuels.

8.3.3 PLS evaluation using reference analysis

In the first step, the feasibility of the fuel parameter prediction is checked with the help of reference analysis. The measurement data is a mix of sensor measurement data and reference analysis. The relative permittivity and the conductivity are used as sensor data. The near infrared spectrum, viscosity, density, kinematic viscosity and acid number are used as reference measurement data. For the measurement data, a distinction must be made between sensor or reference measurement data and the measurement data from viscosity, density, kinematic viscosity and acid number. The latter are only required for teaching the PLS, whereas the sensor measurement data have to be measured online in the car from the unknown fuel. In addition, the sensor data for the fuels in the training matrix must also have been measured for a comparison with the online measurements.

To determine the fuel composition for diesel fuels, three parameters are used to describe the fuel. The three parameters are biodiesel content, aromatic content and hydrocarbon content. A total of 35 fuels and fuel blends are used in the training matrix. The prediction accuracy of the three parameters is shown in Figure 62. The admixtures of FAME, hydrocarbons and aromatics are given in percent by volume. The training matrix contains fuels with RME and HVO that contain 100% FAME or 100% hydrocarbons. For the aromatic content, the upper limit for the fuels used is approx. 30%, which results in the respective axis scaling. The predicted volume fraction is plotted on the y-axis and the measured fraction on the x-axis. The partially clustered distribution for the data set results from the typical composition of fossil fuels. Fuel blends from FAME and HVO result in a systematic distribution between 0 and 100% admixture for the parameters FAME and hydrocarbons. The data set used with 35 fuels results in an average prediction accuracy of FAME with +/- 1.2%, of aromatics with +/- 0.6 and hydrocarbons with +/- 1.5%.

In addition to the prediction accuracy, the areas in the near-infrared spectrum can also be identified that best describe the parameters FAME, hydrocarbons and aromatics with a high regression coefficient. In Figure 63, the regression coefficient is plotted against the data points from the near-infrared spectrum and permittivity. Since, in contrast to the near-infrared spectrum, only a single value is available for the relative permittivity, the data points in Figure 63 correspond to the NIR spectrum. Only the last data point represents the relative permittivity. Only the first two components are shown in Figure 63, as they already describe 99% of the variance.

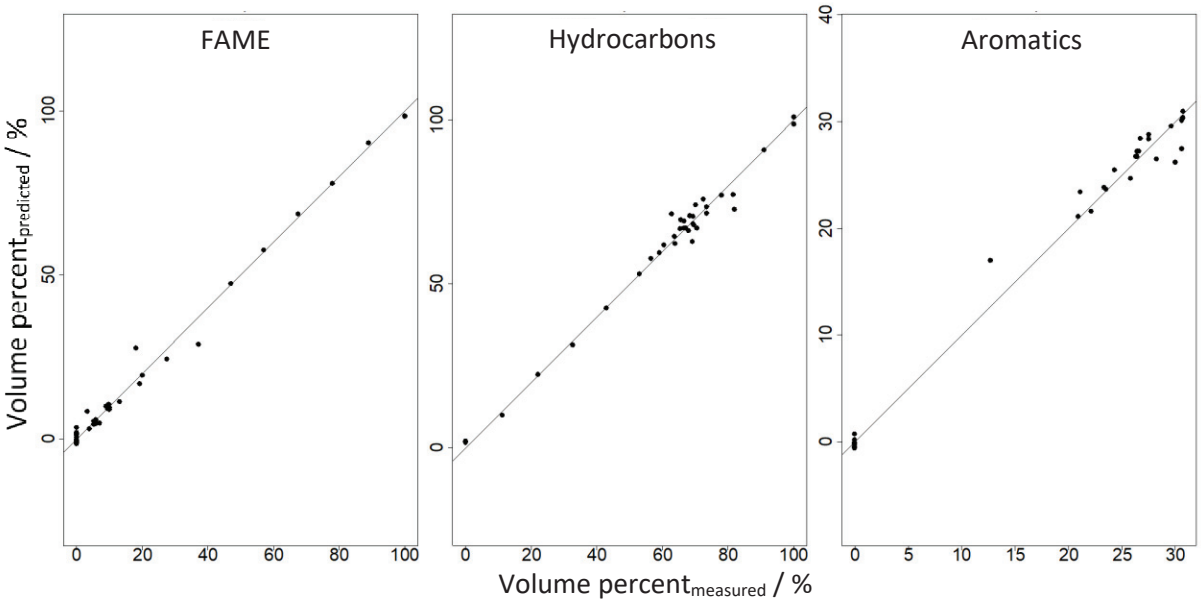

Figure 62: Comparison between predicted and measured values of the three parameters FAME, hydrocarbons and aromatics.

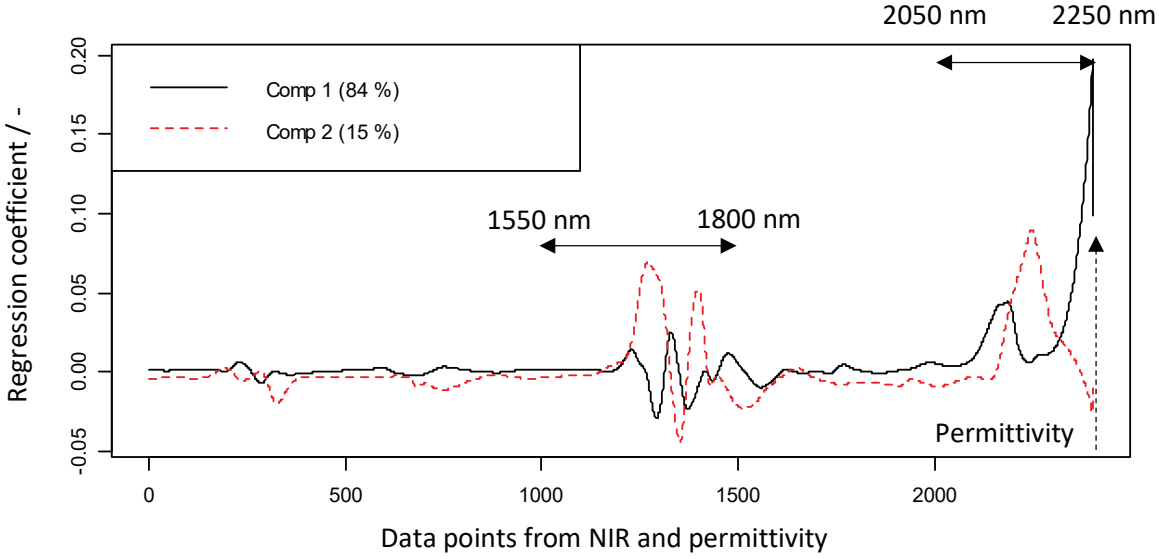

Figure 63: Regression coefficient as a function of the data points used.

From Figure 63 it can be seen that two areas in the NIR spectrum and the permittivity are important for the evaluation. The first range covers the wavelength range from 1550 nm to 1800 nm, which contains the CH_2 and CH_3 oscillation bands. The second range from 2050 nm to 2250 nm contains the carbonyl vibration of the ester group with λ_{max} = 2155 nm and the aromatic C-H vibration band with λ_{max} = 2177 nm. Consequently, component 1 describes the FAME content and component 2 describes the aromatic content. In addition to the respective oscillation bands, combination oscillations of the C=O or C-H oscillation and the CH_2 or CH_3 oscillations always occur in the NIR spectrum. In addition to the CH_2 and CH_3 oscillations of the hydrocarbons, the range between 1550 nm and 1800 nm also has a corresponding share in the parameters FAME and aromatics. The relative permittivity as a measured variable represents the sum of FAME, aromatics and hydrocarbons as a measured value. For this reason, it is not surprising that the permittivity has a large weight in the forecast. For the hydrocarbons,

the regression coefficient for the CH_2 and CH_3 bands at 1550 nm to 1800 nm shows only small values. The best way to determine the hydrocarbons is by means of permittivity.

A separate PLS with its own data set is carried out to determine fuel ageing. 14 fuels are used which are available in two ageing stages (24 and 48 hours in the Rancimat) in addition to the unaged fuels. However, evaluating the degree of ageing requires a different procedure than determining the fuel composition. The reason is that ageing cannot be recorded with a direct parameter, as is possible with FAME and aromatics. For this reason, the measurable quantities acid number and density are used to characterise the ageing of the fuel. In addition, another parameter called the oxidation index is used. The parameter oxidation index is the attempt to describe the ageing itself with a defined parameter. It represents the difference between the relative permittivity (ε_r') of the aged fuel and the relative permittivity of the unaged fuel (equation 11).

$$Oxidation\ index = \varepsilon_r'(aged\ fuel) - \varepsilon_r'(unaged\ fuel) \quad (10)$$

The reason is that the change in relative permittivity is related to the oxidation of the fuel. However, the oxidation index is not only based on the permittivity itself, but can also be recorded in the NIR spectrum by the carbonyl oscillation band. In unaged fuel, the carbonyl vibration band is composed only of the carbonyl vibration of the ester group. Oxidation creates additional functional groups such as ketones, alcohols and epoxides, which lead to a band increase at the same point in the NIR spectrum during ageing. For the determination, the ageing can therefore be recorded with the aid of the oxidation index and the known aromatics and biodiesel concentration. Together with the acid number and density of the fuel, ageing can finally be defined with three separate parameters.

The results of the PLS evaluation are shown in Figure 64 for the acid number, the density and the oxidation index. For all 42 fuels, the predicted value is compared with the measured value. The prediction of the acid number (Figure 64 above) must be interpreted from two standpoints. On the one hand, DIN EN 14104 specifies a defined limit value for the acid number that the fuels must not exceed. The limit value is 0.5 mg KOH/g. From Figure 64 above, there is a trend for predicting the acid number that the higher the acid number, the greater the accuracy of the prediction. In the reference evaluation, the limit value of 0.5 mg KOH/g can be used as an ageing indicator. However, acid numbers below 0.5 mg KOH/g are subject to a rapidly increasing inaccuracy.

In order to compensate for deviations in the acid number prediction, the density is also taken into account when determining the degree of ageing (Figure 64 middle). The prediction of the fuel density is independent of the fuel with an accuracy of the second decimal place. The minimum and maximum limit values for density of 800 kg/m^3 and 845 kg/m^3 specified in DIN EN 590 can therefore be accurately predicted. However, the density is the measurand that changes only slightly due to ageing compared to the acid number and oxidation index. While the density is still within the limit values, other parameters can already be far outside the limit values. For this reason, another ageing parameter with the oxidation index is used. By predicting the oxidation index, the aged fuels can be highlighted as a cluster for 24 hours and 48 hours. Easily oxidisable fuels such as pure RME can be clearly identified by the strong change in the oxidation index. On the other hand, fuels such as HVO, which hardly change during the ageing period of 48 hours, are identified as such. For fuels with a blend of biodiesel, the oxidation index can be reliably predicted, with exceptions. Viewed as a whole, a prediction of the state of ageing is possible. The accuracy and thus the reliability can be considerably improved by expanding the underlying data set.

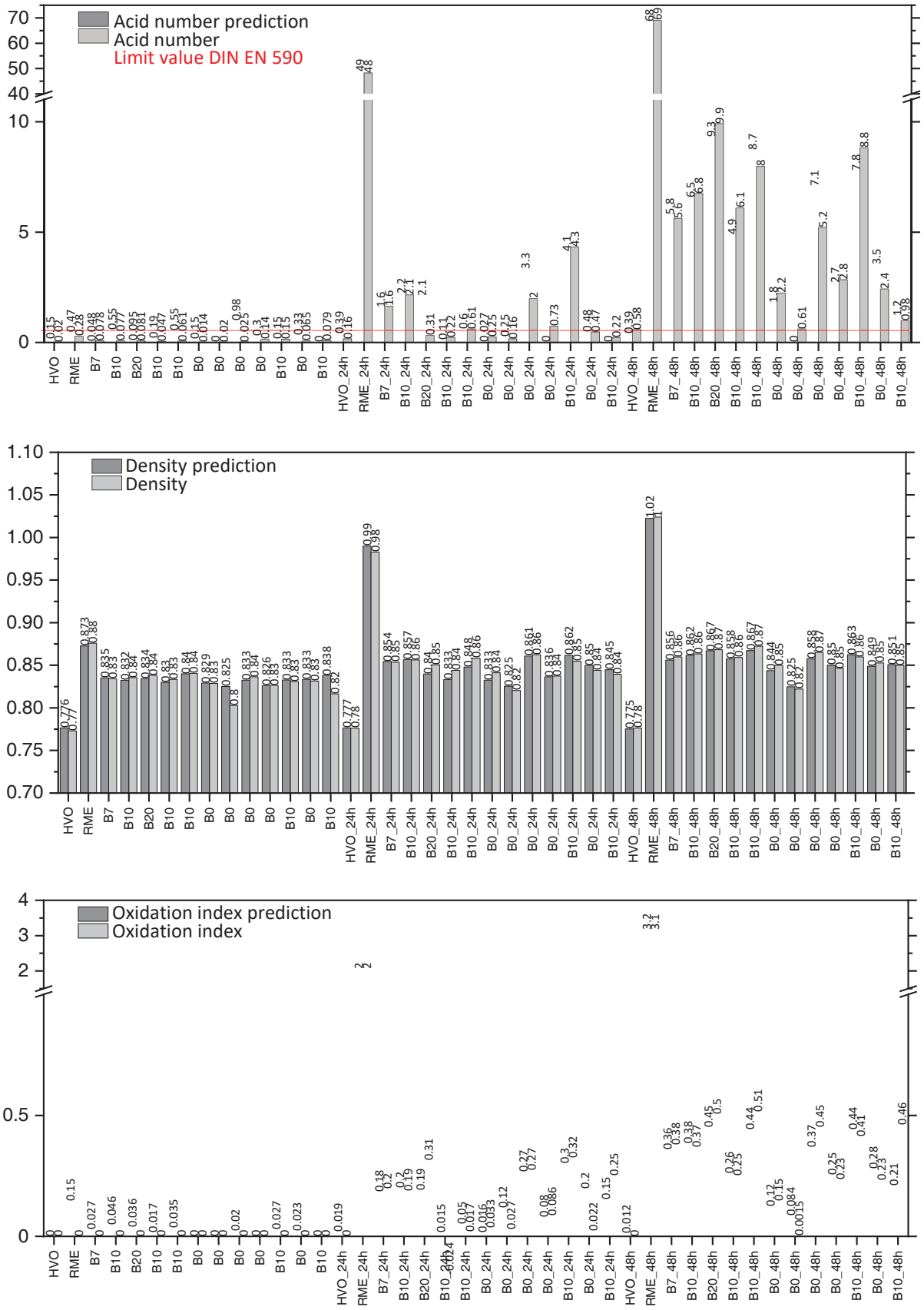

Figure 64: Comparison between predicted and measured values for the three parameters acid number, density and oxidation index.

To evaluate the PLS evaluation, the regression coefficients are plotted against the data points used for the three parameters acid number, density and oxidation index based on the components in Figure 65. The focus of this evaluation is on the identification of the data points that are relevant for the prediction. The data points are made up of the NIR spectrum and the permittivity like in Figure 63, with the permittivity as a single variable representing the last data point in Figure 65. The acid number is related to the measurement data in the NIR spectrum from a wavelength of 2000 nm. This is exactly the area in which a general increase in the baseline can be observed due to the addition of acid. The large wavelength range used to predict the acid number proves the quality of the assignment. Only the low level of increase in the baseline at very low acid numbers makes the prediction more difficult. The prediction of the density is based equally on the wavelength range from 2000 nm. However, the regression coefficient is here several orders of magnitude smaller. Due to the combination vibrations, the range from 1550 nm to 1800 nm is also taken into account. In contrast to the density and acid number, the prediction of the oxidation index is based more on the range of carbonyl oscillation and permittivity. As a result of the definition in equation 11, the prediction of the oxidation index occurs exactly as expected, which is a good indicator of fuel ageing.

The fuel composition can be predicted with good accuracy through the PLS evaluation of the reference measurement values. When determining the fuel ageing, several parameters have to be used because of the larger deviations for individual fuels in the matrix used in order to reliably determine the ageing. By using three parameters, criteria can be determined as of when a fuel is classified as aged. In this way, a reliable prediction can be made in which all three parameters must indicate ageing. The oxidation index must be interpreted in combination with the FAME admixture. Low FAME admixtures and a high oxidation index indicate severe fuel ageing. The evaluation of the composition and the degree of ageing possible for reference analysis is used in the following for the pure sensor-based evaluation.

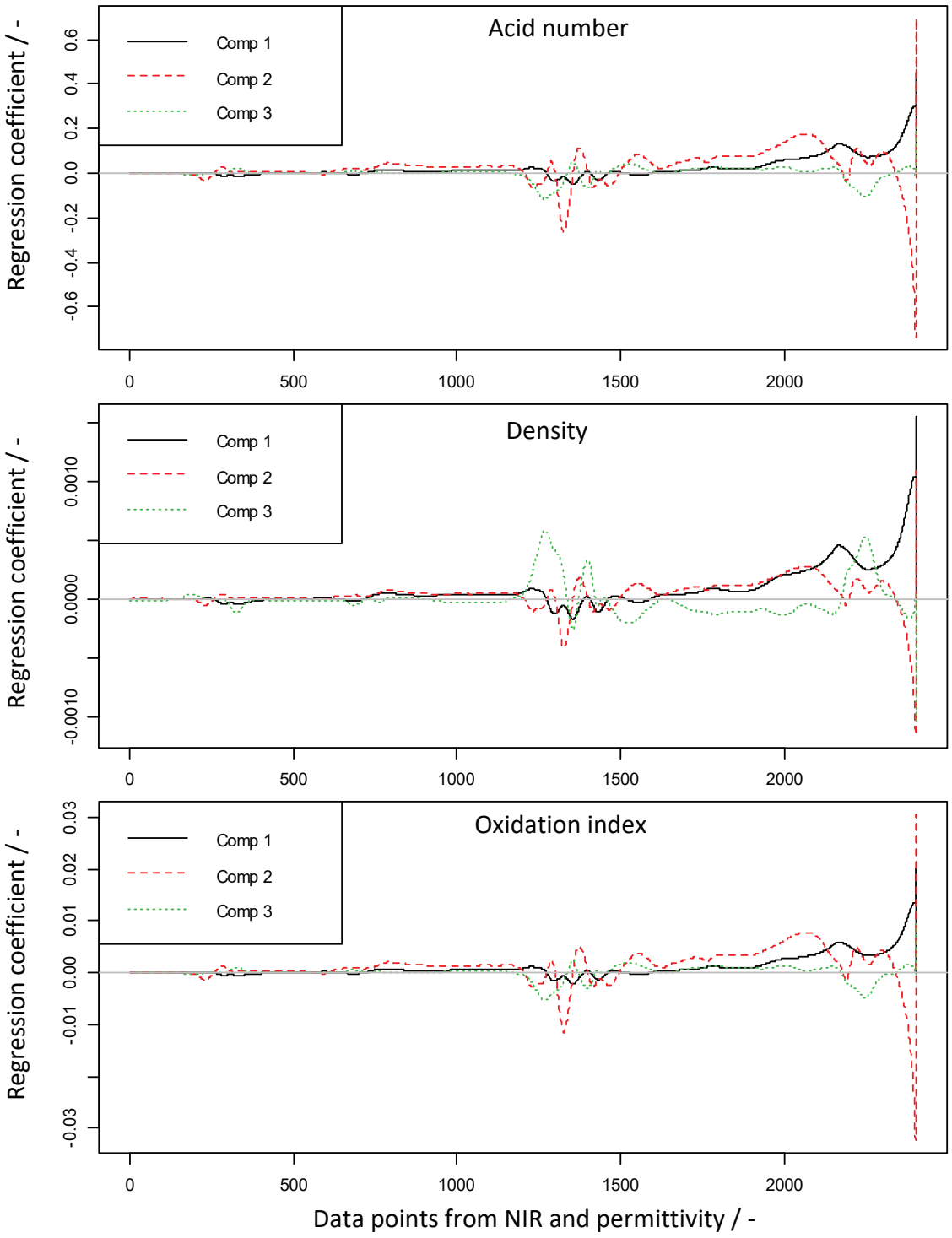

Figure 65: Regression coefficient as a function of the data points used.

8.3.4 Sensor-based prediction

The sensor-based forecast differs from the reference evaluation in the measurement data collection of the NIR spectrum. A mini-spectrometer with 8 nm resolution is used for the sensor-based prediction (reference NIR: 1 nm resolution). The determination of the permittivity takes place in both evaluations with the sensor concept. The sensor-based evaluation uses 12 diesel fuels, which differ in terms of aromatics and FAME admixture. The sensors used are described in detail in Section 8.1.

The results of the fuel composition prediction are summarised in Table 2. As with the reference evaluation, FAME, aromatics and hydrocarbons are used as fuel parameters for the prediction. The predicted and measured values are given for each of the three parameters in Table 2. The individual deviations for the FAME forecast result in a mean forecast deviation of +/- 0.5%. Due to the relatively small data set, the maximum deviation results in a prediction accuracy of +/- 2%. The aromatic content is predicted with an average forecast deviation of +/- 0.4%. From the maximum deviation, the prediction accuracy is +/- 0.7%. The prediction of the hydrocarbons is carried out with an average accuracy of +/- 0.5% and a maximum deviation of +/- 1.4%.

Table 2: Comparison of the predicted with the measured values of the three parameters FAME, aromatics and hydrocarbons.

Fuel	FAME		Aromatics		Hydrocarbons	
	Predicted	Measured	Predicted	Measured	Predicted	Measured
B0	0.0	0	30.6	30.6	69.4	69.4
B0	0.3	0	30.7	30.7	69.0	69.3
B0	0.0	0	29.8	30.0	70.5	70.0
B0	0.0	0	26.7	26.6	73.9	73.4
B0	2.0	0	29.0	29.6	69.0	70.4
B7	3.0	3.4	27.8	27.5	69.2	69.1
B10	19.7	19.2	23.9	24.3	56.4	56.5
B10	9.5	10.1	26.2	26.4	64.3	63.5
B10	9.2	9.5	24.4	23.3	66.5	67.2
B10	10.5	10	22.8	23.5	66.7	66.5
B10	11.8	13.2	27.0	26.3	61.2	60.5
B20	20.4	20.1	20.8	20.9	58.8	59.0

With the developed sensors and the evaluation of the measurement data it can be successfully shown that an online prediction of the fuel composition is possible. The training matrix used with 12 fuels represents the greatest limitation here. Despite this small dataset of fuels, there is a prediction accuracy with which the aromatic content and hydrocarbons can be determined with an accuracy of less than +/- 1.4%. Due to the intensity of the vibration band of the carbonyl vibration of the FAME, it is generally more difficult to achieve a high degree of prediction accuracy. For this reason, for the further development of the prototype towards series production, the amount of fuels used for the training must be further increased.

To evaluate the prediction of the three parameters FAME, aromatics and hydrocarbons, the regression coefficients are shown as a function of the NIR well length or permittivity in Figure 66. The range of the NIR spectrum relevant for the prediction is between 1600 nm and 2250 nm. The permittivity has an influence on the forecast for all three parameters. For NIR spectroscopy of the sensor system, the regression coefficients can be used to limit the detector unit to two smaller ranges from 1600 nm to 1750 nm and 2050 nm to 250 nm for further optimisation. The lower measurement resolution of the mini spectrometer used (8 nm) compared to the reference measurement with 1 nm resolution does

not significantly affect the accuracy of the prediction. The reason for this is likely to be the combination oscillations in the NIR spectrum. As a result, the information content is divided over a larger wavelength range, so that the point-by-point collection of the absorption is less important for the information content. The decisive factor for the prediction accuracy of the FAME admixture is the absorption band with λmax = 2155 nm. The absorption band at λmax = 2177 nm has the greatest influence on the prediction of the aromatic concentration. The absorption band of the aromatic C-H oscillation is, however, much more pronounced compared to the carbonyl oscillation band of FAME.

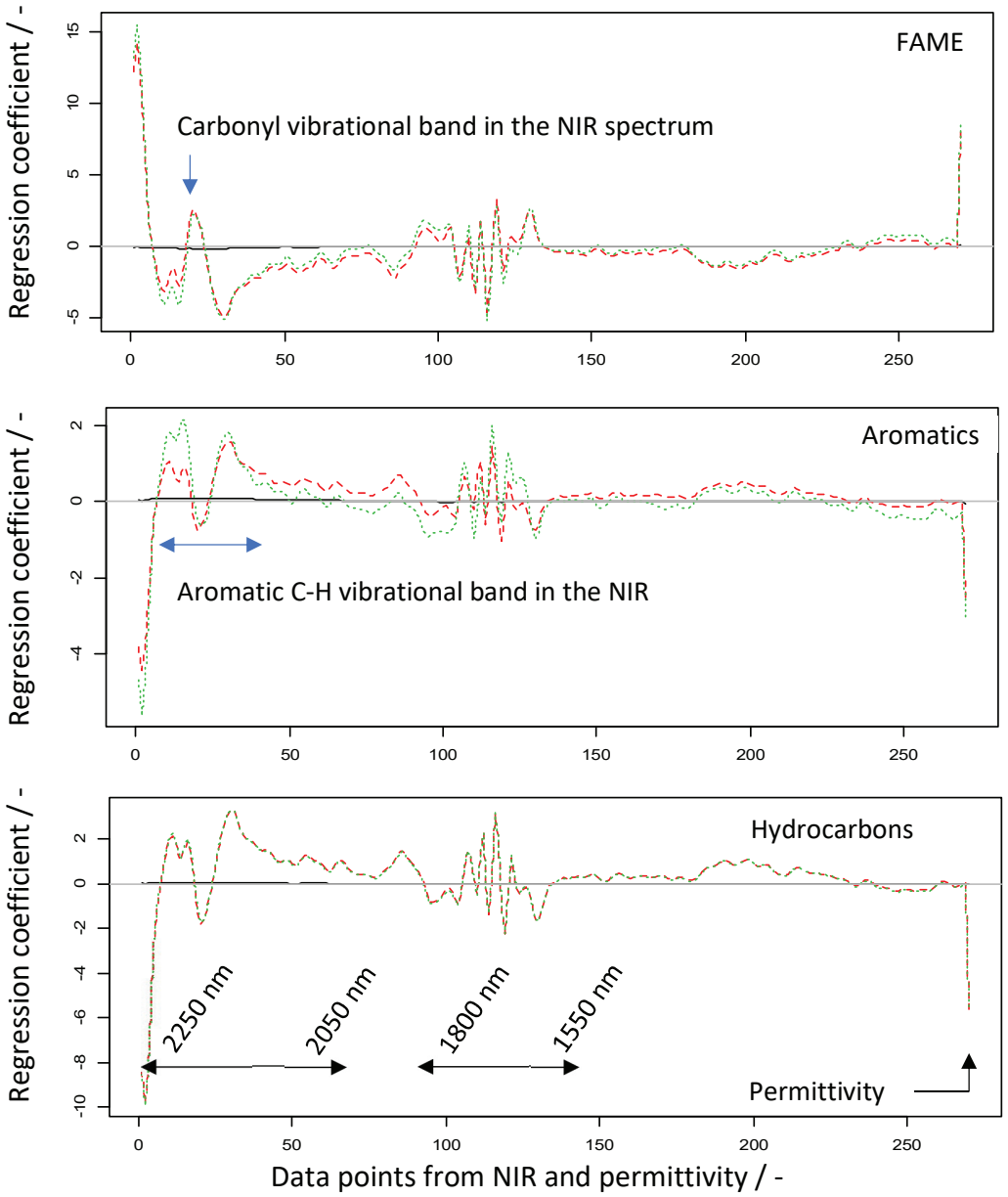

Figure 66: Regression coefficient as a function of the data points used.

The narrow-band absorption band of FAME can be clearly seen in Figure 66 above (blue arrow). The course of the regression coefficient over the data points in the aromatics prediction in Figure 66 middle extends over a larger area. In the wavelength range of the carbonyl oscillation band for the FAME determination, a negative regression coefficient can be seen for the aromatic determination. In this area, the influence of the FAME determination on the aromatics determination must be adjusted by

the overlaying of the bands. Figure 66 clearly shows that the PLS evaluation successfully takes into account the cross-influence of the carbonyl band and the aromatic C-H oscillation band.

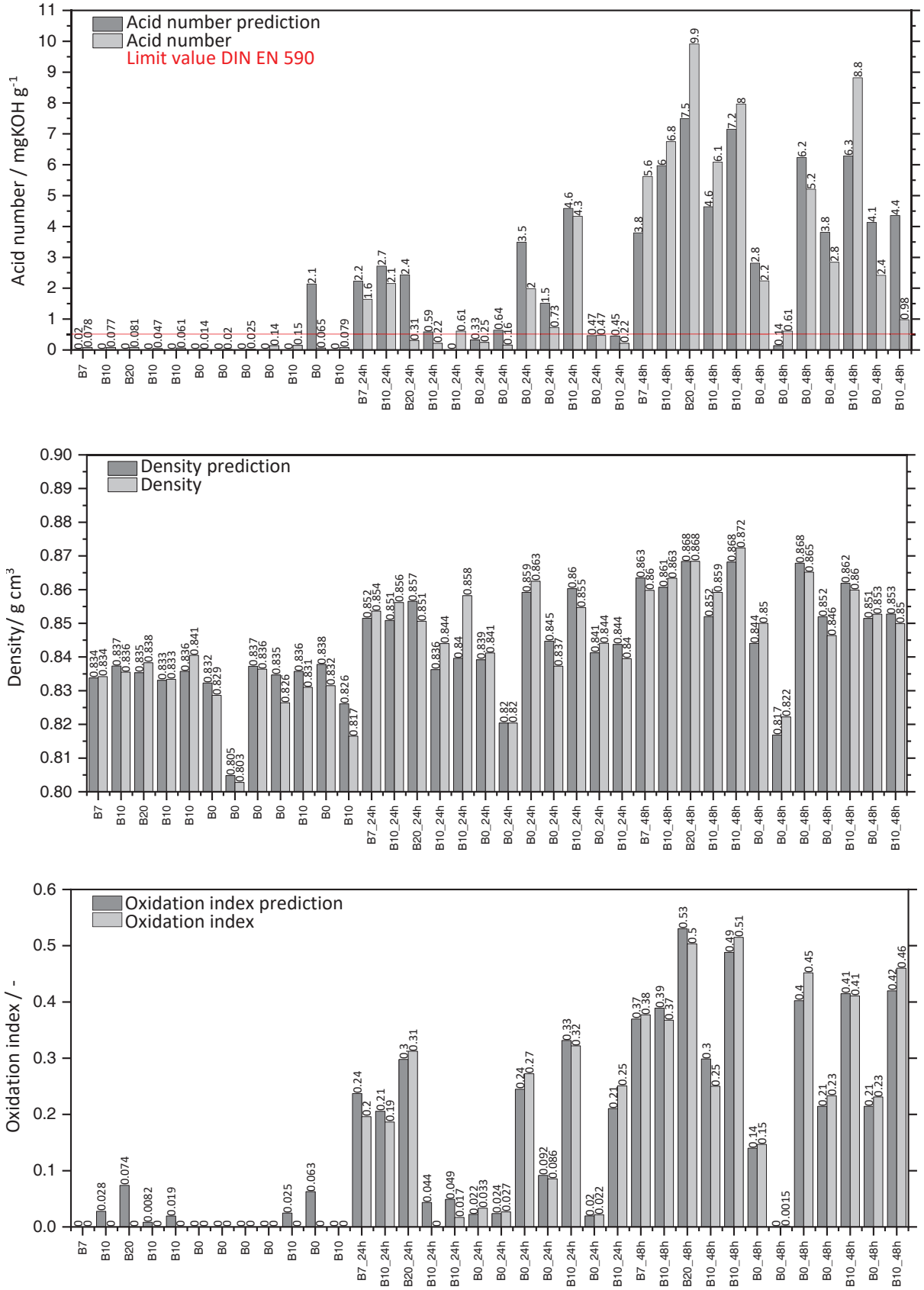

Figure 67: Comparison between predicted and measured values for the three parameters acid number, density and oxidation index.

In addition to the fuel composition, it is possible to determine the ageing with the developed sensors. The same three parameters are used for this as for the reference evaluation. With the help of acid number, density and oxidation index, the chemical and physical effects of oxidation on the fuel can be recorded. Due to the significantly larger deviations in the prediction of these three ageing parameters, the three parameters should be used together for the prediction of ageing in order to achieve a reliable prediction. The results of the prediction are shown in Figure 67. The measured values for the acid number, density and oxidation index show that the ageing of the 12 fuels is very different. The different ageing of the fuels is a great advantage for assessing the reliability of the developed sensors. In this way it can be clearly shown that ageing detection is possible for different effects of ageing. For the three parameters there is an average prediction deviation of the acid number of 0.8 mg KOH/g, for the density of 0.0044 g/cm^{-3} and for the oxidation index of 0.02. The mean prediction accuracy is very accurate for the density and the oxidation index with the small data set of 12 fuels. When predicting the acid number, the accuracy must be optimised even further with a larger data set. However, the mean forecast deviations must be supplemented by a detailed examination of the individual fuels. In the case of the acid number, individual strong deviations contribute significantly to the mean deviation. With a larger data set, these isolated large deviations can be recorded more precisely. In addition, when predicting ageing, it is of great importance whether a fuel is aged at all. And it is precisely this statement that can be clearly shown with the results shown here. With an enlargement of the dataset of fuels, whereby individual strong deviations can be compensated, the prediction of the acid number can also be used reliably below the limit value of 0.5 mg KOH/g.

The prediction of the density is made with a maximum deviation of 0.018 g/cm^{-3}, which means that sufficient accuracy is achieved here even with the small data set. With the densities in Figure 67 middle, which fluctuate greatly from fuel to fuel, a very reliable forecast can be assumed here overall. Thus, with the prediction of the density, selectively aged fuels that are outside the norm can be identified.

There are no limit values for the oxidation index with which the accuracy can easily be assessed. Since the oxidation index results from the relative permittivity and the correlation with the NIR spectra of the fuels, a comparison with the measurement accuracy of the relative permittivity is a good measure. The relative permittivity can be measured to the second decimal place with the sensor system. The measurement accuracy to the second decimal place is one of the outstanding properties of the developed sensor system. The mean deviation of the oxidation index at the second decimal place therefore represents a more than sufficient forecast accuracy. For a further classification of the prediction accuracy, the order of magnitude of the oxidation index between unaged and maximum measured ageing can also be used. The heaviest aged fuel has an oxidation index of 0.5. This means that 25 intermediate stages of ageing can theoretically be recorded. And here too, the larger the data set, the greater the accuracy and reliability of the prediction.

For the validation of the PLS evaluation, the regression coefficients of the data points of NIR and permittivity are plotted against each other in Figure 68. By looking at the regression coefficient, the areas in the NIR spectrum can be made visible that contribute to the prediction. These ranges can be compared with the effects that, for example, the acid number has on the NIR spectrum. If they match, the plausibility of the PLS evaluation can be interpreted. Acidic compounds lead to a baseline increase in the range of 1700 nm and 2200 nm in the NIR spectrum. Due to combination vibrations, the range between 1550 nm and 1800 nm is also important in the NIR. In both areas, there is a correlation with the acid number in the PLS. Accordingly, when determining the acid number, a plausible application of the PLS can be assumed. The prediction of the density is made up of all areas that are important for determining the composition of FAME, aromatics and hydrocarbons. The high accuracy of the prediction of these three parameters is also reflected in the prediction of density. The oxidation index is based much more strongly on the correlation with the permittivity, which is shown by the regression

coefficient in all three curves of components 1 to 3. In addition, the region around 2143 nm, which represents the maximum of the carbonyl vibrational band, is used heavily in component 1 for the correlation. Overall, the prediction of the three ageing parameters acid number, density and oxidation index is focused on the areas that should contribute to the prediction as expected. The developed sensor system with the PLS evaluation method and a sophisticated selection of parameters is an effective tool for determining the fuel composition and the degree of ageing.

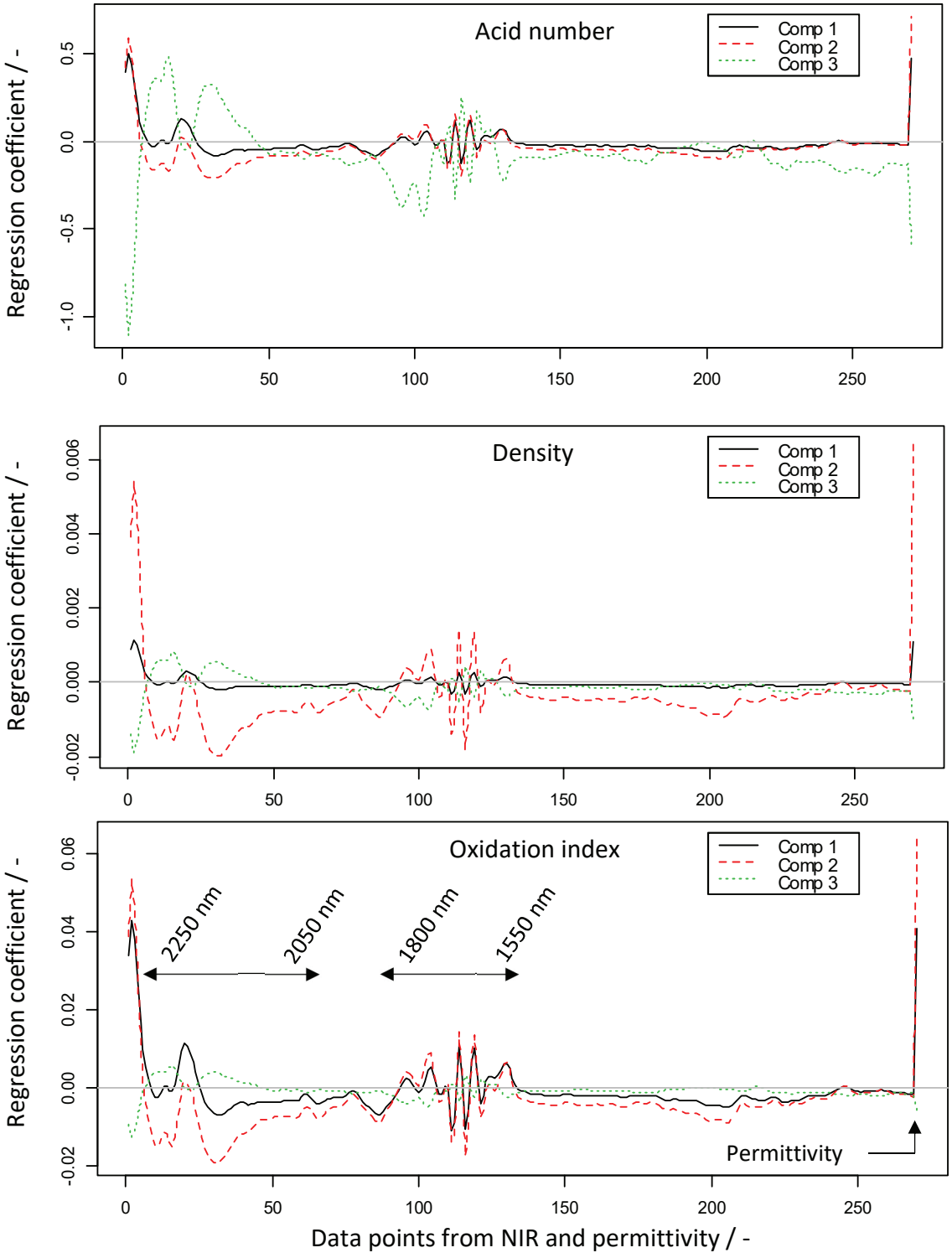

Figure 68: Regression coefficient as a function of the data points used.

9 Summary

For the increased use of rapeseed oil methyl ester (RME) in the future, also in connection with new regenerative fuels, understanding ageing is an important aspect in order to be able to ensure stable fuel formulations. The investigation of the ageing products from RME represents a very complex system due to the different fatty acid methyl esters (FAME) with single, double, triple unsaturated and saturated fatty acids and the resulting large number of different oxidation products. For this reason, a suitable method must be used in the elucidation of ageing products. For this reason, ageing is being investigated in this research project using high-resolution mass spectrometry coupled with liquid chromatography. The interaction of the chromatographic separation and the high-resolution mass spectrometry makes it possible to examine the complexity of biodiesel ageing. For the ageing products of RME isolated in this way, the structure elucidation can be carried out with high-resolution mass spectrometry with the help of MS/MS experiments. The data thus collected from the RME investigation show that a limitation of the oxidation can be observed (fourfold oxidation). In addition, short-chain ageing products can be identified with their structure. By elucidating the structure of long-chain ageing products, the mechanism of oligomerisation can be traced back to an esterification of oxidation products. Contrary to expectations, the long-chain ageing products are composed predominantly of dimers. The main products of the oligomers are dimers from short-chain degradation products and simply oxidised FAME. Larger ageing products, on the other hand, can only be observed in traces. In addition to the structural elucidation of the ageing products, the time course of fuel ageing was also investigated. With the help of mass spectrometry, individual masses can be specifically represented over the course of ageing. Thus, the oxidation products within the categories found (1-fold, 2-fold, 3-fold, 4-fold oxidation, acids, short-chain degradation products, dimers) can be examined for the reaction kinetics. Furthermore, the influence of the fuel composition of HVO and OME on RME ageing was investigated. The results show that the miscibility of the individual components affects the ageing of RME. Increased ageing of RME can be observed in areas with poor miscibility. The mass-selective investigation can also show that the oxidation of the individual fatty acid methyl esters is influenced by the composition of the ternary mixtures and the resulting solubility of individual fatty acid methyl esters. In the case of poor miscibility, there is stronger RME ageing of poorly soluble unsaturated fatty acids. The structure elucidation and the associated identification of the reaction mechanism offers the possibility of being able to better control ageing behaviour in the future. With esterification as the underlying reaction of oligomerisation, targeted measures can now be developed to minimise or prevent the dimerization that occurs during ageing. Investigations into the ageing behaviour of ternary RME/OME/HVO mixtures show that, by varying the composition, even poorly miscible fuels such as HVO and OME can be used as solubilizers in conjunction with RME. Based on the investigated effects of ageing, a basic additive (tributylamine) is checked for applicability as an additive with the approach of neutralising acids that occur. For this purpose, the effects of tributylamine on the formation of ageing products have been investigated. Together with the identification of the degradation products of tributylamine and the studies carried out on synergistic effects, the effectiveness of tributylamine can be confirmed.

In the second part of the final report, a sensor system is presented with which the composition and the degree of ageing of the fuel can be determined. The prediction of fuel parameters with the sensor system is based on a combination of near-infrared spectroscopy, dielectric relaxation spectroscopy and the measurement of conductivity. With the fuel composition, the FAME content, the aromatic content and the content of hydrocarbons can be predicted. Based on the number of fuels used, the PLS evaluation carried out can determine the parameters with a maximum deviation of 2% for FAME, 0.7% for aromatics and 1.4% for hydrocarbons. The degree of ageing is determined with the help of three other parameters (acid number, density and oxidation index), which can record the changes in

the fuel due to oxidation. The acid number and the density are two parameters with which the fuel can be compared directly with the limit values of the fuel standard DIN EN 590. The third parameter is called the oxidation index and represents the changes in relative permittivity caused by the oxidation. With the developed sensors it can be shown that the fuel composition and above all the fuel ageing can be determined with simple measuring methods.

10 Outlook

Due to the unsaturated FAME, biodiesel is more susceptible to oxidation. With the presented studies on biodiesel ageing, ageing can be characterised from oxidation to oligomerisation. This results in new starting points for minimising or even suppressing biodiesel ageing in a more targeted manner with regard to oligomerisation. As a next step in biodiesel research, the possibilities should be examined whether the esterification can be specifically prevented by additives, fuel matrix or other factors.

With the developed sensor system, a tool is also available with which the ageing can be recognised. This, in addition to further improving fuel ageing, can identify the fuel that should no longer be used in the automobile. For the further development of the on-board sensor system, a further simplification and cost minimisation must primarily take place. The relevant areas in the NIR spectrum are identified with the evaluation data, which means that individual wavelength ranges can also be used for the sensor design. With a larger fuel base, the accuracy of the sensors can be further improved in the future, as a result of which a greater simplification can be compensated for in individual areas.

11 Bibliography

[1] https://www.dwd.de/DE/leistungen/nationalerklimareport/download_report_auflage-4.pdf?__blob=publicationFile&v=11

[2] M. Unglert et al. Action areas and the need for research in biofuels, Fuel, 2020, 268, 117227.

[3] K. Araujo, D. Mahajan, R. Kerr, M. da Silva, Global Biofuels at the Crossroads: An Overview of Technical, Policy, and Investment Complexities in the Sustainability of Biofuel Development, *Agriculture* 2017, *7*, 32.

[4] M. Mofijur, M.G. Rasul, J. Hyde, M.M.K. Bhuyia, Role of Biofuels on IC Engines Emission, Energy Procedia, 2015, 75, 886-892.

[5] L. Bemert, Diesel-Mikroemulsionen als alternativer Kraftstoff, Cuviller Verlag, Göttingen, Dissertation, 2009.

[6] O. P. Bhardwaj, A. Omari, J. Nuottimaki, R. Hervé, Optimierte Motorkalibrierung für erneuerbare Dieselkraftstoffe, MTZ, März 2018, 79. Jahrgang,26-34.

[7] Adolf, J., Fehrenbach, H., Fritsche, U. *et al.* Welche Rolle können Biokraftstoffe im Verkehrssektor spielen? *Wirtschaftsdienst* 2013, 93, 124–131.

[8] Verband der Automobilindustrie, Antriebe und Kraftstoffe der Zukunft, 2009, 2. Überarbeitete Auflage.

[9] Neste Corporation, Neste Renewable Diesel Handbook, 2020.

[10] R. H. Boyd, Some Physical Properties of Polyoxymethylen Dimethyl Ethers, Journal of Polymer Science, 1961, Vol L, 133-141.

[11] S. Fischer, C. Beidl, A. Viehmann, S. Rinderknecht, Plug-in-Hybride für den Volumenmarkt, MTZ, März 2017, 30-39.

[12] A. F. Aguilera, P. Tolvanen, K. Eränen, S. Leveneur, Epoxidation of oleic acid under conventional heating and microwave radiation, Chemical Engineering and Processing: Process Intensification, 2016, 102, 70-87.

[13] W. Xia, S. M. Budge, M. D. Lumsden, 1H-NMR Characterization of Epoxides Derived from Polyunsaturated Fatty Acids, J. Am. Oil Chem. Soc. 2016, 93, 467-478.

[14] B. S. Levison, R. Zhang, Z. Wang, X. Fu, J. A. DiDonato, Quantification of fatty acid oxidation products using online high-performance liquid chromatography tandem mass spectrometry, Free Radical Biology and Medicine, 2013, 59, 2-13.

[15] T. Püssa, P. Raudsepp, P. Toomik, R. Pällin, U. Mäeorg, S. Kuusik, R. Soidla, M. Rei, A study of oxidation products of free polyunsaturated fatty acids in mechanically deboned meat, Journal of Food Composition and Analysis, 2009, 22, 307-314.

[16] M. G. Simic, M. Karel, Autoxidation in Food and biological Systems, Springer Science+Business Media, New York, 1980.

[17] K. Ingold, Inhibition of the Autoxidation of Organic Substances in the Liquid Phase, Chem. Rev. 1961, 61, 563–589.

[18] I. Ernest, Radikalische Reaktionen. In: Bindung, Struktur und Reaktionsmechanismen in der organischen Chemie. Springer, Vienna, 1972.

[19] J. Lee, Y. Lee, E. Choe, Temperature dependence of the autoxidation and antioxidants of soybean, sunflower, and olive oil, *Eur Food Res Technol*, 2007, 226, 239-246.

[20] K. Waterman, R. Adami, Accelerated aging: prediction of chemical stability of pharmaceuticals, International Journal of Pharmaceutics, 2005, 293, 101–125.

[21] J. Hioe, H. Zipse, Radical stability and its role in synthesis and catalysis, Org. Biomol. Chem. 2010, 8, 3609-3617.

[22] N. E. Schore, K. P. C. Vollhardt, Organische Chemie. Wiley-VCH, Weinheim, 2020.

[23] J. Hioe, H. Zipse, Radical stability and ist role in synthesis and catalysis, Org.Biomol.Chem. 2010, 8, 3609-3617.

[24] K. Herwig, P. Lorenz, C. Rüchardt, Zur Reaktivität elektronenreicher Olefine, 5. Reaktionen von Tetraaminoäthylenen mit Lactamen und Imiden, Chemische Berichte, 1975, 108, 214-224.

[25] A. Gansäuer, Radicals in Synthesis I - Methods and Mechanisms, Springer, Berlin Heidelberg, 2006, 163.

[26] F. Becker, Hyperkonjugation, Angew. Chem. 1953, 4, 97-107.

[27] H. P. Latscha, U. Kazmaier, H. A. Klein, Organische Chemie, 7. Auflage, Springer-Verlag, Berlin Heidelberg, 2016.

[28] R. R. Hiatt, W. M. Strachan, The Effect of Structure on the Thermal Stability of Hydroperoxides, Journal of Organic Chemistry, 1963, 28, 1893-1894.

[29] E. N. Frankel, Lipid Oxidation, Prog. Lipid. Res. 1980, 19, 1-22.

[30] V. M. Samokyszyn, L. J. Marnett, Hydroperoxide-dependent Cooxidation of 13-cis-Retinoic Acid by Prostaglandin H Synthase, J. Biol. Chem. 1987, 262, 29, 14119-14133.

[31] R.E. Parker, N.S. Isaacs, Mechanisms of Epoxide Reactions, *Chem. Rev.* 1959, 59, 4, 737–799.

[32] S. Jain, M.P. Sharma, Stability of biodiesel and its blends: A review, Renewable and Sustainable Energy Reviews, 2010, 14, 667-678.

[33] G. Knothe, J. VanGerpen, J. Krahl, The biodiesel handbook, Urbana, Illinois: AOCS Press, 2005.

[34] G. Knothe, L. F. Razon, Biodiesel fuels, Progress in Energy and Combustion Science, 2017, 58, 36-59.

[35] Arbeitsgemeinschaft Qualitätsmanagement Biodiesel e.V., Kälteeigenschaften von Biodiesel, 2018.

[36] S. Proschke, M. Unglert, Charakterisierung der Mischbarkeit gealterter Kraftstoffe, Tagungsbandbeitrag 10. Biokraftstoffsymposium, 2019.

[37] M. Mittelbach, S. Schober, The Influence of Antioxidants on the Oxidation Stability of Biodiesel, JAOCS, 2003,80, 817-823.

[38] J. Zhou, Y. Xiong, S. Xu, Evaluation of the oxidation stability of biodiesel stabilized withantioxidants using the PetroOXY method, Fuel, 2016, 184, 808-814.

[39] P. Geladi, B. R. Kowalski, Partial Least-Squares regression: a Tutorial, Analytica Chimica Acta, 1986, 85, 1-17.

[40] https://www.agilent.com/cs/library/usermanuals/public/G3335-90231_TOF_Q-TOF_Concepts.pdf

[41] https://www.agilent.com/cs/library/eseminars/public/Making%20LC%20Methods%20MS%20Friendly.pdf

[42] A. Küchler, Hochspannungstechnik. Berlin: Springer, 2009. 978-3-540-78412-8.

[43] W. von Münch, Elektrische und magnetische Eigenschaften der Materie. Stuttgart: B. G. Teubner Verlag, 1987. 978-3-6630-9910-9.

[44] E. Philippow, Grundlagen der Elektrotechnik. Berlin: Huss-Medien, 2000. 978-3-3410-1241-3.

[45] K. Simonyi, Theoretische Elektrotechnik. Leipzig et al.: Barth Verlagsgesellschaft, 1993. 978-3-3350-0375-5.

[46] D. P. Demarque, A. E. M. Crotti, R. Vessecchi, J. L. C. Lopes, N. P. Lopes, Fragmentation reactions using electrospray ionization mass spectrometry: an important tool for the structural elucidation and characterization of synthetic and natural products, Nat. Prod. Rep. 2016, 33, 432-455.

[47] K. Heusler, J. Kalvoda, Intramolecular Free-Radical Reactions, Angewandte Chemie International Edition, 1964, 3, 525-596.

[48] S. Schulze, H. Vogel, Aspects of the Safe Storage of Acrylic Monomers: Kinetics of the Oxygen Consumption, Chem. Eng. Technol. 1998, 21, 829-837.

[49] A. Munack, M. Petchatnikov, L. Schmidt, J. Krahl, Spektroskopische Untersuchungen zur Ergründung der Wechselwirkungen zwischen Biodiesel und Dieselkraftstoff bei Blends, Abschlussbericht, 2009.

[50] D. Corradini, Handbook of HPLC, Taylor & Francis Inc, 2010.

[51] Heimann W., Wisser K. (1965) Das Redox-Potential. In: Belitz HD. et al. (eds) Analytik der Lebensmittel. Handbuch der Lebensmittelchemie, vol 2 / 1. Springer, Berlin, Heidelberg.

[52] U. Lüning, Organische Reaktionen. Eine Einführung in Reaktionswege und Mechanismen, Spektrum Akademischer Verlag, 2. Edition, 2007.

[53] J. Pecha, L. Sanek, T. Fürst, K. Kolomaznik, A kinetics study of the simultaneous methanolysis and hydrolysis of triglycerids, Chemical Engineering Journal, 2016, 288, 680–688.

[54] Z. Fan, Fluoreszenzspektroskopische Charakterisierung und Identifizierung von Kraftstoffgemischen zur Entwicklung eines Kraftstoffsensors, Cuvilli Verlag, Göttingen, 2016.